
RUNNING OF RADIATIVE NEUTRINO MASSES
A Study of the Zee-Babu Model

Michael Volpp



München 2017

RUNNING OF RADIATIVE NEUTRINO MASSES

A Study of the Zee-Babu Model

Masterarbeit
im Elitemasterstudiengang
Theoretical and Mathematical Physics
der Ludwig-Maximilians-Universität
München

eingereicht von
Michael Volpp
aus Ostfildern

München, den 16. April 2017



Masterarbeit

am
Max-Planck-Institut für Physik
(Werner-Heisenberg-Institut)
Föhringer Ring 6
80805 München

eingereicht von Michael Volpp
am 16. April 2017

im Elitemasterstudiengang
Theoretical and Mathematical Physics
der Ludwig-Maximilians-Universität München

Betreuer: Dr. Alexander Merle
Erstgutachter: Dr. habil. Georg Raffelt
Zweitgutachter: Prof. Dr. Gerhard Buchalla

Tag der mündlichen Prüfung: 19. April 2017

Abstract

Experiments unambiguously show that neutrinos have tiny – but nonzero – masses, contradicting the prediction of the Standard Model of Particle Physics (SM). Radiative models are extensions of the SM, in which neutrinos get their masses not from tree-level terms in the Lagrangian, as for example in the well-known seesaw-type scenarios. Rather, the masses appear as effective terms at loop level, which become possible by postulating new particles circulating in the loops.

Radiative models have various appealing features, making them interesting candidate neutrino mass models. In contrast to the seesaw setting, the new particles do not have to be exceedingly heavy, rendering them potentially observable in near-future experiments. Indeed, they explain the high suppression of neutrino masses naturally, as these come out as the product of multiple (small) couplings. This also leads to neutrino parameters generically showing a strong energy dependence (“running”). It was shown in previous work on the Scotogenic model that the running in radiative settings can explain the deviation of measured neutrino data taken at energies below the electroweak scale from theoretical predictions at much higher energies.

In this thesis, we study the running of neutrino parameters in another radiative model, the Zee-Babu model. It is an economical extension of the SM by only two charged scalar particles, leading to neutrino masses at two-loop order. The main topic of this work is the computation of the full set of renormalisation group equations (RGEs) in the Zee-Babu model and in its effective theories (EFTs), which one obtains by subsequently integrating out the additional scalars. Furthermore, we derive the matching equations relating the parameters of the different EFTs. We consistently organise the calculations in loop orders, which is a convenient and powerful method for deciding which effects are relevant for obtaining a desired accuracy. Finally, we present the results of a numerical evaluation of the RGEs, yielding the running of neutrino masses and leptonic mixing angles in the Zee-Babu model for fixed high-energy mixing patterns.

Contents

1	Introduction	1
2	Theoretical Preliminaries	3
2.1	Neutrinos in the Standard Model and Beyond	3
2.1.1	The Standard Model of Particle Physics	3
2.1.2	Mixing in the Lepton Sector	11
2.2	Renormalisation and Effective Field Theory	14
2.2.1	Renormalisation Group Evolution of Model Parameters	15
2.2.2	Effective Field Theory	20
2.3	Neutrino Mass Models	22
2.3.1	Extending the Standard Model by Neutrino Masses	22
2.3.2	The Zee-Babu Model	24
2.3.3	The Top-Down Approach of RG Evolution	26
3	Running of the Neutrino Mass Matrix in the Zee-Babu Model	31
3.1	Systematics of the Calculations	32
3.1.1	Expansion in Loop Orders	32
3.1.2	Application to the Zee-Babu Model	37
3.2	Full Theory	39
3.2.1	Mass Matrix	39
3.2.2	Renormalisation Group Equations	41
3.2.3	Calculation of the Wavefunction Renormalisation Constants	43
3.3	EFT- h	48
3.3.1	Effective Operators	48
3.3.2	Calculation of the Counterterms	49
3.3.3	Matching	56
3.3.4	Mass Matrix	68
3.3.5	Renormalisation Group Equations	68
3.4	EFT- k	71
3.4.1	Effective Operators	71

3.4.2	Matching	71
3.4.3	Mass Matrix	72
3.4.4	Renormalisation Group Equations	73
3.5	EFT-0	75
3.5.1	Matching	75
3.5.2	Mass Matrix	76
3.5.3	Renormalisation Group Equations	76
4	Numerical Results	79
4.1	Evaluation of the Neutrino Mass Matrix	79
4.2	Solution of the RGEs	80
4.2.1	Simplification and Solution of the RGEs	80
4.2.2	Initial Values for the RGEs	81
4.3	Discussion of the Results	84
5	Conclusions and Outlook	91
A	Symbols and Notation	95
B	Spinor Algebra	99
C	Feynman Rules of the Zee-Babu Model	101
C.1	Unbroken Phase	101
C.1.1	Propagators and Wavefunction Renormalisation Counterterms	102
C.1.2	Leptonic Gauge Couplings	103
C.1.3	Scalar Couplings	105
C.1.4	Leptonic Yukawa Couplings	106
C.1.5	Effective Couplings	107
C.2	Broken Phase	108
D	RGEs of the Zee-Babu Model and its EFTs	109
D.1	RGEs of the Full Theory	109
D.2	RGEs of EFT- h	111
D.3	RGEs of EFT- k	112
D.4	RGEs of EFT-0	113

Chapter 1

Introduction

The Standard Model of Particle Physics (SM) provides the modern understanding for all of the interactions among known subatomic particles, except for those due to gravity. It came together in its modern form in the mid-1970s, as the result of almost half a century of experimental and theoretical research. Since then, the SM has been tested thoroughly in experiments, and it provided remarkably accurate predictions [1].

However, physicists agree that the SM cannot be the ultimate description of Nature, for example due to its inability to describe phenomena such as gravity or Dark Matter [2], and also because of various theoretical flaws. Furthermore, this view is affirmed strongly by direct experimental contradictions of the SM coming from the field of neutrino physics.

A revolution in neutrino physics started in June 1998, when the Super-Kamiokande collaboration announced the discovery of neutrino oscillations of atmospheric neutrinos [3], an effect which is absent in the SM as it predicts neutrinos to be massless. This focused attention on solar neutrinos, for which experiments like SNO [4] soon could show the existence of flavour conversion. These experimental results have further been confirmed and refined [5, 6], leading to a clear phenomenological picture of neutrino oscillations [7].

The observation that neutrinos do have tiny masses has led to lively and still ongoing experimental and theoretical efforts trying to shed light on the origin of these masses. One of the most important aspects of this question is whether neutrinos are of Majorana or of Dirac type, i.e., whether neutrinos are or are not their own antiparticles, respectively. This question might be settled through experiments trying to observe neutrinoless double beta decay, one example being the GERDA experiment [8]. From a theoretical standpoint, the odds are good for neutrinos being Majorana particles, as the Dirac case would probably imply the existence of three right-handed (RH) sterile neutrinos with a highly fine-tuned mass configuration. Nevertheless, extending the SM by RH neutrinos is a very popular approach, since, by making these very heavy, one can explain tiny (and in this case Majorana) neutrino masses by the seesaw mechanism [9–11].

In this thesis, we investigate another type of SM extension, in which neutrino masses do not appear in the tree-level Lagrangian but are generated at loop order. In such radiative models, one postulates new particles which circulate in loops, thus generating effective

mass terms for the neutrinos. Neutrino masses are then given by the product of multiple (small) couplings, naturally leading to their observed strong suppression. An advantage of such models compared to seesaw-type settings is that the mass scale of the new particles can potentially be reached in near-future experiments. Furthermore, running effects may be capable of explaining the deviation of theoretical predictions for mixing patterns at very high energy scales from the measured data at energies below the electroweak scale. Indeed, corrections to neutrino masses and mixings beyond leading order are generically strong in radiative models, since the corrections to the couplings in the aforementioned product tend to add up. One popular radiative model is the Scotogenic model [12], in which neutrino masses are generated at one-loop order. The running in this model has been studied extensively in previous works, confirming that it can explain the measured neutrino parameters at low energies, which motivates further research in this field [13, 14].

Therefore, in this thesis, we consider another radiative model, the so-called Zee-Babu model [15]. It is an extension of the SM by only two charged scalar particles, leading to neutrino masses at two-loop order. Regarding its low-energy properties, the model has been examined thoroughly [16, 17] in the light of current data, which constrains the free parameter space but does not rule the model out. However, the running of neutrino parameters in this model has not yet been studied in the literature. We will help to close this gap by deriving the full set of renormalisation group equations (RGEs) in the Zee-Babu model and its effective field theories (EFTs), which follow from successively integrating out the new particles at energies below their masses. This allows us to study the running of neutrino parameters in the whole range from very high energies down to energies below the electroweak scale.

We structure this thesis as follows: In Chapter 2, we review the basic aspects of the SM with focus on neutrino masses and leptonic flavour mixing. Subsequently, we introduce the techniques we need for computing RGEs, as well as the concept of integrating out particles and matching the resulting EFTs. In addition, we discuss popular extensions of the SM for neutrino masses and introduce the Zee-Babu model. Chapter 3 is devoted to the main task of this work: the derivation of the two-loop mass matrix, the matching equations, and the RGEs in the Zee-Babu model as well as in the EFTs derived from it. We structure the calculations consistently in loop orders, which allows us to compare the relative importance of different contributions to the running in a systematic way. We present the results of a numerical evaluation of the RGEs in Chapter 4, yielding first insights into the running of neutrino masses and leptonic mixing angles in the Zee-Babu model. Finally, we summarise our work in Chapter 5. In the appendices, we present our conventions on notation as well as a list of the Feynman rules and RGEs of the Zee-Babu model.

Theoretical Preliminaries

In this chapter, we introduce the basic concepts and calculational techniques, which we will use throughout this thesis. We discuss how to describe neutrino masses by extending the Standard Model of Particle Physics (SM) and present the Zee-Babu model. Furthermore, we shortly summarise the techniques we need to investigate the energy dependence (“running”) of neutrino masses and mixing parameters.

2.1 Neutrinos in the Standard Model and Beyond

In the SM, neutrinos are – unlike all other fermions – massless particles. We will now review the most important aspects of the SM with respect to fermion masses, and present current experimental data which shows that the SM has to be extended: we observe leptonic flavour mixing, implying nonzero neutrino masses.

2.1.1 The Standard Model of Particle Physics

We present the SM Lagrangian and discuss the Higgs mechanism, through which all fermions except the neutrinos acquire masses. Furthermore, we show how this leads to flavour mixing in the quark sector but not in the lepton sector. This is reflected in the presence of accidental symmetries in the SM, which will be the last topic of this section.

Lagrangian

The SM [18–21] is a gauge theory based on the gauge group

$$SU(3)_C \times SU(2)_L \times U(1)_Y, \tag{2.1.1}$$

and the particle content summarised in Tab. 2.1. We obtain the Lagrangian of the SM by writing down all renormalisable (cf. Sec. 2.2.1) terms which transform as singlets under

Field name	Spin	Representation
B_μ	1	$(\mathbf{1}, \mathbf{1}, 0)$
W_μ^A	1	$(\mathbf{1}, \mathbf{3}, 0)$
G_μ^B	1	$(\mathbf{8}, \mathbf{1}, 0)$
$Q_{I,L} = \begin{pmatrix} u_{I,L} \\ d_{I,L} \end{pmatrix}$	$\frac{1}{2}$	$(\mathbf{3}, \mathbf{2}, +\frac{1}{6})$
$u_{I,R}$	$\frac{1}{2}$	$(\mathbf{3}, \mathbf{1}, +\frac{2}{3})$
$d_{I,R}$	$\frac{1}{2}$	$(\mathbf{3}, \mathbf{1}, -\frac{1}{3})$
$L_{I,L} = \begin{pmatrix} \nu_{I,L} \\ e_{I,L} \end{pmatrix}$	$\frac{1}{2}$	$(\mathbf{1}, \mathbf{2}, -\frac{1}{2})$
$e_{I,R}$	$\frac{1}{2}$	$(\mathbf{1}, \mathbf{1}, -1)$
$\phi = \frac{1}{\sqrt{2}} \begin{pmatrix} \phi^+ \\ \phi^0 \end{pmatrix}$	0	$(\mathbf{1}, \mathbf{2}, +\frac{1}{2})$

Table 2.1: Particle content of the Standard Model of Particle Physics. The representation of the gauge group under which a field transforms is specified by its dimension (for $SU(3)_C$ and $SU(2)_L$, first two bold numbers) and its $U(1)_Y$ -hypercharge (third number). For fields which transform as doublets under $SU(2)_L$, we also provide the names of their components. Note that there are eight gauge fields associated with $SU(3)_C$, i.e. $B \in \{1, 2, \dots, 8\}$, three gauge fields associated with $SU(2)_L$, i.e. $A \in \{1, 2, 3\}$, and three families of fermions, i.e. $I \in \{1, 2, 3\}$.

the Lorentz group as well as under the gauge group,¹

$$\mathcal{L}_{\text{SM}} \supset \mathcal{L}_{\text{kin}} + \mathcal{L}_{\text{Yuk}} - \mathcal{V}_{\text{scal}}, \quad (2.1.2)$$

where

$$\begin{aligned} \mathcal{L}_{\text{kin}} = & (\overline{Q}_{I,L})_i (i\not{D}Q_{I,L})_i + \overline{u}_{I,R} (i\not{D}u_{I,R}) + \overline{d}_{I,R} (i\not{D}d_{I,R}) \\ & + (\overline{L}_{I,L})_i (i\not{D}L_{I,L})_i + \overline{e}_{I,R} (i\not{D}e_{I,R}) + (D_\mu \phi^\dagger)_i (D^\mu \phi)_i, \end{aligned} \quad (2.1.3a)$$

$$-\mathcal{L}_{\text{Yuk}} = Y_{u,IJ} \overline{u}_{I,R} (Q_{J,L})_i \phi_j \epsilon_{ij} + Y_{d,IJ} \overline{d}_{I,R} (Q_{J,L})_i \phi_i^\dagger + Y_{e,IJ} \overline{e}_{I,R} (L_{J,L})_i \phi_i^\dagger + \text{h.c.}, \quad (2.1.3b)$$

$$\mathcal{V}_{\text{scal}} = \mu_\phi^2 \phi_i^\dagger \phi_i + \lambda_\phi (\phi_i^\dagger \phi_i)^2. \quad (2.1.3c)$$

Here, we introduced the up- and down-type quark Yukawa matrices Y_u and Y_d , respectively, the leptonic Yukawa matrix Y_e , as well as the Higgs mass parameter μ_ϕ^2 and the Higgs quartic coupling λ_ϕ . We use lower case Latin letters i, j, \dots from the middle of the alphabet to denote $SU(2)_L$ -indices, and upper case Latin letters I, J, \dots from the middle of the alphabet for family indices. Furthermore, we suppress $SU(3)_C$ -indices and use Dirac spinors to describe fermions. We summarise our conventions on notation as well as the symbols that we use in App. A.

The gauge-covariant derivatives of the fields are defined by:

$$D_\mu \equiv \partial_\mu + ig_1 Y B_\mu + ig_2 \frac{\sigma^A}{2} W_\mu^A + ig_3 \frac{\lambda^B}{2} G_\mu^B. \quad (2.1.4)$$

Here, Y denotes the hypercharge of the field on which D_μ acts. Furthermore, σ^A denote the three Pauli matrices and λ^B are the eight Gell-Mann matrices. Note that the terms proportional to g_2 and g_3 have to be omitted for fields which transform as singlets under $SU(2)_L$ or $SU(3)_C$, respectively.

Higgs Mechanism

To prepare the discussion in the following paragraphs, let us first review some important aspects of the Higgs mechanism [22–25]. We can parameterise the Higgs doublet ϕ by writing

$$\phi(x) = P(x) \frac{1}{\sqrt{2}} \begin{pmatrix} 0 \\ v + \phi_H(x) \end{pmatrix}, \quad (2.1.5)$$

where v is a real constant and $\phi_H(x)$ a real-valued field with vanishing vacuum expectation value, which we call the *Higgs field*. Then, ϕ acquires a vacuum expectation value (vev) of the form

$$\langle \phi(x) \rangle = \frac{1}{\sqrt{2}} \begin{pmatrix} 0 \\ v \end{pmatrix}, \quad (2.1.6)$$

¹We suppress the kinetic and Θ -terms of gauge fields as well as peculiarities such as ghost fields because these are not relevant for our purposes.

where v was recently determined experimentally [26]:

$$v = 246 \text{ GeV}. \quad (2.1.7)$$

In what follows, we will call this quantity the *Higgs vev*. $P(x)$ is a special-unitary basis transformation, which produces the most general complex doublet from the doublet with vanishing upper and real-valued lower component. We can eliminate $P(x)$ by an $SU(2)_L$ -gauge transformation, which amounts to a specific choice of basis, making the manifest number of scalar degrees of freedom minimal, namely one. This specific choice of gauge is called *unitarity gauge*:

$$\phi(x) = \frac{1}{\sqrt{2}} \begin{pmatrix} 0 \\ v + \phi_H(x) \end{pmatrix}. \quad (2.1.8)$$

The Higgs vev v is related to the parameters μ_ϕ^2 and λ_ϕ in the scalar potential via

$$v^2 = \frac{-\mu_\phi^2}{\lambda_\phi}, \quad (2.1.9)$$

which arises from minimising the scalar potential in terms of $|\phi| \equiv \left(\phi_i^\dagger \phi_i\right)^{1/2}$.

The specific choice of vacuum given in Eq. (2.1.6) spontaneously breaks the gauge symmetry of the SM in the following way:

$$SU(3)_C \times SU(2)_L \times U(1)_Y \rightarrow SU(3)_C \times U(1)_{\text{em}}. \quad (2.1.10)$$

In particular, one of the four generators of the gauge group factor $SU(2)_L \times U(1)_Y$ remains unbroken. This symmetry breaking pattern yields three massive gauge bosons (the *W-bosons* W_μ^\pm and the *Z-boson*) and one massless gauge boson (the *photon*).

By substituting Eq. (2.1.8) into the kinetic term of the Higgs doublet ϕ , we find the mass of the physical Higgs particle described by ϕ_H :

$$m_H^2 = -2\mu_\phi^2 = 2\lambda_\phi v^2. \quad (2.1.11)$$

Furthermore, by writing the kinetic term of ϕ in terms of the gauge boson mass eigenstates, we find that W_μ^\pm couple to the *charged fermion currents*:

$$J_W^{\mu+} = \frac{1}{\sqrt{2}} (\overline{v}_{I,L} \gamma^\mu e_{I,L} + \overline{u}_{I,L} \gamma^\mu d_{I,L}), \quad J_W^{\mu-} = (J_W^{\mu+})^\dagger. \quad (2.1.12)$$

Note that the charged fermion currents are the only terms in the SM Lagrangian which couple different flavours of fermions. This will be of importance in the context of flavour mixing, which we discuss below.

Fermion Masses and Physical Parameters

Not all parameters in the Lagrangian of the SM are physical. The defining property of an unphysical parameter is that there exist no observable effects that depend on this parameter. In Eqs. (2.1.3) and (2.1.4) we introduced three real gauge couplings g_1 , g_2 , and g_3 , two real scalar parameters, μ_ϕ^2 and λ , as well as 27 complex Yukawa couplings Y_e , Y_u , and Y_d . We now discuss which of those parameters are physical. This will help us later in identifying the physical parameters in the Zee-Babu model. For the numerical calculations in Chap. 4 it is crucial to know which parameters are physical, as we want to deal with a parameter space which is as small as possible in order to reduce the complexity of the calculations.

As already noted, g_1 , g_2 , g_3 , μ_ϕ^2 , and λ_ϕ are real parameters. Otherwise, the Lagrangian would not be Hermitean, thus violating unitarity. Turning to the Yukawa sector, recall that any nonsingular complex matrix A can be diagonalised bi-unitarily, i.e., there exist two unitary matrices U and W such that

$$A = WD_AU^\dagger, \quad (2.1.13)$$

where D_A is diagonal with real and positive elements [27, 28]. Although these diagonal elements are often referred to in the literature as the “eigenvalues” of A , it is worth emphasizing that they are not eigenvalues in the mathematical sense, as Eq. (2.1.13) is no similarity transformation. We now use this result to study how many of the Yukawa couplings are physical. First, consider the Yukawa couplings Y_u and Y_d of the quark sector, which we rewrite as:

$$Y_u = W_u D_u U_u^\dagger, \quad (2.1.14a)$$

$$Y_d = W_d D_d U_d^\dagger. \quad (2.1.14b)$$

Note that the unitary matrices U_u , U_d , W_u , and W_d act on the family space. W_u and W_d are unphysical parameters, as we can make them disappear from the theory entirely by redefining the right-handed quark fields. Indeed, consider the following unitary transformations:

$$u_R \equiv W_u u'_R, \quad (2.1.15a)$$

$$d_R \equiv W_d d'_R. \quad (2.1.15b)$$

They leave the gauge-kinetic terms as given in Eq. (2.1.3a) invariant and eliminate both W_u and W_d from the Yukawa terms in Eq. (2.1.3b). Therefore, W_u and W_d disappear from the theory and are thus unphysical parameters.

The situation is a bit more complicated for the matrices U_u and U_d . When plugging ϕ in unitarity gauge into the Yukawa part of the Lagrangian, we find that in the term proportional to Y_u the upper component of the doublet Q_L survives, while in the term proportional to Y_d , the lower component survives. This allows us to eliminate U_u and U_d

from the Yukawa part of the Lagrangian by rotating the upper and lower components of Q_L individually:

$$u_L \equiv U_u u'_L, \quad (2.1.16a)$$

$$d_L \equiv U_d d'_L. \quad (2.1.16b)$$

The field rotations given by Eqs. (2.1.15) and (2.1.16) define the *mass eigenbasis* of the quark fields, the basis vectors of which we denote by primed fields. As in the case of the right-handed fields, the kinetic terms of the left-handed fields remain diagonal when rotated to the mass eigenbasis. Thus, in the mass eigenbasis, the free-particle Hamiltonian of the quark fields is diagonal, which implies that mass eigenstates do not mix during free propagation. Indeed, in the mass eigenbasis, the Lagrangian contains the flavour-diagonal terms

$$\mathcal{L}_{\text{SM}} \supset \overline{u'_{I,L}} (i\cancel{\partial} u'_{I,L}) + \overline{u'_{I,R}} (i\cancel{\partial} u'_{I,R}) - \frac{v}{\sqrt{2}} (\overline{u'_{I,L}} D_{u,II} u'_{I,R} + \text{h.c.}). \quad (2.1.17)$$

Analogous terms appear for the down-type quarks. From the terms bilinear in the quark fields we can read off the masses of the quarks,

$$m_{u,I} = \frac{v y_{u,I}}{\sqrt{2}}, \quad m_{d,I} = \frac{v y_{d,I}}{\sqrt{2}}, \quad (2.1.18)$$

where we have defined

$$y_{u,I} \equiv D_{u,II}, \quad y_{d,I} \equiv D_{d,II}. \quad (2.1.19)$$

We will discuss fermion mass terms in Sec. 2.1.2 in more detail.

In contrast to the case of the right-handed quark fields, the rotations of the left-handed quark fields do not leave the *full* gauge-kinetic terms invariant. Indeed, rewriting Eq. (2.1.12) in the mass eigenbasis yields the central result

$$J_W^{\mu+} \supset \frac{1}{\sqrt{2}} \overline{u_{I,L}} \gamma^\mu d_{I,L} = \frac{1}{\sqrt{2}} \overline{u'_{I,L}} \gamma^\mu U^{\text{CKM}} d'_{J,L}, \quad (2.1.20)$$

where we have defined the *Cabibbo-Kobayashi-Maskawa* (CKM) mixing matrix U^{CKM} [29–31] via:

$$U^{\text{CKM}} = U_u^\dagger U_d. \quad (2.1.21)$$

Experimentally, one finds that the CKM-matrix is non-diagonal. The important point to understand here is that the presence of the CKM-matrix leads to mixings between different families of quarks, which we call *flavour mixing*. More precisely, there is a mismatch between the mass eigenbasis, in which the free-particle Hamiltonian is diagonal, and the *flavour eigenbasis*, in which the charged quark current is diagonal. We will discuss this in more detail for the lepton sector below.

We learned that not all entries of the matrices U_u and U_d are unphysical, since we cannot eliminate these matrices completely by field redefinitions. Rather, there remain as many physical parameters as we need to parameterise the CKM-matrix. This matrix is

a 3×3 unitary matrix (as it is a product of two unitary matrices), and it can therefore be parameterised by nine real parameters, three of which are angles and six of which are phases. However, not all of these parameters are physical, as we still have the freedom of performing quark field redefinitions which do not change any term in the Lagrangian except the term appearing on the right-hand side of Eq. (2.1.20). Indeed, we can multiply any of the six left-handed quark fields $u'_{I,L}$ and $d'_{I,L}$ by an individual complex phase and thereby eliminate five of the six phases of the CKM-matrix [32]. Since a global phase rotation leaves Eq. (2.1.20) invariant, we can only eliminate one phase less than the number of quark fields we have at our disposal. Furthermore, this also fixes the phases of the right-handed fields u'_R and d'_R , as we have to rotate them accordingly in order to leave the mass terms as given in Eq. (2.1.17) invariant.

We arrive at the final result that only eleven of the 36 real parameters contained in the Yukawa matrices Y_u and Y_d are physical. These are six real and positive diagonal elements $y_{u,I}$ and $y_{d,I}$ (which can be traded for the quark masses), three *CKM mixing angles*, and one *CKM phase*.

Let us investigate the same aspects in the lepton sector. In analogy to the quark sector, we can diagonalise the leptonic Yukawa matrix,

$$Y_e = W_e D_e U_e^\dagger, \quad (2.1.22)$$

and eliminate the rotation matrices W_e and U_e by going to the mass eigenbasis of the leptons using the rotations

$$e_R \equiv W_e e'_R, \quad (2.1.23a)$$

$$e_L \equiv U_e e'_L. \quad (2.1.23b)$$

Note that we did not specify any rotation of the left-handed neutrino fields ν_L . This is not necessary in order to eliminate U_e from the Yukawa terms as there is no analogue to the right-handed quark singlet u_R in the lepton sector: there are no right-handed neutrinos in the SM. Therefore, we have only one leptonic Yukawa term in the SM Lagrangian. When fixing unitarity gauge, the left-handed neutrinos drop out completely from the Yukawa terms and therefore acquire no mass term. Indeed, we only find a mass term for the charged leptons:

$$\mathcal{L}_{\text{SM}} \supset \overline{\nu_{I,L}} (i \not{\partial} \nu_{I,L}) + \overline{e'_{I,L}} (i \not{\partial} e'_{I,L}) + \overline{e'_{I,R}} (i \not{\partial} e'_{I,R}) - \frac{v}{\sqrt{2}} (\overline{e'_{I,L}} D_{e,II} e'_{I,R} + \text{h.c.}). \quad (2.1.24)$$

Thus, neutrinos are exactly massless in the SM,

$$m_I = 0, \quad (2.1.25)$$

where we introduced the notation $m_{1,2,3}$ for neutrino masses, which we will use in this thesis. In contrast, the charged leptons acquire masses,

$$m_{e,I} = \frac{v y_I}{\sqrt{2}}, \quad (2.1.26)$$

where the y_I denote the diagonal entries of D_e :

$$D_e \equiv \text{diag}(y_e, y_\mu, y_\tau). \quad (2.1.27)$$

As there is no preferred mass eigenbasis of the neutrino fields, we are free to rotate them using the same matrix U_e as for the left-handed charged leptons:

$$\nu_L \rightarrow U_e \nu_L. \quad (2.1.28)$$

We have deliberately not introduced a primed neutrino field, as there is no distinguished mass eigenbasis for the neutrinos in the SM. Looking at the term of Eq. (2.1.12) containing the leptons, we find that there appears no analogue to the CKM-matrix:

$$J_W^{\mu+} \supset \frac{1}{\sqrt{2}} \overline{\nu_{I,L}} \gamma^\mu e_{I,L} = \frac{1}{\sqrt{2}} \overline{\nu_{I,L}} \gamma^\mu U_e e'_{I,L} \rightarrow \frac{1}{\sqrt{2}} \overline{\nu_{I,L}} \gamma^\mu e'_{I,L}. \quad (2.1.29)$$

In the first step, we rotated to the mass eigenbasis of the charged leptons, which we compensated by the rotation given in Eq. (2.1.28). We now understand that Eq. (2.1.28) amounts to the *definition* of the flavour eigenbasis in the lepton sector: the electron-neutrino $\nu_{e,L}$ is defined to be the state which couples to the charged lepton mass eigenstate $e'_{e,L}$ via W -exchange, and analogously for the flavours μ and τ . As there is no distinguished mass eigenbasis for the neutrinos, in the lepton sector of the SM there is no mismatch between the mass eigenbasis and the flavour eigenbasis, leading to the absence of flavour mixing. Thus, the only physical parameters in the leptonic Yukawa sector are the three real and positive diagonal elements $y_{e,I}$ (which can be traded for the masses of the charged leptons).

In summary, the SM Lagrangian contains 18 real parameters: $y_{u,I}$, $y_{d,I}$, $y_{e,I}$, g_1 , g_2 , g_3 , μ_ϕ^2 , λ_ϕ , and four CKM parameters. Those parameters are independent “input parameters” in the sense that they cannot be calculated from the SM but have to be supplied by experiments [26].

Accidental Symmetries

The SM possesses a global accidental symmetry,² described by the symmetry group:

$$G_{\text{SM}}^{\text{acc}} = U(1)_B \times U(1)_e \times U(1)_\mu \times U(1)_\tau. \quad (2.1.30)$$

Here, $U(1)_B$ leads to conservation of baryon number (or, equivalently, of quark number), and $U(1)_{e,\mu,\tau}$ describe the conservation of the three lepton family numbers. This symmetry

²The SM is *defined* via the postulate of its gauge group and its particle content: the Lagrangian is the sum of all Lorentz-invariant, gauge-invariant, and renormalisable terms which can be formed out of the particle content. Therefore, the gauge symmetry (as well as the Lorentz symmetry) are fundamental in the sense that they define the model. In contrast, the Lagrangian following from these fundamental symmetries may be invariant under further global symmetries. As those symmetries are not imposed a priori on the model, they appear somehow accidentally and are therefore called *accidental symmetries*. In particular, there is no fundamental principle (such as gauge invariance) which may prevent new physics from breaking these symmetries.

reflects our discussion in the previous section: in the quark sector, only the total number of quarks is a conserved quantity, while we have inter-family mixing due to the presence of the CKM-matrix. In contrast, in the lepton sector, not only the total lepton number,

$$L \equiv L_e + L_\mu + L_\tau, \quad (2.1.31)$$

but moreover the individual lepton family numbers are conserved as there is no inter-family mixing in the SM.

The presence of the conserved quantity L tells us that, in the SM, neutrinos are not only massless at tree level (which we discussed at length above), but also that neutrino masses are not generated by loop effects. Indeed, as we will see below, the only type of mass term, which can be formed using only the SM particle content, is a Majorana mass term. However, such a term would break L . As global symmetries such as L cannot be broken by perturbative effects, Majorana mass terms are protected from being generated at loop order. Thus, neutrinos are massless at all orders of perturbation theory in the SM. Moreover, it turns out that the subgroup $U(1)_{B-L}$ is non-anomalous. As Majorana mass terms break $B - L$, too, neutrino masses may not even be produced by non-perturbative effects [33].

2.1.2 Mixing in the Lepton Sector

We learned in the previous section that, in the SM, neutrinos are massless particles, implying the absence of mixing effects. We now show that experiments contradict this prediction: neutrinos do have masses. To understand the experimental data, we first discuss, which types of mass terms for neutrinos are generally possible and how mixing effects are parameterised in the lepton sector.

Mass Terms for Fermions

There is plenty of experimental evidence that neutrinos are massive particles. However, we will see that the nature of the neutrino mass terms is not yet known. Therefore, from a model-building point of view, we have to take into account various possibilities. We will now investigate, which types of mass terms are possible for fermions in general [34, 35]. In App. B, we summarise the algebraic rules for spinors, which we need in this section.

Mass terms for fermions are terms bilinear in fermion fields. The only non-vanishing Lorentz-invariant possibility is to combine a left-handed field ψ_L with a right-handed field χ_R as follows:

$$- \mathcal{L}_{\text{Mass}} = m (\overline{\psi}_L \chi_R + \overline{\chi}_R \psi_L). \quad (2.1.32)$$

From this observation, two possibilities for fermion mass terms arise. If we use the left- and right-handed components of a single Dirac field $\psi = \psi_L + \psi_R$, we arrive at a *Dirac mass term*:

$$- \mathcal{L}_{\text{Dirac}} = m (\overline{\psi}_L \psi_R + \overline{\psi}_R \psi_L). \quad (2.1.33)$$

Note that, if ψ carries a $U(1)$ -charge, the Dirac mass term conserves this charge. In Sec. 2.1.1 we found that Dirac masses are generated for the quarks and for the charged leptons in the SM.

The second possibility is to start from a single, say, left-handed field ψ_L . As the charge-conjugated field $(\psi_L)^c$ transforms as a right-handed spinor, we can build a mass term using only ψ_L , yielding a so-called *Majorana mass term*:

$$-\mathcal{L}_{\text{Majorana}} = m \left[\overline{(\psi_L)^c} \psi_L + \overline{\psi_L} (\psi_L)^c \right]. \quad (2.1.34)$$

Clearly, the same construction is possible starting from a right-handed field. In contrast to the Dirac mass term, a Majorana mass term does not conserve $U(1)$ -charges. Particularly, a Majorana mass term violates fermion number by two units, leading to “clashing arrows” on fermion lines. We describe in App. C, how Feynman rules can be applied in such a case.

If the fields carry flavour indices, the masses in the above equations get promoted to mass matrices. While in the case of Dirac mass terms, the mass matrix does not have any particular symmetry properties, only the symmetric part of Majorana mass matrices is physical. This follows from Eq. (B.0.9) and we will discuss it in more detail in an analogous case below, cf. footnote 9.

PMNS-matrix

In order to understand the current experimental data on neutrino masses and mixings, let us assume that, due to some (yet unspecified) beyond-SM (BSM) mechanism, neutrino masses are generated. We know from Sec. 2.1.1 that if neutrinos are massive particles, we have inter-family mixing in the lepton sector and vice-versa. Then, as is the case for the quark sector, there is also a mismatch between the primed mass eigenbasis and the unprimed flavour eigenbasis in the lepton sector. Indeed, the rotation as given in Eq. (2.1.28) would in general not diagonalise the free-particle Hamiltonian of massive neutrinos. Rather, we would have to use a matrix $U_\nu \neq U_e$ to transform to the (now well-defined) mass eigenbasis of the neutrinos:

$$\nu_L \equiv U_\nu \nu'_L. \quad (2.1.35)$$

This results, in contrast to Eq. (2.1.29), into the appearance of a CKM-like matrix U^{PMNS} , the so-called *Pontecorvo-Maki-Nakagawa-Sakata* (PMNS) mixing matrix [36, 37], when writing the charged leptonic currents in the mass eigenbasis,

$$J_W^{\mu+} \supset \frac{1}{\sqrt{2}} \overline{\nu_{I,L}} \gamma^\mu e_{I,L} = \frac{1}{\sqrt{2}} \overline{\nu'_{I,L}} \gamma^\mu (U^{\text{PMNS}})^\dagger_{IJ} e'_{I,L}, \quad (2.1.36)$$

where

$$U^{\text{PMNS}} \equiv U_e^\dagger U_\nu. \quad (2.1.37)$$

In the lepton sector, we retain the definition that a neutrino of a given flavour is the state which couples via W -exchange to the corresponding charged lepton mass eigenstate, cf. the

discussion below Eq. (2.1.29). Thus, according to this definition, by rotating the charged leptons e_L to their mass eigenbasis and performing the same rotation on the neutrinos ν_L according to Eq. (2.1.28), we end up in the flavour eigenbasis. Then, the PMNS-matrix coincides with U_ν , and therefore describes the rotation from the mass eigenbasis of the neutrinos to the flavour eigenbasis:

$$\begin{pmatrix} \nu_e \\ \nu_\mu \\ \nu_\tau \end{pmatrix} = U^{\text{PMNS}} \begin{pmatrix} \nu'_1 \\ \nu'_2 \\ \nu'_3 \end{pmatrix}. \quad (2.1.38)$$

Recall that we denote the masses corresponding to the mass eigenstates $\nu'_{1,2,3}$ by $m_{1,2,3}$.

Let us count how many parameters of U^{PMNS} are physical [38, 39]. To this end, we have to distinguish the cases of Dirac and Majorana mass terms for the neutrinos. If neutrinos acquire Dirac mass terms through some BSM mechanism, the situation is analogous to what we had for the CKM-matrix in the quark sector in Sec. 2.1.1. Indeed, for Dirac mass terms, we are free to rephase all six left-handed fields e'_L and ν'_L since this phase shift can be compensated by shifting the corresponding right-handed fields e'_R and ν'_R by the same phase, leaving the mass terms invariant. Therefore, for Dirac mass terms, the PMNS-matrix is parameterised by three *leptonic mixing angles* θ_{12} , θ_{13} , and θ_{23} , as well as by one phase δ , the so-called *Dirac phase*. However, for Majorana mass terms, we cannot freely rephase the neutrino fields ν'_L , as the mass terms are not invariant under a phase shift. Thus, in that case, we end up with two additional phases ϕ_1 and ϕ_2 , the so-called *Majorana phases*.

There are infinitely many ways to parameterise the PMNS-matrix. In this thesis we choose the so-called *standard parameterisation* [28],

$$U^{\text{PMNS}} = \text{diag}(e^{i\delta_e}, e^{i\delta_\mu}, e^{i\delta_\tau}) \cdot V \cdot \text{diag}(e^{-i\phi_1/2}, e^{-i\phi_2/2}, 1), \quad (2.1.39)$$

where

$$V = \begin{pmatrix} c_{12}c_{13} & s_{12}c_{13} & s_{13}e^{-i\delta} \\ -c_{23}s_{12} - s_{23}s_{13}c_{12}e^{i\delta} & c_{23}c_{12} - s_{23}s_{13}s_{12}e^{i\delta} & s_{23}c_{13} \\ s_{23}s_{12} - c_{23}s_{13}c_{12}e^{i\delta} & -s_{23}c_{12} - c_{23}s_{13}s_{12}e^{i\delta} & c_{23}c_{13} \end{pmatrix}. \quad (2.1.40)$$

Here, we have used the abbreviations $c_{ij} \equiv \cos(\theta_{ij})$ and $s_{ij} \equiv \sin(\theta_{ij})$. As described above, if neutrinos have Majorana mass terms, the phases δ_e , δ_μ , δ_τ can be absorbed into the fields. For Dirac mass terms, we can additionally absorb the Majorana phases ϕ_1 and ϕ_2 .

Experimental Data in the Neutrino Sector

We learned that nonzero neutrino masses lead to a mismatch between the flavour and mass eigenbases in the lepton sector. Experimentally, this results in *neutrino oscillations* [38, 40, 41], which means that a neutrino produced with a definite flavour will change its identity when propagating. Regarding the neutrino masses $m_{1,2,3}$, neutrino oscillation experiments are only sensitive to the *mass splittings*:

$$\Delta m_{ij}^2 \equiv m_i^2 - m_j^2. \quad (2.1.41)$$

	Normal ordering		Inverted ordering	
	best fit ($\pm 1\sigma$)	3σ range	best fit ($\pm 1\sigma$)	3σ range
$\theta_{12}/^\circ$	$33.56^{+0.77}_{-0.75}$	$31.38 \rightarrow 35.99$	$33.56^{+0.77}_{-0.75}$	$31.38 \rightarrow 35.99$
$\theta_{23}/^\circ$	$41.6^{+1.5}_{-1.2}$	$38.4 \rightarrow 52.8$	$50.0^{+1.1}_{-1.4}$	$38.8 \rightarrow 53.1$
$\theta_{13}/^\circ$	$8.46^{+0.15}_{-0.15}$	$7.99 \rightarrow 8.90$	$8.49^{+0.15}_{-0.15}$	$8.03 \rightarrow 8.93$
$\delta/^\circ$	261^{+51}_{-59}	$0 \rightarrow 360$	277^{+40}_{-46}	$145 \rightarrow 391$
$\frac{\Delta m_{21}^2}{10^{-5}}/\text{eV}^2$	$7.50^{+0.19}_{-0.17}$	$7.03 \rightarrow 8.09$	$7.50^{+0.19}_{-0.17}$	$7.03 \rightarrow 8.09$
$\frac{\Delta m_{32}^2}{10^{-3}}/\text{eV}^2$	$+2.524^{+0.039}_{-0.040}$	$+2.407 \rightarrow +2.643$	$-2.514^{+0.038}_{-0.041}$	$-2.635 \rightarrow -2.399$

Table 2.2: Neutrino oscillation parameters from a fit to global data as of November 2016 [51, 52].

From measurements with solar [42–45] as well as with reactor neutrinos [46, 47] we know that $\Delta m_{21}^2 > 0$, while the sign of Δm_{32}^2 is not yet known. This leaves open the possibility for two different mass orderings, the so-called *normal ordering*, in which we have $\Delta m_{32}^2 > 0$ and the *inverted ordering* in the opposite case. However, measurements involving atmospheric neutrinos [48] and neutrinos produced in accelerators [49, 50] allow for the determination of $|\Delta m_{31}^2|$. In Tab. 2.2 we summarise the current results of a global fit [51, 52] of neutrino oscillation experiments.

Besides neutrino oscillation experiments, there are projects which use β -decay [53–55] to determine the *absolute scale* of neutrino masses.³ Until now, only an upper bound of about 2 eV could be obtained. Furthermore, experiments looking for neutrinoless double β -decay are trying to answer the question whether neutrinos are Dirac or Majorana particles [56].

Finally, a third method, including observations of the cosmic microwave background, is able to obtain an upper bound on the *sum* of neutrino masses. The most recent upper bound was obtained by combining results from different measurements including the Planck experiment [57]:

$$\sum_{i=1}^3 m_i < 0.23 \text{ eV, at 95\% C.L.} \quad (2.1.42)$$

2.2 Renormalisation and Effective Field Theory

In this thesis, we want to investigate the energy dependence (running) of the neutrino mass matrix in the Zee-Babu model, cf. 2.3.2. This mass matrix is a combination of tree-level model parameters, so we obtain its running from the running of these parameters. We now introduce the basic concepts we will need to compute this running, namely the renormalisation group (RG) evolution of model parameters and effective field theory (EFT). The profound conceptual ideas behind these concepts are discussed in all elementary textbooks

³To be precise, the corresponding observable is the so-called *effective electron neutrino mass* m_β , defined by $m_\beta^2 \equiv m_1^2 c_{12}^2 c_{13}^2 + m_2^2 s_{12}^2 c_{13}^2 + m_3^2 s_{13}^2$ [38].

on QFT [20, 25, 58] and in much more detail in Refs. [21, 59]. We will not review these here in detail, and focus on the calculational techniques [60].

2.2.1 Renormalisation Group Evolution of Model Parameters

We start with discussing how we can relate parameters in the Lagrangian to experimentally measurable values, and how we can set up the theory a priori in terms of measurable parameters. Afterwards, we introduce the calculational tools we will use throughout this thesis, and finally show how to use them to compute the running of model parameters.

Bare and Renormalised Parameters, Renormalisability

We already discussed in detail the Lagrangian of the SM and identified, which parameters are physical in the sense that they can be determined experimentally. Now, we have a look at how these physical parameters relate to the measured values.

Loosely speaking, what experimentalists measure as a particle's mass or as couplings between particles, is described perturbatively as the sum of *infinitely many* Feynman diagrams. These describe all possible *quantum corrections*, which correspond to *loop diagrams*, while the lowest order terms are the *tree-level* propagators and vertices. These tree-level diagrams correspond directly to the so-called *bare* fields, masses, and couplings, appearing in the Lagrangian. Adding the loop corrections, yields – after the process of *renormalisation* – the corresponding *dressed* or *renormalised* quantities, which are accessible through experiment.

Generically, the loop corrections one has to compute when renormalising a quantity turn out to be infinite due to the arbitrarily high momenta, which are allowed to circulate in the loops, and which have to be summed up in loop integrals. Naturally, at first sight, this is a conceptually problematic observation. However, there exist numerous *regularisation techniques*, which enable us to deal with these infinities. All those techniques have in common that one first introduces some kind of *regulator*, for example a simple momentum cutoff, which renders the loop integrals finite at the cost of now having a regulator-dependent theory. Such a regulator has no physical meaning in this context. Indeed, when renormalising the regulated theory, i.e., when fixing the computed quantities to equal⁴ measured values, the regulator drops out at the end of the calculation, given that the theory is physically sensible. Such theories are called *renormalisable theories*.

Renormalisation yields *finite* renormalised parameters, which are directly related to measurable quantities. On the contrary, the bare parameters are formally infinite and unphysical, i.e., they are not accessible by experiment.

⁴Strictly speaking, renormalised quantities are only *equal* to the measured ones in *physical* renormalisation schemes, cf. below.

Renormalised Perturbation Theory

We get more insight by introducing the concept of *counterterms* yielding so-called *renormalised perturbation theory*. The basic idea is to rewrite the Lagrangian (which is written in terms of bare parameters) in terms of renormalised parameters, thus incorporating renormalisation already at the level of the Lagrangian.⁵ To illustrate this procedure, let us consider φ^4 -theory as a toy example:

$$\mathcal{L}_\varphi = (\partial_\mu \varphi_B)^\dagger (\partial^\mu \varphi_B) - m_B^2 \varphi_B^\dagger \varphi_B - \lambda_B (\varphi_B^\dagger \varphi_B)^2. \quad (2.2.1)$$

By adding the subscript B to the field φ , the mass parameter m , and the quartic scalar coupling λ , we indicate that the Lagrangian is written in terms of bare quantities. Note that we omitted these subscripts in Sec. 2.1. We now introduce the renormalised field, which we denote simply by φ , via the relation

$$\varphi_B \equiv Z_\varphi^{\frac{1}{2}} \varphi. \quad (2.2.2)$$

We call the quantity Z_φ the *wavefunction renormalisation constant*. Furthermore, we introduce the abbreviation

$$\delta Z_\varphi \equiv Z_\varphi - 1. \quad (2.2.3)$$

By plugging this into the Lagrangian and using the definitions⁶

$$m_B^2 \equiv Z_\varphi^{-1} (m^2 + \delta m^2) \quad \text{and} \quad (2.2.4a)$$

$$\lambda_B \equiv Z_\varphi^{-2} (\lambda + \delta \lambda), \quad (2.2.4b)$$

with δm^2 and $\delta \lambda$ being the renormalisation constants corresponding to the mass parameter and the quartic scalar coupling, we arrive at

$$\mathcal{L}_\varphi = \mathcal{L}_{\varphi,\text{ren}} + \mathcal{L}_{\varphi,\text{ct}}, \quad (2.2.5)$$

with the *renormalised Lagrangian*

$$\mathcal{L}_{\varphi,\text{ren}} = (\partial_\mu \varphi)^\dagger (\partial^\mu \varphi) - m^2 \varphi^\dagger \varphi - \lambda (\varphi^\dagger \varphi)^2, \quad (2.2.6)$$

and the *counterterm Lagrangian*

$$\mathcal{L}_{\varphi,\text{ct}} = \delta Z_\varphi (\partial_\mu \varphi)^\dagger (\partial^\mu \varphi) - \delta m^2 \varphi^\dagger \varphi - \delta \lambda (\varphi^\dagger \varphi)^2. \quad (2.2.7)$$

⁵Note that this is not the only way of renormalising a theory. One may also use the bare Lagrangian to compute measurable quantities (up to a given order in perturbation theory), and pin them down to experimental data *afterwards*. This is called *bare perturbation theory*.

⁶We want to prepare for more general cases and thus renormalise λ additively here. Note that multiplicative renormalisation is a special case thereof, but not always applicable, for example when couplings carry additional indices with particular symmetry properties.

The terms making up the counterterm Lagrangian are called the counterterms. In slight abuse of terminology, we will often call the parameters δZ_φ , δm^2 , and $\delta\lambda$ themselves counterterms.

We choose δZ_φ , δm^2 , and $\delta\lambda$ real here in order to preserve unitarity. However, in more general cases, renormalisation constants of couplings do not necessarily have to be real. Examples we will meet in this thesis are renormalisation constants of Yukawa and of effective couplings. Furthermore, if fields carry family indices, the renormalised fields in general are superpositions of the fields of different families, leading to wavefunction renormalisation constants carrying family indices.

The usage of counterterms is as follows. First, we determine the renormalisation constants. To this end, we treat the counterterms as independent fundamental terms in the Lagrangian, yielding new vertices with Feynman rules following from $\mathcal{L}_{\varphi,\text{ct}}$ as usual. This allows us to determine the counterterms order by order in perturbation theory by applying so-called *renormalisation conditions* (defining the *renormalisation scheme*). All renormalisation schemes have in common that the infinite, i.e. regulator-dependent parts, of the bare quantities are absorbed into the counterterms. This is the way how regulators vanish from the theory in renormalised perturbation theory.

However, the renormalisation schemes differ in the way how one defines the finite parts of the counterterms. In the *physical renormalisation scheme*, one fixes the finite parts by the condition that the remaining renormalised quantities coincide with the corresponding measured values. This may be the most intuitive way of carrying out renormalisation, but the calculations often turn out to be quite cumbersome in practice. In the following section, we introduce a more convenient renormalisation scheme, the so-called *minimal subtraction* (MS) *scheme*, which we will use throughout this thesis. In other renormalisation schemes than the physical one, the renormalised quantities are not equal to the measured values. Thus, one says that renormalised quantities are *scheme-dependent*. However, renormalised quantities can be calculated from measured values, which makes them measurable in this sense, too.

The question of whether a theory is renormalisable or not can now be rephrased in the counterterm language: is it always possible to absorb all infinities into counterterms? This is clearly not the case if our theory has the property that diagrams with some arbitrarily high, but fixed, number of external legs are divergent at some sufficiently high loop order. In this case, one would be forced to add an arbitrarily high number of counterterms to the Lagrangian in order to render all Green's functions finite. Thereby, an infinite number of parameters would enter the theory, each of which would have to be matched to experiment (by applying some renormalisation scheme). Thus, the theory would lose all predictive power and we call it a *non-renormalisable* theory. In the opposite case, where a finite number of counterterms is enough to render all Green's functions finite, the theory is renormalisable. Although hard to prove in full generality, there is a surprisingly simple way for deciding whether a theory is renormalisable or not: if all couplings of the theory have mass dimension greater or equal to zero, the theory is renormalisable [61–66].

Dimensional Regularisation and the MS Renormalisation Scheme

We now introduce the MS renormalisation scheme which, together with the so-called *dimensional regularisation* (dimreg) technique, provides a powerful method of performing renormalisation [67].

In dimreg, we write the loop integrals in d instead of four spacetime dimensions and parameterise d by a regularisation parameter, which we denote by ε :

$$d \equiv 4 - \varepsilon. \quad (2.2.8)$$

Thus, for $\varepsilon = 0$ we have $d = 4$. The results of loop integrals now depend on d and we can expand them in a Laurent series in ε . Then, the divergencies in four spacetime dimensions appear as terms proportional to inverse powers of ε . For practical calculations, we refer the reader to the excellent appendix of Ref. [25], in which the results of many loop integrals as well as other important relations in d dimensions are tabulated. Furthermore, the usage of *Passarino-Veltman functions* greatly simplifies many computations in dimreg, as their divergent terms are tabulated in the literature [68, 69].

When writing the Lagrangian in d spacetime dimensions, the mass dimensions of scalar, spinor, and vector fields φ , ψ , and A , respectively, can be read off from their kinetic terms by requiring the Lagrangian to have mass dimension d (since the action is dimensionless):

$$[\varphi] = \frac{d-2}{2}, \quad (2.2.9a)$$

$$[\psi] = \frac{d-1}{2}, \quad (2.2.9b)$$

$$[A] = \frac{d-2}{2}. \quad (2.2.9c)$$

We use this to rescale the couplings by powers of the *renormalisation scale* μ in such a way that their mass dimension remains the same as in four spacetime dimensions:

$$Q \rightarrow \mu^{D_Q \varepsilon} Q. \quad (2.2.10)$$

For example, for quartic scalar couplings λ we have $D_\lambda = 1$, for gauge couplings g one finds $D_g = 1/2$, and for Yukawa couplings Y we also obtain $D_Y = 1/2$.

Renormalisation is particularly simple using the minimal subtraction (MS) scheme, in which – as its name suggests – the counterterms are defined by the prescription that they cancel *only* the divergences. Thus, in dimreg, the renormalisation constants δZ_ϕ and δQ , respectively, have the simple form:

$$\delta Z_\phi = \sum_{k=1}^{\infty} \delta Z_{\phi,k} \frac{1}{\varepsilon^k}, \quad \delta Q = \sum_{k=1}^{\infty} \delta Q_k \frac{1}{\varepsilon^k}. \quad (2.2.11)$$

Here and in the following sections, we use the notation ϕ to denote any field without specifying whether it is of scalar, spinor or vector type. There should be no confusion with

the SM Higgs doublet, which we also denoted by the letter ϕ in Sec. 2.1.1. Analogously, Q denotes any coupling of the theory and can be of scalar, vectorial, or a more general tensorial nature. Note that in MS, the renormalisation constants do *not* contain any UV-finite terms, i.e., no terms finite in the limit $\varepsilon \rightarrow 0$. Indeed, all finite terms belong to the renormalised quantities.

Calculating β -functions

The renormalisation scale μ , which appeared above for dimensional reasons, is to be identified with the energy scale of the processes under consideration [59]. The fact that the bare Lagrangian is independent of μ has the profound implication that physical, i.e. renormalised, quantities in turn *do* depend on μ : they *run* with the energy scale at which they are measured [70–73]. We call this phenomenon the *renormalisation group (RG) evolution* of model parameters.

We now present a general equation which allows us to compute the energy dependence, i.e., the *running* of some model parameter Q . Recall that we do not specify whether Q is of scalar, vectorial or some more general tensorial nature, making our result applicable for all types of couplings we will encounter in Chap. 3. The derivation is quite lengthy and does not give much insight into the physics involved, which is why we do not repeat it here in detail. We refer the reader to Refs. [35, 60], which we follow closely.

Extending our introductory example of φ^4 -theory to a case where multiple fields ϕ_i are involved, Eq. (2.2.4) reads for a general coupling Q :

$$Q_B = \left(\prod_{i \in S_L} Z_{\phi_i}^{n_i} \right) [Q + \delta Q] \mu^{D_Q \varepsilon} \left(\prod_{j \in S_R} Z_{\phi_j}^{n_j} \right). \quad (2.2.12)$$

Note that due to their tensorial nature we have to distinguish between renormalisation constants which multiply $Q + \delta Q$ from the left and from the right as indicated by the index sets S_L and S_R .

We want to compute the so-called β -function of Q , defined by:

$$\beta_Q \equiv \mu \frac{dQ}{d\mu}. \quad (2.2.13)$$

To this end, we employ the aforementioned condition that bare quantities do not depend on the renormalisation scale, i.e.:

$$\frac{dQ_B}{d\mu} = 0. \quad (2.2.14)$$

By setting the total derivative of the right-hand side of Eq. (2.2.12) to zero, one finds after

some algebra the central equation:

$$\begin{aligned}
\beta_Q &= D_Q \left\langle \frac{d\delta Q_1}{dQ} \middle| Q \right\rangle + \sum_k D_{P_k} \left\langle \frac{d\delta Q_1}{dP_k} \middle| P_k \right\rangle - D_Q \delta Q_1 \\
&+ \sum_{i \in S_L} n_i \left[D_Q \left\langle \frac{d\delta Z_{\phi_i,1}}{dQ} \middle| Q \right\rangle + \sum_k D_{P_k} \left\langle \frac{d\delta Z_{\phi_i,1}}{dP_k} \middle| P_k \right\rangle \right] Q \\
&+ Q \sum_{j \in S_R} n_j \left[D_Q \left\langle \frac{d\delta Z_{\phi_j,1}}{dQ} \middle| Q \right\rangle + \sum_k D_{P_k} \left\langle \frac{d\delta Z_{\phi_j,1}}{dP_k} \middle| P_k \right\rangle \right].
\end{aligned} \tag{2.2.15}$$

Here, we denoted all running parameters, on which δQ and δZ_{ϕ_i} depend (in addition to Q itself), by P_k :

$$\delta Q = \delta Q [Q(\mu), \{P_k(\mu)\}], \tag{2.2.16a}$$

$$\delta Z_{\phi_i} = \delta Z_{\phi_i} [Q(\mu), \{P_k(\mu)\}]. \tag{2.2.16b}$$

If Q or P_k are complex quantities, we have to treat their complex conjugates Q^* and P_k^* as additional independent variables. Furthermore, we introduced the notation

$$\left\langle \frac{dF}{dx} \middle| y \right\rangle \equiv \begin{cases} \frac{dF}{dx} y, & \text{for scalars } x, y, \\ \frac{dF}{dx_n} y_n, & \text{for vectors } x_n, y_n, \\ \frac{dF}{dx_{mn}} y_{mn}, & \text{for matrices } x_{mn}, y_{mn}, \end{cases} \tag{2.2.17}$$

where repeated indices are implicitly summed. This is easily adapted to the case when x and y are higher-rank tensors. Note that Eq. (2.2.15) only depends on the $1/\varepsilon$ -coefficients of the counterterms, cf. (2.2.11). This property will simplify our calculations in Chap. 3.

2.2.2 Effective Field Theory

Imposing renormalisability greatly reduces the number of allowed terms in a Lagrangian. Indeed, as discussed above, in four spacetime dimensions the Lagrangian is of mass dimension four. Then, the condition that all couplings have non-negative mass dimension is equivalent to the condition that no operator appearing in the Lagrangian has mass dimension greater than four.

Despite its name, a non-renormalisable theory can be useful as a low-energy approximation of some more fundamental theory, which we call the *full theory* or the *UV-completion* in this context. The low-energy theory is then called an *effective field theory* (EFT). In such cases, there exists a natural cutoff energy, above which the EFT becomes invalid and where one has to use the full theory instead. In contrast to the unphysical cutoff we discussed above in the context of regularisation, the cutoff in EFTs is a concrete physical quantity.

We can use the EFT viewpoint in two complementary ways, known as the *bottom-up approach* and the *top-down approach*. Both rely on allowing non-renormalisable terms in the Lagrangian, which we write collectively as:

$$\mathcal{L}_{\text{eff}} = \sum_{n \geq 5} \frac{C_n}{\Lambda^{n-4}} \mathcal{O}^{(n)}. \quad (2.2.18)$$

Here, Λ is some high energy scale, C_n are dimensionless couplings and $\mathcal{O}^{(n)}$ denotes an *effective operator* of mass dimension n . Thus, effective operators of higher mass dimension are suppressed by higher powers of the high scale Λ . By grouping all calculations in inverse orders of Λ , and discarding all contributions higher than a fixed order (which determines the accuracy of the results), finitely many counterterms are sufficient, and we can treat the effective theory like a renormalisable one [59, 74, 75].

The two approaches are different in the aspects of where the high scale Λ comes from and which symmetries and particle content one uses to construct the effective operators. In the bottom-up approach, we use the particle content and symmetries of a given theory and treat it as a low-energy approximation to some unknown UV-completion. Λ then represents the scale above which new physics is expected to become relevant. Using this approach, one can make, for instance, general and model-independent statements about extensions of the SM by neutrino masses, cf. Sec. 2.3.1.

On the contrary, in the top-down approach we consider a given and renormalisable theory which we assume to be a valid description of Nature. In this thesis, we use the Zee-Babu model as an example of such a theory, cf. Sec. 2.3.2. At low energies, heavy particles *decouple* from the theory [76]. at tree level, this is obvious: a heavy particle cannot be produced as an external state for energies below its mass m , and its propagator in loops can be expanded as

$$\frac{1}{p^2 + m^2} = \frac{1}{m^2} \left(1 - \frac{p^2}{m^2} + \frac{p^4}{m^4} - \dots \right), \quad (2.2.19)$$

showing that for $p^2 \ll m^2$ there is no propagation of the particle. The *Appelquist-Carazzone decoupling theorem* [77] states that this decoupling also takes place *after* renormalisation, i.e., when taking into account quantum corrections to the propagator. However, the decoupling is *not* manifest in the MS-scheme we are using, leading to *large logarithms* in the IR-limit. Thus, perturbation theory cannot be trusted for energies way below the particle's mass, and we obtain meaningless results if we do not take care of the decoupling by hand. We do this by *integrating out* the particle at its *mass threshold*, i.e., at the energy which equals the particle's mass. This means to take the particle out of the theory and capture its residual effects by effective operators [78, 79].⁷ We say that the effective operators get *switched on* at the mass threshold. The resulting EFT has to be *matched* to the full theory by employing *matching conditions*, stating that both the full theory and the EFT yield the same predictions at the threshold energy.

⁷The parlance “integrate out” particles, stemming from the path integral formulation, is misleading in this context.

2.3 Neutrino Mass Models

We now look at some approaches of extending the SM by neutrino masses. This leads us to the Zee-Babu model, which we will study in this thesis, focusing on the running of neutrino masses and mixing angles. To prepare this, we explain at the end of this section in detail the top-down approach, which we will use to investigate this running.

2.3.1 Extending the Standard Model by Neutrino Masses

In this section, we discuss shortly how the SM may be extended in order to incorporate neutrino masses, leading us to *beyond-SM* (BSM) *physics*. A generic approach to extending the SM by neutrino masses is to think of it as an effective low energy theory [33]. This means that we retain the SM gauge group as well as its particle content, but allow also non-renormalisable terms. We already discussed this bottom-up approach in Sec. 2.2.2.

Allowing terms up to mass-dimension $\mathcal{D} = 5$, we obtain a single effective operator, the so-called *Weinberg operator* given by [80, 81]:

$$\mathcal{L}_{\mathcal{D}=5} = -\kappa_{W,IJ} \overline{(L_{I,L})^c}_i (L_{J,L})_j \phi_k \phi_l \epsilon_{ik} \epsilon_{jl} + \text{h.c.} \quad (2.3.1)$$

We can make the scale Λ_{NP} of new physics explicit by introducing the dimensionless couplings $C_{W,IJ}$ via:

$$\kappa_{W,IJ} \equiv \frac{C_{W,IJ}}{\Lambda_{\text{NP}}}. \quad (2.3.2)$$

Upon electroweak symmetry breaking, this operator leads to a Majorana mass term for the neutrinos:

$$\mathcal{L}_{\mathcal{D}=5} \supset -\frac{v^2}{\Lambda_{\text{NP}}} \frac{C_{W,IJ}}{2} \overline{(\nu_{I,L})^c} \nu_{J,L} + \text{h.c.} \quad (2.3.3)$$

Note that this term breaks lepton number by two units, and does also not conserve the individual lepton family numbers, cf. Sec. 2.1.1.

Seesaw Mechanism

A popular approach for generating a term of the form Eq. (2.3.1) is by introducing a set of right-handed *sterile neutrinos*⁸:

$$\nu_{I,R} \sim (\mathbf{1}, \mathbf{1}, 0). \quad (2.3.4)$$

Then, by gauge symmetry, there is a new Yukawa term allowed in addition to the SM:

$$-\mathcal{L}_{\text{Yuk},\nu} = Y_{\nu,IJ} \overline{\nu_{I,R}} (L_{J,L})_i \phi_j \epsilon_{ij} + \text{h.c.} \rightarrow M_{D,IJ} \overline{\nu_{I,R}} \nu_{J,L} + \text{h.c.} \quad (2.3.5)$$

⁸Although there is no physical reason to do so at this point, let us assume that we have *three* sterile neutrinos for simplicity.

On the right-hand side of this equation, we already wrote down the Dirac mass term for the neutrinos appearing upon EWSB. The Dirac mass matrix is given by:

$$M_{D,IJ} = \frac{Y_{\nu,IJ}v}{\sqrt{2}}. \quad (2.3.6)$$

If this new Yukawa term was the only term we added to the SM Lagrangian, we would *impose* lepton number symmetry, thus not treating the SM as a low-energy effective theory (as in the SM, lepton number is only an accidental symmetry). Indeed, gauge symmetry allows a Majorana mass term for the sterile neutrinos:

$$-\mathcal{L}_{\text{Maj},\nu} = \frac{1}{2}M_{R,IJ}\overline{(\nu_{I,R})^c}\nu_{J,R} + \text{h.c.} \quad (2.3.7)$$

Before studying the implications of this term, let us assume that for some reason we have $M_R = 0$. Then, neutrinos would be Dirac particles, as their masses arised solely from the Dirac term. The only way of explaining their smallness would be through exceedingly small Yukawa couplings Y_ν (compared to the SM Yukawa couplings), as the Higgs-vev v is fixed by experiment. This represents a fine-tuned and thus quite unsatisfactory scenario from a theoretical point of view.

In the general case $M_R \neq 0$ we can rewrite the neutrino mass terms in the form

$$-\mathcal{L}_{M,\nu} = \frac{1}{2} \begin{pmatrix} \overline{(\nu_L)^c} & \overline{\nu_R} \end{pmatrix} \begin{pmatrix} 0 & M_D^T \\ M_D & M_R \end{pmatrix} \begin{pmatrix} \nu_L \\ (\nu_R)^c \end{pmatrix}, \quad (2.3.8)$$

where we used Eq. (B.0.9) to rewrite the Dirac term. The eigenstates we obtain by diagonalising this mass matrix contain both left- and right-handed neutrino species, forming six Majorana particles. However, if the eigenvalues of M_R are much greater than those of M_D , i.e., if $M_R \gg M_D$, we can approximately block-diagonalise the mass matrix and obtain a mass matrix of the form:

$$M_\nu = -M_D^T M_R^{-1} M_D. \quad (2.3.9)$$

for three Majorana neutrino eigenstates which coincide with ν_L (in this approximation). By making M_R large enough, we can explain the tinyness of the neutrino masses M_ν . Note that the mass matrix M_R has no connection to the electroweak scale, making it *not* unnatural to assume M_R being very large. This is the famous *seesaw type I mechanism*. There exist various modifications of this idea, leading to further seesaw-type scenarios [38].

Radiative Models

Another popular approach for generating Majorana neutrino masses are so-called *radiative models*. In these models, one also introduces additional heavy particles in such a way that in contrast to the seesaw-mechanism no mass term for the neutrinos is generated at tree level. Rather, neutrino masses appear as effective terms due to diagrams in which the additional particles circulate in loops, i.e., neutrino masses are generated by loop-effects. Thus, the neutrino mass matrix in such models generically is a product of many (small)

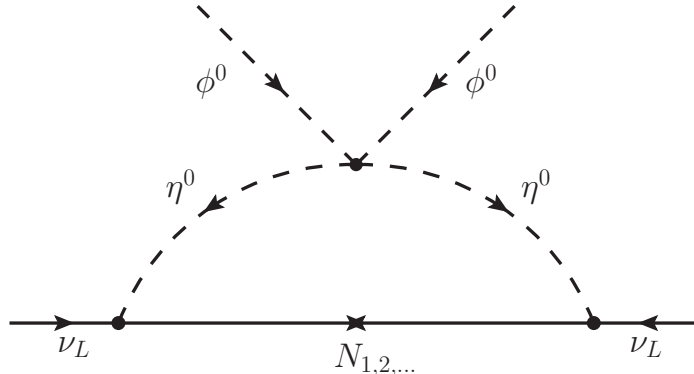


Figure 2.1: The one-loop diagram responsible for neutrino mass generation in the Scotogenic model.

tree-level couplings and loop factors of $1/16\pi^2$, leading to a strong suppression. Therefore, such models have the advantage over seesaw-type models that the additional particles do not have to be exceedingly heavy for explaining tiny neutrino masses, and thus may be found in near-future experiments.

One famous example of radiative models is the *Scotogenic model*, which is an extension of the SM by right-handed sterile neutrinos $N_{1,2,\dots}$, a second $SU(2)_L$ -doublet $\eta \equiv (\eta^+, \eta^0)$, and a discrete \mathbb{Z}_2 -symmetry, under which all SM particles are even and all new particles are odd [12]. This symmetry forbids a mass term for the SM neutrinos at tree level. The lowest-order contribution is through the diagram depicted in Fig. 2.1, leading to radiative neutrino masses at one-loop level. An interesting property of the Scotogenic model is that the corrections of the tree-level parameters add up in the product forming the neutrino mass matrix, leading to strong running of neutrino masses and leptonic mixing angles. It was shown in Refs. [13,14] that this running can explain the deviation of measured neutrino data from theoretical predictions at very high energy scales. This motivates to investigate the running in other radiative models, too.

In this thesis, we study the running in the Zee-Babu model. This is another radiative model, in which neutrino masses are two-loop effects. We will introduce this model in the following section.

2.3.2 The Zee-Babu Model

In this section we introduce the Zee-Babu model, which we will study in great detail in this thesis. First, we present the Lagrangian of the model and discuss related topics such as symmetry breaking and physical parameters. Afterwards, we show that in the Zee-Babu model lepton number is violated, which allows Majorana neutrino masses to be generated at two-loop order.

Lagrangian

The Zee-Babu model [15] is an economical extension of the SM by only two scalar particles h^+ and k^{++} , both of which transform as singlets under the $SU(2)_L$ and $SU(3)_C$ gauge groups and have hypercharges +1 and +2, respectively:

$$h^+ \sim (\mathbf{1}, \mathbf{1}, +1), \quad (2.3.10a)$$

$$k^{++} \sim (\mathbf{1}, \mathbf{1}, +2). \quad (2.3.10b)$$

Writing down all possible renormalisable and gauge-invariant terms following from this particle content, we arrive at the Lagrangian density

$$\mathcal{L}_{\text{ZB}} \supset \mathcal{L}_{\text{kin}} + \mathcal{L}_{\text{Yuk}} - \mathcal{V}_{\text{scal}}. \quad (2.3.11)$$

Here, \mathcal{L}_{kin} , \mathcal{L}_{Yuk} , and $\mathcal{V}_{\text{scal}}$ denote the gauge-kinetic, Yukawa, and scalar potential terms, respectively:

$$\begin{aligned} \mathcal{L}_{\text{kin}} = & (\overline{Q_{I,L}})_i (i\not{D}Q_{I,L})_i + \overline{u_{I,R}} (i\not{D}u_{I,R}) + \overline{d_{I,R}} (i\not{D}d_{I,R}) \\ & + (\overline{L_{I,L}})_i (i\not{D}L_{I,L})_i + \overline{e_{I,R}} (i\not{D}e_{I,R}) + (D_\mu \phi^\dagger)_i (D^\mu \phi)_i \\ & + (D_\mu h^-) (D^\mu h^+) + (D_\mu k^{--}) (D^\mu k^{++}), \end{aligned} \quad (2.3.12a)$$

$$\begin{aligned} -\mathcal{L}_{\text{Yuk}} = & Y_{e,IJ} \overline{e_{I,R}} (L_{J,L})_i \phi_i^\dagger + Y_{u,IJ} \overline{u_{I,R}} (Q_{J,L})_i \phi_j \epsilon_{ij} + Y_{d,IJ} \overline{d_{I,R}} (Q_{J,L})_i \phi_i^\dagger \\ & + f_{IJ} (\overline{L_{I,L}})_i^c (L_{J,L})_j \epsilon_{ij} h^+ + g_{IJ} (\overline{e_{I,R}})_i^c e_{J,R} k^{++} + \text{h.c.}, \end{aligned} \quad (2.3.12b)$$

$$\begin{aligned} \mathcal{V}_{\text{scal}} = & \mu_\phi^2 \phi_i^\dagger \phi_i + \mu_h^2 h^+ h^- + \mu_k^2 k^{++} k^{--} + \lambda_\phi (\phi_i^\dagger \phi_i)^2 + \lambda_h (h^+ h^-)^2 \\ & + \lambda_k (k^{++} k^{--})^2 + \lambda_{\phi h} (\phi_i^\dagger \phi_i) (h^+ h^-) + \lambda_{\phi k} (\phi_i^\dagger \phi_i) (k^{++} k^{--}) \\ & + \lambda_{hk} (h^+ h^-) (k^{++} k^{--}) + \mu_{hk} (h^+ h^+ k^{--} + h^- h^- k^{++}). \end{aligned} \quad (2.3.12c)$$

Comparing this Lagrangian to the SM Lagrangian, Eq. (2.1.3), we find two new Yukawa matrices f and g as well as new scalar mass parameters μ_h^2 , μ_k^2 , and new quartic scalar couplings λ_h , λ_k , $\lambda_{\phi h}$, $\lambda_{\phi k}$, and λ_{hk} . Most notably, there also appears a trilinear scalar coupling μ_{hk} , which is of importance in the context of neutrino masses.

Let us discuss which parameters of the model are physical, cf. Sec. 2.1.1. We follow [17] and work in a basis where the charged lepton Yukawa matrix Y_e is diagonal with real and positive elements as given in Eq. (2.1.27). In addition, we define the Yukawa matrix f to be antisymmetric and the Yukawa matrix g to be symmetric.⁹ Furthermore, we shift

⁹We do not necessarily have to impose those symmetry properties on f and g , but it is convenient to do so as for f only the antisymmetric part and for g only the symmetric part is physical. This can be seen as follows. First, consider the Yukawa term involving k^{++} . Suppose we started with the term $\tilde{g}_{IJ} T_{IJ} k^{++}$, where we defined $T_{IJ} \equiv (\overline{e_{I,R}})_i^c e_{J,R}$ and suppressed the Hermitean conjugate term. Assume that we do not impose any symmetry properties on $\tilde{g}_{IJ} = \tilde{g}_{IJ}^s + \tilde{g}_{IJ}^a$, which we split into its symmetric and antisymmetric parts. Using Eq. (B.0.9), we find that T is symmetric $T_{IJ} = T_{JI}$. Therefore, in the sum over I, J only the symmetric part \tilde{g}_{IJ}^s survives, $\tilde{g}_{IJ} T_{IJ} = \tilde{g}_{IJ}^s T_{IJ}$, and hence the antisymmetric part turns out to be physically irrelevant. This is the reason why we can define the Yukawa matrix to be symmetric from the beginning: $g_{IJ} \equiv \tilde{g}_{IJ}^s$. Following the same arguments and taking into account the presence of the antisymmetric symbol ϵ , we find that only the antisymmetric part of the Yukawa matrix f_{IJ} is physical.

the phases of the fermion fields in order to remove three phases from the elements of g . Analogously, by shifting phases of the charged scalars, we remove one phase from f and set μ_{hk} real and positive. This choice turns out to be compatible with the standard parameterisation of the PMNS-matrix as given in Eq. (2.1.40) [82]. In total, in the lepton and scalar sectors, we have 22 moduli (3 from Y_e , 6 from g , 3 from f and 10 from the parameters in the scalar potential), as well as 5 phases (3 from g and 2 from f). We will discuss in Sec. 4.2.2, how these physical parameters are related to the parameters of the PMNS-matrix.

Upon EWSB, the physical scalar particles ϕ_H , h^+ and k^{++} acquire masses given by:

$$m_H^2 = -2\mu_\phi^2 = 2\lambda_\phi v^2, \quad (2.3.13a)$$

$$m_h^2 = \mu_h^2 + \frac{1}{2}\lambda_{\phi h}v^2, \quad (2.3.13b)$$

$$m_k^2 = \mu_k^2 + \frac{1}{2}\lambda_{\phi k}v^2. \quad (2.3.13c)$$

Note that we assume $m_h^2, m_k^2 \gg m_H^2$, as otherwise the charged particles h^+ and k^{++} should already have been seen in experiments, cf. Sec. 2.3.3. However, interestingly, the current bounds on the scalar masses m_h and m_k are accessible to the second run of the LHC [17].

Neutrino Masses

The central property of the Zee-Babu model is that a Majorana mass term of the form

$$\mathcal{L}_{M_\nu} = -\frac{1}{2}M_{\nu,IJ}\overline{\nu_{I,L}}(\nu_{J,L})^c + \text{h.c.} \quad (2.3.14)$$

for the neutrinos is generated at two-loop order. Indeed, the Yukawa terms proportional to f and g together with the trilinear term proportional to μ_{hk} in the scalar potential violate lepton number by two units. Using these couplings, we can build the two-loop diagram shown in Fig. 2.2, which is the lowest-order contribution to neutrino masses in the Zee-Babu model. We will compute the mass matrix M_ν in Sec. 3.2.

There exist several references [15, 16], which investigate, whether the Zee-Babu model is consistent with neutrino data. Refs. [17, 83] take into account most recent data from neutrino experiments, to constrain the free parameters of the model. The authors conclude that this data is not enough to rule the model out. Therefore, the Zee-Babu model still is a popular candidate neutrino mass model.

2.3.3 The Top-Down Approach of RG Evolution

We discussed in the previous section that the Zee-Babu model is a viable candidate neutrino mass model, since its predictions are consistent with current experiments. In this thesis, we will analyse the RG evolution of the parameters in this model. In Ref. [17], the running in the Zee-Babu model was already studied in the context of the stability of the Higgs potential. In this thesis, we will go one step further and take into account the full RG

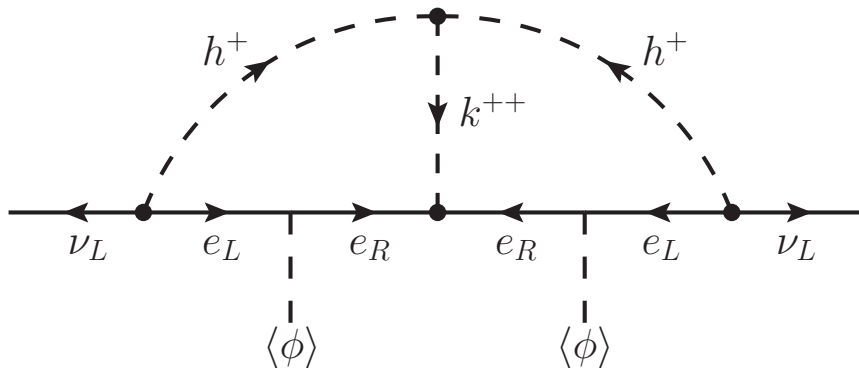


Figure 2.2: The two-loop diagram responsible for neutrino mass generation in the Zee-Babu model.

evolution of all model parameters. This allows us to investigate the running of neutrino masses and leptonic mixing angles.

Top-Down Approach

We will investigate the running in a top-down approach, cf. Sec. 2.2.2. This means that we start with some parameter configuration at a high input energy scale, which we choose to be the scale of *grand unification* $\mu_{\text{GUT}} \approx 10^{16}$ GeV.¹⁰ We will often simply call this scale the *high scale*. This approach is interesting, as there exist several theoretically well-motivated leptonic mixing patterns, for example from GUTs, at the high scale. One example is the *bimaximal mixing pattern*, in which $\theta_{13} = 0^\circ$ and $\theta_{12} = \theta_{23} = 45^\circ$ [84]. The mixing pattern measured at much lower energies deviates considerably from this prediction, cf. Sec. 2.1.2, which makes it interesting to study, whether the running can explain this discrepancy. In this thesis, we will impose a bimaximal mixing pattern at μ_{GUT} and run the parameters down to the *electroweak scale* $\mu_{\text{EW}} \approx 100$ GeV (the *low scale*), where we check whether the predicted neutrino observables are consistent with experimental data.

Neutrino experiments take place at energies even lower than μ_{EW} . For example, solar neutrinos have energies in the range 1-10 MeV, while both atmospheric neutrinos and neutrinos produced in accelerators are in the GeV range. In the context of neutrino masses, the paramount reason for studying the running is not to connect the outcomes of measurements taken at different energies, as their current uncertainties are much higher than the running. Indeed, at μ_{EW} the BSM particles are necessarily integrated out, a setting in which we know that neutrino parameters show barely any running [14, 85]. This makes it consistent to compare neutrino parameters at the common scale μ_{EW} with experimental results.

Considering the Zee-Babu model, we will show in Sec. 4 that a given mixing pattern does

¹⁰*Grand unified theories* predict the unification of the gauge couplings at this scale. However, in the Zee-Babu model such a unification does not take place. Thus, in our setting, the GUT-scale is an arbitrary but motivated choice for a high input scale.

not fix all model parameters. Rather, we have a large space of parameter configurations, all of which produce, say, the bimaximal mixing pattern. Therefore, we have much freedom in initialising the RGEs at μ_{GUT} . In order to find out whether the Zee-Babu model is a physically sensible theory, we will scan this space for configurations which make the model parameters run into the measured values at the low scale. Furthermore, the parameters have to stay confined to physically meaningful bounds on the way down from the high to the low scale. If one does not find such an initial parameter configuration, we can either rule out the model completely, or gain information about possible modifications of the model. To come to a conclusive answer, one would have to perform a scan of the whole free parameter space. Clearly, this is beyond the scope of this thesis, but our results presented in Chap. 4 provide a useful starting point for a more thorough investigation.

One could ask the question why we would choose a top-down approach in the first place. Indeed, we saw in Sec. 2.1.2 that, at the low scale, experiments constrain the parameter configuration quite tightly. In contrast, we have not much more to say about parameter configurations at the high scale than which ones might be theoretically more appealing than others. So, why don't we just fix the measured parameter configuration at the low scale and run it up using the RGEs of the Zee-Babu model to higher energies in order to study whether the parameters run out of physically meaningful regions? This approach is taken for example in Ref. [17], in the context of vacuum stability. However, we do not choose it for our extended analysis, since it is, strictly speaking, *not* correct. Indeed, we saw in Sec. 2.2.2 that if we inspect the running at energy scales below a particle's mass threshold, it has to be integrated out of the theory. Thus, at these energies, we have to use the RGEs of the corresponding EFT. In the Zee-Babu model, the masses of the charged scalars h^+ and k^{++} are assumed to be substantially larger than μ_{EW} , as they have not yet been seen in experiments. Therefore, it is not correct to use the RGEs of the full Zee-Babu model at energies near μ_{EW} , as here h^+ and k^{++} cannot be treated as propagating degrees of freedom.

EFT-Structure of the Zee-Babu Model

Let us briefly discuss in more detail the structure of the EFTs derived from the Zee-Babu model. In a top-down approach, we start with specific initial values of the masses m_h and m_k of h^+ and k^{++} at μ_{GUT} , and calculate the running of those masses (together with the other model parameters) using the RGEs of the full theory. This yields the solutions $m_h = m_h(\mu)$ and $m_k = m_k(\mu)$. From these solutions, we can determine the mass thresholds μ_h^* and μ_k^* of h^+ and k^{++} .

For example, μ_k^* is given by the point at which $m_k(\mu)$ intersects the angle bisector, i.e., at the solution of the implicit equation:

$$\mu_k^* = m_k(\mu_k^*). \quad (2.3.15)$$

At this energy, we say that k^{++} hits its mass threshold. Below μ_k^* , we have to use the EFT, which results from integrating out k^{++} , and we have to match this EFT to the

higher-energy theory at μ_k^* . Clearly, the same considerations apply when h^+ hits its mass threshold μ_h^* given by:

$$\mu_h^* = m_k(\mu_h^*). \quad (2.3.16)$$

Which of the particles hits its mass threshold first will depend on the parameter configuration at μ_{GUT} .

If we integrate out k^{++} first, we call the resulting theory EFT- h (as h^+ remains). In the opposite case, we use the name EFT- k . Going further down to lower energies after the first particle was integrated out, the remaining particle will eventually also hit its mass threshold and be integrated out, too. We will call the theory which results after we have integrated out both h^+ and k^{++} , i.e., which only contains SM particles, EFT-0.

Thus, there are two different routes for getting from the full high-energy theory to EFT-0. The matching equations which determine the initial values in EFT-0 will therefore differ depending on which route follows from the initial parameter configuration at μ_{GUT} . Therefore, although those theories do formally have the same Lagrangian, we will distinguish between an EFT-0 h and an EFT-0 k in the context of the matching. Here, EFT-0 h means that we are in EFT-0 and took the route

$$\text{full theory} \rightarrow \text{EFT-}h \rightarrow \text{EFT-0},$$

while EFT-0 k refers to the route

$$\text{full theory} \rightarrow \text{EFT-}k \rightarrow \text{EFT-0}.$$

We illustrate this graphically in Fig. 2.3.

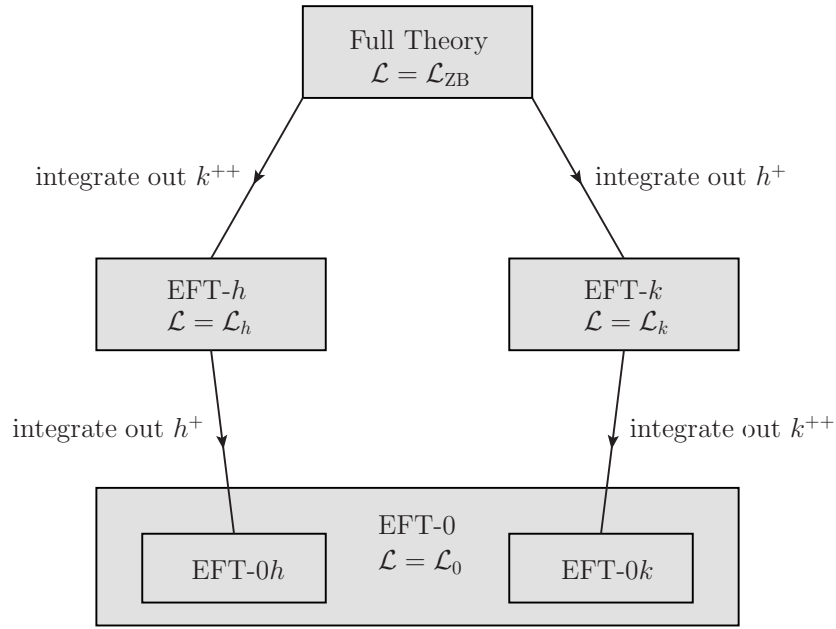


Figure 2.3: Matching structure of the EFTs derived from the Zee-Babu model. Which route is taken on the way from the full theory down to EFT-0 depends on the initial parameter configuration at the high energy scale μ_{GUT} . The comparison of the resulting neutrino parameters with experimental data takes place at the low energy scale μ_{EW} , at which both h^+ and k^{++} are already integrated out (EFT-0).

Running of the Neutrino Mass Matrix in the Zee-Babu Model

This chapter makes up the main part of this thesis: the computation of the running of neutrino masses and leptonic mixing parameters in the Zee-Babu model. In Sec. 2.1.2, we learned that these are encoded in the neutrino mass matrix M_ν . Thus, one central task of this chapter is the computation of M_ν , which is no tree-level parameter in radiative models. Rather, M_ν is an effective quantity given by a product of tree-level parameters. Thus, the computation of the running of M_ν amounts to calculating the running of these parameters, i.e. the derivation of their RGEs. Eventually, we will end up with a large system of coupled RGEs, which cannot be solved analytically in full generality. We therefore have to resort to numerical methods, which we will present in Chap. 4.

In Sec. 2.3.3, we discussed that we have to integrate out the scalars h^+ and k^{++} at their respective mass thresholds in order to decouple them properly from the theory. Therefore, we have to consider the RGEs not only in the full Zee-Babu model, but also in the effective theories EFT- h , EFT- k , and EFT-0. Furthermore, we have to find the matching equations, which we will employ in order to compute the initial values of the running parameters in the EFTs from the parameters in the respective higher-energy theories. The derivation of these matching equations is another central task of this chapter.

We do not have to compute all RGEs by hand, as there exists a computer program named SARAH, which is able to derive RGEs, given a Lagrangian [86, 87]. Unfortunately, SARAH cannot compute RGEs of effective couplings, which we therefore have to derive by hand. Nevertheless, SARAH saves us much work: first of all, it gives us the RGEs of the full theory. In addition, these results are helpful in the EFTs, too, as we can easily deduce the RGEs of those full-theory couplings, which are still present in the EFTs, from the corresponding RGEs in the full theory. Indeed, we will find that in these RGEs do not appear any new terms compared to the full theory. Thus, we obtain these RGEs by just setting the full-theory couplings, which are not present in the EFTs anymore, to zero.

In summary, we only have to calculate the RGEs of the effective couplings in the EFTs by hand. As we learned in Sec. 2.2.1, computing the RGE of some coupling using

Eq. (2.2.15) basically amounts to calculating its counterterm and the wavefunction renormalisation constants appearing in the expression connecting the bare and renormalised versions of this coupling, cf. Eq. (2.2.12). Thus, we have to calculate the counterterms of all relevant effective couplings as well as the respective wavefunction renormalisation constants. Although we will not need them there, we do some preparatory work and calculate the wavefunction renormalisation constants already in the full theory. This turns out to be only slightly more effortful than doing the calculations in the EFTs directly, and the full-theory results may be useful for future reference. In the EFTs, we then only have to compute the counterterms of the effective couplings from scratch.

Finally note that, in a top-down approach one not only has to care about whether some high-energy parameter configuration can reproduce the measured neutrino parameters at the low scale. In addition, one also has to check whether model parameters leave physically sensible regions on the way from the high scale down to the low scale. Therefore, we will derive the RGEs of *all* model parameters, regardless of whether we eventually need them to compute the mass matrix or not.

3.1 Systematics of the Calculations

In this section, we prepare the subsequent calculations by introducing our approach of organising them in loop orders. This allows us to decide, which diagrams we have to compute and which we can safely neglect in order to arrive at a given accuracy of the running of the neutrino mass matrix. Note that, in principle, we do nothing more special than renormalising a Lagrangian. However, as the mass matrix in radiative models is a composite quantity containing various tree-level parameters, it is intricate to keep track of the relative importance of the running effects. Thus, it will prove useful to systematise the calculations.

We introduce our technique in general, without sticking to a specific radiative neutrino mass model, in order to make it applicable for a wide range of models. Afterwards, we investigate the Zee-Babu model in particular, using this very technique. It will give us important information about the structure of the running in the EFTs, even before carrying out the computations in detail.

3.1.1 Expansion in Loop Orders

As is very common in QFT, the calculations presented in this chapter are of a perturbative nature. This means that the running of neutrino parameters is mathematically expressed as a superposition of infinitely many quantum effects. Therefore, we need a means of estimating the relative importance of these effects. Only then we can decide which effects we have to include in our calculations and which we can safely neglect in order to arrive at a specific accuracy. In this thesis, we chose to structure our calculations by expanding

all quantities in *loop orders*, i.e., in a series in so-called *loop factors* [88],

$$\alpha \equiv \frac{1}{16\pi^2} \ll 1, \quad (3.1.1)$$

and by cutting this expansion at a specific loop order. This may at first seem to be a very crude measure of the relative importance of the effects involved. Indeed, one should in principle expand all effects in a series in coupling constants and use this as the measure. Unfortunately, this approach is not of much use here for several reasons. First, there are many different coupling constants involved which would lead to multiple nested expansions, making the calculations cumbersome. Even worse, the relative strengths of the coupling constants of BSM physics are not known a priori. Therefore, we have no means of deciding which effects we have to consider before we actually did the calculations and evaluated the results for a specific parameter configuration. This would make our work unbearably complicated, as we would have to compute much more diagrams than are actually necessary. In contrast, the expansion in loop orders turns out to be a very convenient way to structure the calculations, since we always know beforehand how many loop factors are associated with a specific effect. Therefore, this approach is very suitable for a first study of radiative neutrino mass models. The results give important insight into the structure of a model, and may subsequently be refined easily by taking into account information about the relative strength of the coupling constants.

Using the loop order expansion, we will find that there are two important aspects where things are conceptually different in a full theory, i.e., a theory which only contains renormalisable couplings, compared to an EFT. First, in a full theory, n -loop contributions to the mass matrix come exclusively from n -loop diagrams. In contrast, in an EFT, n -loop contributions to the mass matrix may also come from m -loop diagrams with $m < n$. Such diagrams then contain effective couplings which are switched on beyond tree-level. This is a quite trivial observation, since clearly the “missing loops” are implicitly included in the effective operators. More importantly, in full theories, the loop expansion of the β -function β_λ of a running coupling λ always starts at a loop order N_λ^β beyond tree-level, i.e. $N_\lambda^\beta > 0$. In EFTs however, the loop expansion of the β -function of an effective coupling κ may start at the same order N_κ^β as the order N_κ at which the coupling itself is switched on. This means that we can have $N_\kappa^\beta = N_\kappa$.¹ The presence of an effective coupling with this property in an EFT leads to the effect that the running of the mass matrix in this EFT is stronger (in terms of loop orders) than in the full theory.

Let us now express this mathematically. We start with the full theory. In general, the neutrino mass matrix M_ν of a model featuring the radiative generation of neutrino masses at N -th loop order is of the form

$$M_\nu = \sum_{n=N}^{\infty} M_\nu^{(n)} = \sum_{n=N}^{\infty} \alpha^n \widetilde{M}_\nu^{(n)}, \quad (3.1.2)$$

¹If we use the same language in full theories, we would say that any full theory coupling λ is “switched on” at tree level, i.e. $N_\lambda = 0$, and we always have $N_\lambda^\beta > N_\lambda$. The same is true for effective couplings which are switched on an tree-level.

where a term $M_\nu^{(n)}$ is defined to denote the sum of all n -loop contributions to the neutrino mass matrix. This means that $M_\nu^{(n)}$ comes intrinsically with a loop factor α^n of order n , which we made explicit on the right-hand side of the above equation. Assume now that there are several different contributions to the mass matrix at n -loop order which we denote by $M_{\nu,k}^{(n)}$:

$$M_\nu^{(n)} = \sum_k M_{\nu,k}^{(n)}. \quad (3.1.3)$$

In a full theory, every term $M_{\nu,k}^{(n)}$ simply denotes an n -loop diagram $\mathcal{M}_{\nu,k}^{(n)}$,

$$M_{\nu,k}^{(n)} = \mathcal{M}_{\nu,k}^{(n)}, \quad (3.1.4)$$

each of which evaluates to some combination of the running model parameters (which we denote collectively by λ_i here) and in particular comes with a factor of α^n (as it contains n loops):

$$\mathcal{M}_{\nu,k}^{(n)} = \alpha^n \prod_i \lambda_i. \quad (3.1.5)$$

Clearly, this equation may contain some further constants which are not energy-dependent or more complex combinations of the λ_i such as loop integrals, but this is not important for the general point we want to make here since it does not bring any further factors of α into play. Therefore, we ignore such complications and assume each term to be a simple product of the λ_i . Then, in order to connect the running of M_ν with the running of the λ_i , we calculate the derivative of M_ν with respect to the energy parameter μ . Following Eqs. (3.1.2)–(3.1.5), this will be a sum of terms of the form:

$$\frac{dM_{\nu,k}^{(n)}}{d\mu} = \alpha^n \sum_j \prod_{i \neq j} \lambda_i \beta_{\lambda_j}. \quad (3.1.6)$$

Here,

$$\beta_{\lambda_j} \equiv \frac{d\lambda_j}{d\mu} \quad (3.1.7)$$

is the β -function of the parameter λ_j , cf. Sec. 2.2.1. Just as we did for the mass matrix, those β -functions can be organised in loop orders,

$$\beta_{\lambda_j} = \sum_{n=N_{\lambda_j}^\beta}^{\infty} \beta_{\lambda_j}^{(n)} = \sum_{n=N_{\lambda_j}^\beta}^{\infty} \alpha^n \tilde{\beta}_{\lambda_j}^{(n)}, \quad (3.1.8)$$

where again $\beta_{\lambda_j}^{(n)}$ denotes all n -loop contributions to β_{λ_j} and therefore contains a loop factor α^n . As we will discuss below, for full theory couplings there is no zeroth order term here: $N_{\lambda_j}^\beta > 0$. Combining Eqs. (3.1.6) and (3.1.8), we arrive at the result that the leading order effect of the running of the neutrino mass matrix is (at least) of loop order $N + 1$.

This result seems rather trivial and the derivation may therefore appear to be overly complicated. Nevertheless, this rigorous counting of loop orders pays off when it comes to the EFTs, as here we additionally have to take into account that *effective operators may be switched on at loop orders beyond tree-level*. Indeed, it is convenient to structure the matching (cf. Sec. 2.2.2) of effective couplings to higher-energy theories also by an expansion of the effective couplings in loop orders. Given an effective coupling κ , we write

$$\kappa = \sum_{n=N_\kappa}^{\infty} \kappa^{(n)} = \sum_{n=N_\kappa}^{\infty} \alpha^n \tilde{\kappa}^{(n)}, \quad (3.1.9)$$

where $N_\kappa \in \{0, 1, 2, \dots\}$ is the loop order at which κ is switched on. In analogy to the case of the neutrino mass matrix and the β -functions, we use $\kappa^{(n)}$ to denote all contributions to the effective coupling coming from n -th loop order effects in the higher-energy theory. Therefore, as indicated in the above equation, $\kappa^{(n)}$ contains a factor of α^n . Note that it is useful in this context to think of full theory couplings λ_i as being “switched on” at tree level: $N_{\lambda_i} = 0$.

In an EFT there will be diagrams, which contain effective couplings, contributing to the neutrino mass matrix. Considering the analogue of Eq. (3.1.4) in an EFT, it is not true anymore that each contribution to the mass matrix at n -th loop order is just an n -loop diagram. Rather, we have

$$M_{\nu,k}^{(n)} = \mathcal{M}_{\nu,k}^{(m)}, \quad (3.1.10)$$

with $m \leq n$. If $m = n$, $\mathcal{M}_{\nu,k}^{(m)}$ is an n -loop diagram and can therefore only contain couplings which are present at tree level, i.e., either full-theory couplings which have been already present in the higher-energy theory, or the tree-level terms $\kappa^{(0)}$ of effective couplings κ with $N_\kappa = 0$. Otherwise, the diagram would describe an effect of an order higher than n . On the other hand, for $m < n$, we have to have effective couplings in the diagram which come with so many factors of α that the diagram effectively describes a process of loop order n . Therefore, we can write:

$$\mathcal{M}_{\nu,k}^{(m)} = \alpha^m \left(\prod_i \lambda_i \right) \left(\prod_j \kappa_j^{(n_j)} \right). \quad (3.1.11)$$

Recall that we denote the full-theory couplings by λ_i . Furthermore, we use an index j to enumerate the effective couplings. Then, in Eq. (3.1.10) the loop orders only match if we have:

$$m + \sum_j n_j = n. \quad (3.1.12)$$

We now again compute the derivative of the neutrino mass matrix M_ν with respect to μ in order to connect the running of M_ν with the running of the model parameters:

$$\frac{dM_{\nu,k}^{(n)}}{d\mu} = \alpha^m \left(\sum_{j'} \prod_{i \neq j'} \lambda_i \beta_{\lambda_{j'}} \right) \left(\prod_j \kappa_j^{(n_j)} \right) + \alpha^m \left(\prod_i \lambda_i \right) \left(\sum_{j'} \prod_{j \neq j'} \kappa_j^{(n_j)} \beta_{\kappa_{j'}}^{(n_{j'})} \right). \quad (3.1.13)$$

The first term on the right-hand side of this equation is the analogue of Eq. (3.1.6), as it contains the β -functions β_{λ_i} of the full-theory couplings λ_i . As explained above, their loop expansions start beyond tree-level, i.e. $N_{\lambda_i}^\beta > 0$. Therefore, the first term on the right-hand side is (at least) of loop order $n + 1$. In the EFT, however, there appears a second term on the right-hand side. It contains the β -functions $\beta_{\kappa_j^{(n_j)}}$ of the effective couplings $\kappa_j^{(n_j)}$. As we have already anticipated, it can happen that the loop expansion of the β -function of some effective coupling κ starts at the same order N_κ at which κ is switched on, i.e., we can have:

$$N_\kappa = N_\kappa^\beta. \quad (3.1.14)$$

If an effective coupling with this property is present in an EFT, the second term on the right-hand side of Eq. (3.1.13) contains terms which are of order n . Thus, in this case, the running effects are of *the same* loop order as the corresponding term of the neutrino mass matrix itself.

Let us now discuss in more detail how we can have $N_\kappa^\beta = N_\kappa$ in an EFT, in contrast to $N_\lambda^\beta > N_\lambda$ in the full theory. More precisely, we now show that $N_Q^\beta > N_Q$ if $N_Q = 0$, while $N_Q^\beta = N_Q$ may be the case if $N_Q > 0$. Using the notation of Sec. 2.2.1, we denote by Q any coupling of a theory. In particular, we do not specify whether it is a full-theory coupling or an effective coupling. We learned that the β -function β_Q of Q is calculated from the $1/\varepsilon$ -coefficients δQ_1 and $\delta Z_{\phi_i,1}$ of its counterterm and of the wavefunction renormalisation constants, respectively. These appear in Eq. (2.2.12), which connects the bare coupling Q_B with its renormalised counterpart Q . Both δQ_1 and $\delta Z_{\phi_i,1}$ are calculated as a series in loop orders:

$$\delta X_1 = \sum_{n=N_X^\delta}^{\infty} \delta X_1^{(n)}. \quad (3.1.15)$$

Here, X stands either for Q or for some Z_{ϕ_i} and, as above, $\delta X_1^{(n)}$ denotes the sum of all n -loop contributions to δX_1 .

The expansions of $\delta Z_{\phi_i,1}$ start beyond tree-level. The same is true for the counterterm δQ_1 of any coupling with $N_Q = 0$, i.e., for full-theory couplings and for effective couplings which get switched on at tree level. These statements are trivial, since at tree level there cannot occur any infinities which would have to be absorbed by counterterms. We therefore have:

$$N_{\phi_i}^\delta > 0, \quad N_Q^\delta > 0 \quad \text{if} \quad N_Q = 0. \quad (3.1.16)$$

In particular, this means:

$$N_Q^\delta > N_Q \quad \text{if} \quad N_Q = 0. \quad (3.1.17)$$

Using Eq. (3.1.16) in Eq. (2.2.15), we find that each summand contains a quantity of loop order greater than zero. We therefore have:

$$N_Q^\beta > N_Q \quad \text{if} \quad N_Q = 0, \quad (3.1.18)$$

which is what we proposed above.

The difference in the case of the counterterm $\delta\kappa$ of some effective coupling κ with $N_\kappa > 0$ is that we may instead have:

$$N_\kappa^\delta = N_\kappa, \quad (3.1.19)$$

in contrast to Eq. (3.1.16). Such a situation will typically occur if we have an EFT with *two or more* different effective couplings which get switched on at *different* loop orders. A nice example for this situation is the EFT- h derived from the Zee-Babu model, where we have (among others) an effective coupling κ_{21} with $N_{\kappa_{21}} = 0$ and another effective coupling κ_{11} with $N_{\kappa_{11}} = 1$. From κ_{21} we can build a one-loop 1PI diagram which is of loop order one and has the same external states as those which κ_{11} connects. The divergence which comes from this loop diagram therefore has to be cured by the counterterm $\delta\kappa_{11}^{(1)}$, so that we have $\delta\kappa_{11}^{(1)} \neq 0$, i.e. $N_{\kappa_{11}}^\delta = N_{\kappa_{11}}$. This is depicted in the following equation:

$$\begin{aligned} & \text{1PI diagram} = \text{one-loop diagram} + \text{counterterm diagram} \\ & \stackrel{!}{=} \text{UV-finite.} \end{aligned} \quad (3.1.20)$$

Upon substituting Eq. (3.1.19) into Eq. (2.2.15) with $Q = \kappa$, we can see that the second and third line of this equation again lead to terms of loop order greater than N_κ , but this does not have to be the case anymore for the first line. Indeed, the third term in the first line will always be of *the same* order as $\delta\kappa$.² Therefore, if we have an effective operator obeying Eq. (3.1.19), we find:

$$N_\kappa^\beta = N_\kappa. \quad (3.1.21)$$

If κ gives a contribution to the neutrino mass matrix at leading order, the running effects of the mass matrix will thus be of this very order, too.

Finally, we would like to point out that such a situation does not occur in the Scotogenic model [14], for example, as there all effective couplings relevant for neutrino masses in the EFTs are switched on at the same loop order. Thus, we cannot have situations as in Eq. (3.1.20).

3.1.2 Application to the Zee-Babu Model

We now apply the results of the previous section to the case of the Zee-Babu model in order to find out which diagrams we have to calculate.

²This is also the case for the first term if κ is of zeroth order and for the second term if some P_k is of zeroth order.

We learned in Sec. 2.3.2 that, in the Zee-Babu model, a Majorana mass term for the neutrinos of the form

$$\mathcal{L}_{M_\nu} = -\frac{1}{2}M_{\nu,IJ}\overline{\nu_{I,L}}(\nu_{J,L})^c + \text{h.c.} \quad (2.3.14)$$

is generated. We define the Majorana mass matrix $M_{\nu,IJ}$ to be symmetric, in order to drop any unphysical parameters from the very beginning, cf. Sec. 2.1.2. We know that the leading order contribution to neutrino masses comes from a two-loop diagram, i.e., we have $N = 2$. In this thesis, we will consider only these leading order effects, i.e., we are going to sum up all diagrams contributing to the mass matrix at second loop order. This yields, according to Eq. (2.3.14):

$$i\mathcal{M}_{\nu,IJ}^{(2)} \equiv \begin{array}{c} \leftarrow \nu_{I,L} \quad \text{2-loop} \quad \nu_{J,L} \rightarrow \end{array} = -2 \cdot \frac{1}{2}iM_{\nu,IJ}P_R = -iM_{\nu,IJ}P_R. \quad (3.1.22)$$

One of our tasks in this chapter is to find concrete expressions for $M_{\nu,IJ}^{(2)}$ in the full theory, as well as in the EFTs derived from it. As we do not want to clutter up the notation, we are going to consistently drop the superscript “(2)” in what follows.

Now let us consider the running of the neutrino mass matrix. As we have $N = 2$, in the full theory, the running of the mass matrix starts *beyond* two-loop order. As it turns out, running effects in the full theory start at third order. Therefore, as we particularly want to investigate the leading order effects of the running in the full theory, we have to consistently take into account all third order effects in the full theory as well as in the EFTs.

In the EFTs, we decided to consider effective operators up to mass dimension $\mathcal{D} = 5$. In Tab. 3.1 we list the subset of those effective couplings which turn out to be relevant for the generation of neutrino masses in the EFTs of the Zee-Babu model together with the loop orders at which they get switched on and the loop orders of the leading term of their respective β -functions. From this table, we can read off that the running in EFT- k and in EFT-0 will start at third loop order, just as it does in the full theory. Indeed, there is only one effective coupling, namely κ_W , present in those EFTs and we have already discussed above that in this case the running necessarily starts beyond the order at which this coupling is switched on.

In contrast, in EFT- h , we will find that there are two effective couplings, namely κ_{11} and κ_W , the β -functions of which receive contributions at the same loop order as at which they are switched on. Indeed, we used the calculation of the counterterm of κ_{11} already as an example for such a situation in Eq. (3.1.20). This leads to running effects already at two-loop order in EFT- h , i.e., at the same loop order at which the neutrino masses itself are generated.

As already noted above, in order to be consistent, we have to consider the running up to *the same* order in the full theory and in all EFTs. In particular, it would be inconsistent to only consider the leading order effects of the running, i.e., to go up to third order in the full theory, EFT- k and EFT-0, but only up to second order in EFT- h . Therefore, as we

κ	EFT-h		EFT-k		EFT-0	
	N_κ	N_κ^β	N_κ	N_κ^β	N_κ	N_κ^β
κ_{21}	0	1	not present		not present	
κ_{11}	1	1	not present		not present	
κ_W	2	2	2	3	2	3

Table 3.1: Effective couplings relevant for the running of the neutrino mass matrix in the Zee-Babu model and the EFTs derived from it. We only consider effective operators of mass dimension $\mathcal{D} = 5$. In EFT- h , three effective couplings, namely κ_{21} , κ_{11} , and κ_W , are relevant for the running, while in EFT- k and EFT-0, κ_W is the only effective coupling we have to consider. Therefore, in EFT- k and EFT-0 we necessarily have $N_{\kappa_W} > N_{\kappa_W}^\beta$. In contrast, in EFT- h the possibility of $N_\kappa = N_\kappa^\beta$ exists due to the presence of multiple different effective couplings being switched on at different orders. As it turns out, EFT- h is indeed an example for such a constellation: we find $N_{\kappa_{11}} = N_{\kappa_{11}}^\beta$, as well as $N_{\kappa_W} = N_{\kappa_W}^\beta$.

decided to take into account all running effects up to third order (otherwise there would be no running at all in the full theory, in EFT- k , and in EFT-0), we are forced to go up to third order, in EFT- h , too.

Thus, as can be seen from Eq. (3.1.13), in EFT- h we have to calculate the β -functions of all tree-level couplings (i.e. of all the λ_i and of κ_{21}) up to first order and the β -functions of κ_{11} and κ_W up to second order. The latter turned out to be computationally unbearable within the scope of this work due to the large number of two-loop Feynman diagrams, which would have to be evaluated in order to calculate counterterms of κ_{11} and κ_W at second order. Nevertheless, we show in Chap. 4 that we obtain meaningful results even without computing these two-loop diagrams.

3.2 Full Theory

We start with the calculations in the full theory. First, we evaluate the two-loop mass matrix diagram. This diagram is finite, which was to be expected, given that there is no counterterm left which could cure an infinity. Afterwards, we present the RGEs calculated by SARAH. Finally, we compute the wavefunction renormalisation constants, which we will need in the EFTs for the calculation of the counterterms of the effective couplings.

3.2.1 Mass Matrix

We have already presented the two-loop diagram which generates neutrino masses in the Zee-Babu model in Sec. 2.3.2. This diagram represents the only contribution to the neutrino mass matrix at two-loop order. Now, we are going to evaluate this diagram, which will result in the expression M_ν^{ZB} for the mass matrix in the full theory.

For the two-loop diagram in the Zee-Babu model we find:

$$\begin{aligned}
i\mathcal{M}_{\nu,IJ}^{\text{ZB}} &\equiv \\
&= \int \frac{d^4q}{(2\pi)^4} \frac{d^4q'}{(2\pi)^4} \left[+2if_{IK}^\dagger P_R \right] \frac{i(-\not{q} + m_{e,K})}{q^2 - m_{e,K}^2} \left[-2ig_{KM} P_R \right] \frac{i(-\not{q}' + m_{e,M})}{q'^2 - m_{e,M}^2} \\
&\quad \cdot \left[-2if_{MJ}^\dagger P_R \right] \left[-2i\mu_{hk} \right] \frac{i}{q^2 - m_h^2} \frac{i}{q'^2 - m_h^2} \frac{i}{(q - q')^2 - m_k^2} \\
&= -8i\alpha^2 v^2 \mu_{hk} f_{IK}^\dagger y_K g_{KM} \mathcal{I}_{1,KM} y_M f_{MJ}^\dagger P_R.
\end{aligned} \tag{3.2.1}$$

Here, we directly worked in $d = 4$ dimensions, since the diagram is finite, and we also set the external momenta to zero as we are only interested in the mass shift induced by this self-energy diagram. Furthermore, we defined the two-loop integral

$$\begin{aligned}
&\alpha^2 \mathcal{I}_{1,KM} (m_h^2, m_k^2, m_{e,K}^2, m_{e,M}^2) \\
&\equiv \int \frac{d^4q}{(2\pi)^4} \int \frac{d^4q'}{(2\pi)^4} \frac{1}{[q^2 - m_{e,K}^2] [q'^2 - m_{e,M}^2] [q^2 - m_h^2] [q'^2 - m_h^2] [(q - q')^2 - m_k^2]},
\end{aligned} \tag{3.2.2}$$

which is symmetric in the flavour indices K and M . Now we plug this result into Eq. (3.1.22) and arrive at the induced Majorana mass matrix in the Zee-Babu theory:

$$\boxed{M_{\nu,IJ}^{\text{ZB}} = 8\alpha^2 v^2 \mu_{hk} f_{IK}^\dagger y_K g_{KM} \mathcal{I}_{1,KM} y_M f_{MJ}^\dagger} \tag{3.2.3}$$

Note that M_{ν}^{ZB} is symmetric in its flavour indices, which directly follows from the symmetry properties of f , g , and \mathcal{I}_1 .

One important property of the neutrino mass matrix in the Zee-Babu model is that one of the neutrinos is *exactly* massless at two-loop order. Indeed, note that $\det f = 0$, as f is a 3×3 antisymmetric matrix. From this we immediately find that $\det M_{\nu}^{\text{ZB}} = 0$, which implies that one mass eigenvalue vanishes. This results in only one Majorana phase of the PMNS-matrix being physical in the Zee-Babu model.

The analytical evaluation of the two-loop integral \mathcal{I}_1 is rather cumbersome and can be found in Refs. [89, 90]. The results contain minor errors which were corrected in [91]. The numerical evaluation of the resulting expression is possible but computationally costly, as one has to resort to high-precision arithmetic since there are delicate cancellations involved. However, as discussed in Sec. 2.3.2, the lepton masses in the denominator are negligible

compared to the scalar masses m_h and m_k , which leads to the simplified expression [16,17]

$$\mathcal{I}_{1,KM}(m_h^2, m_k^2, m_{e,K}^2, m_{e,M}^2) \approx \mathcal{I}_1(m_h^2, m_k^2) = \frac{1}{m_h^2} \tilde{I}\left(\frac{m_k^2}{m_h^2}\right), \quad (3.2.4)$$

where

$$\tilde{I}(r) = - \int_0^1 dx \int_0^{1-x} dy \frac{1-y}{x+(r-1)y+y^2} \log \frac{y(1-y)}{x+ry}. \quad (3.2.5)$$

Here, we defined the ratio $r \equiv m_k^2/m_h^2$. This simplified expression can easily be evaluated numerically. We performed a cross-check using the numerical results for the full analytic expression, and found that the results agree very well for the range of lepton and scalar masses we considered in Sec. 4.

3.2.2 Renormalisation Group Equations

In this section we present the RGEs of the full theory. As described above, these were calculated using the computer program SARAH. Additionally, we performed some cross-checks using the results of Ref. [17] and the counterterms in Sec. 3.2.3.

The system of RGEs is not fully coupled, which allows to solve it in subsequent blocks. These blocks have to be solved in the correct order, as RGEs may depend on the solutions of previous blocks. Therefore, we present the RGEs in this ordered block-wise form.

First, we have to determine the running of the gauge couplings g_1 , g_2 , and g_3 , by solving the equations

$$\alpha\beta_{g_1}^{(1)} = \frac{51}{10}g_1^3, \quad (3.2.6a)$$

$$\alpha\beta_{g_2}^{(1)} = -\frac{19}{6}g_2^3, \quad (3.2.6b)$$

$$\alpha\beta_{g_3}^{(1)} = -7g_3^3, \quad (3.2.6c)$$

where α is the loop factor introduced in Eq. (3.1.1). Note that these equations are not coupled and can be solved analytically,

$$g_i(t) = \frac{g_i(0)}{\sqrt{1 - \frac{b_i}{8\pi^2}g_i^2(0)t}}, \quad (3.2.7)$$

where $b_i = (\frac{51}{10}, -\frac{19}{6}, -7)$.³

³We use the *GUT-normalisation*, relating our gauge coupling $g_1 \equiv g_{1,\text{GUT}}$ to the gauge coupling g'_1 via $g_1 = \sqrt{\frac{5}{3}}g'_1$. This implies $b_1 = \frac{3}{5}b'_1$.

The second block of equations determines the running of the Yukawa couplings:

$$\alpha\beta_{Y_u}^{(1)} = Y_u \left[\frac{3}{2} Y_u^\dagger Y_u - \frac{3}{2} Y_d^\dagger Y_d + T - \frac{17}{20} g_1^2 - \frac{9}{4} g_2^2 - 8g_3^2 \right], \quad (3.2.8a)$$

$$\alpha\beta_{Y_d}^{(1)} = Y_d \left[-\frac{3}{2} Y_u^\dagger Y_u + \frac{3}{2} Y_d^\dagger Y_d + T - \frac{1}{4} g_1^2 - \frac{9}{4} g_2^2 - 8g_3^2 \right], \quad (3.2.8b)$$

$$\alpha\beta_{Y_e}^{(1)} = Y_e \left[\frac{3}{2} Y_e^\dagger Y_e + 2f^\dagger f + T - \frac{9}{4} g_1^2 - \frac{9}{4} g_2^2 \right] + [2gg^\dagger] Y_e, \quad (3.2.8c)$$

$$\alpha\beta_f^{(1)} = f \left[\frac{1}{2} Y_e^\dagger Y_e + 4f^\dagger f + 4\text{Tr}(f^\dagger f) - \frac{9}{10} g_1^2 - \frac{9}{2} g_2^2 \right] + \left[\frac{1}{2} (Y_e^\dagger Y_e)^T \right] f, \quad (3.2.8d)$$

$$\alpha\beta_g^{(1)} = g \left[(Y_e Y_e^\dagger)^T + 4g^\dagger g + 2\text{Tr}(g^\dagger g) - \frac{18}{5} g_1^2 \right] + [Y_e Y_e^\dagger] g. \quad (3.2.8e)$$

The third block of equations yields the running of the scalar couplings:

$$\begin{aligned} \alpha\beta_{\lambda_\phi}^{(1)} &= 4\lambda_\phi T - 2T_4 + 24\lambda_\phi^2 + \lambda_{\phi h}^2 + \lambda_{\phi k}^2 \\ &\quad - \frac{9}{5} \lambda_\phi g_1^2 + \frac{27}{200} g_1^4 - 9\lambda_\phi g_2^2 + \frac{9}{8} g_2^4 + \frac{9}{20} g_1^2 g_2^2, \end{aligned} \quad (3.2.9a)$$

$$\begin{aligned} \alpha\beta_{\lambda_h}^{(1)} &= 16\lambda_h \text{Tr}(f^\dagger f) - 32\text{Tr}(f^\dagger f f^\dagger f) + 20\lambda_h^2 + 2\lambda_{\phi h}^2 + \lambda_{hk}^2 \\ &\quad - \frac{36}{5} \lambda_h g_1^2 + \frac{54}{25} g_1^4, \end{aligned} \quad (3.2.9b)$$

$$\begin{aligned} \alpha\beta_{\lambda_k}^{(1)} &= 8\lambda_k \text{Tr}(g^\dagger g) - 16\text{Tr}(g^\dagger g g^\dagger g) + 20\lambda_k^2 + 2\lambda_{\phi k}^2 + \lambda_{hk}^2 \\ &\quad - \frac{144}{5} \lambda_k g_1^2 + \frac{864}{25} g_1^4, \end{aligned} \quad (3.2.9c)$$

$$\begin{aligned} \alpha\beta_{\lambda_{\phi h}}^{(1)} &= 2\lambda_{\phi h} T + 8\lambda_{\phi h} \text{Tr}(f^\dagger f) - 16\text{Tr}(f^\dagger f Y_e^\dagger Y_e) + 12\lambda_\phi \lambda_{\phi h} + 8\lambda_h \lambda_{\phi h} \\ &\quad + 4\lambda_{\phi h}^2 + 2\lambda_{\phi k} \lambda_{hk} + \frac{27}{25} g_1^4 - \frac{9}{2} \lambda_{\phi h} g_1^2 - \frac{9}{2} \lambda_{\phi h} g_2^2, \end{aligned} \quad (3.2.9d)$$

$$\begin{aligned} \alpha\beta_{\lambda_{\phi k}}^{(1)} &= 2\lambda_{\phi k} T + 4\lambda_{\phi k} \text{Tr}(g^\dagger g) - 16\text{Tr}(g g^\dagger Y_e Y_e^\dagger) + 12\lambda_\phi \lambda_{\phi k} + 8\lambda_k \lambda_{\phi k} \\ &\quad + 4\lambda_{\phi k}^2 + 2\lambda_{\phi h} \lambda_{hk} + \frac{108}{25} g_1^4 - \frac{153}{10} \lambda_{\phi k} g_1^2 - \frac{9}{2} \lambda_{\phi k} g_2^2, \end{aligned} \quad (3.2.9e)$$

$$\begin{aligned} \alpha\beta_{\lambda_{hk}}^{(1)} &= 8\lambda_{hk} \text{Tr}(f^\dagger f) + 4\lambda_{hk} \text{Tr}(g^\dagger g) + 8\lambda_h \lambda_{hk} + 8\lambda_k \lambda_{hk} + 4\lambda_{\phi h} \lambda_{\phi k} + 4\lambda_{hk}^2 \\ &\quad - 18\lambda_{hk} g_1^2 + \frac{432}{25} g_1^4, \end{aligned} \quad (3.2.9f)$$

$$\alpha\beta_{\mu_{hk}}^{(1)} = \mu_{hk} \left[8\text{Tr}(f^\dagger f) + 2\text{Tr}(g^\dagger g) + 4\lambda_h + 4\lambda_{hk} - \frac{54}{5} g_1^2 \right]. \quad (3.2.9g)$$

Here, we have used the abbreviations:

$$T \equiv \text{Tr} \left(3Y_u^\dagger Y_u + 3Y_d^\dagger Y_d + Y_e^\dagger Y_e \right), \quad (3.2.10a)$$

$$T_4 \equiv \text{Tr} \left(3Y_u^\dagger Y_u Y_u^\dagger Y_u + 3Y_d^\dagger Y_d Y_d^\dagger Y_d + Y_e^\dagger Y_e Y_e^\dagger Y_e \right). \quad (3.2.10b)$$

Finally, we need the running of the scalar mass parameters:

$$\alpha\beta_{\mu_\phi^2}^{(1)} = 2\mu_\phi^2 T + 12\lambda_\phi\mu_\phi^2 + 2\lambda_{\phi h}\mu_h^2 + 2\lambda_{\phi k}\mu_k^2 - \frac{9}{10}\mu_\phi^2 g_1^2 - \frac{9}{2}\mu_\phi^2 g_2^2, \quad (3.2.11a)$$

$$\alpha\beta_{\mu_h^2}^{(1)} = 8\mu_h^2 \text{Tr}(f^\dagger f) + 4\lambda_{\phi h}\mu_\phi^2 + 8\lambda_h\mu_h^2 + 2\lambda_{hk}\mu_k^2 + 8\mu_{hk}^2 - \frac{18}{5}\mu_h^2 g_1^2, \quad (3.2.11b)$$

$$\alpha\beta_{\mu_k^2}^{(1)} = 4\mu_k^2 \text{Tr}(g^\dagger g) + 4\lambda_{\phi k}\mu_\phi^2 + 2\lambda_{hk}\mu_h^2 + 8\lambda_k\mu_k^2 + 4\mu_{hk}^2 - \frac{72}{5}\mu_k^2 g_1^2. \quad (3.2.11c)$$

This makes up the full set of RGEs in the Zee-Babu model.

3.2.3 Calculation of the Wavefunction Renormalisation Constants

In this section we present the calculation of the wavefunction renormalisation constants, which we will need later when computing the RGEs of the effective couplings in the EFTs. At this point, we anticipate that we will need δZ_e , δZ_L , δZ_ϕ , and δZ_h , corresponding to the fields e_R , L_L , ϕ , and h^+ , respectively. As explained in Sec. 2.2.1, in the MS-renormalisation scheme, the counterterms are defined to exactly cancel the divergent terms (and only those) appearing in dimreg. This prescription makes the calculations rather straightforward, as we only have to care about these divergent terms. Furthermore, recall from Sec. 3.1 that we only need the wavefunction renormalisation constants at one-loop level. We will present only the calculation of the right-handed lepton wavefunction renormalisation constant $\delta Z_e^{(1)}$ in detail. For the rest of the renormalisation constants, we will only give the final result. For further information we refer the reader to Ref. [35], which is an excellent reference for how to systematise the calculations. Furthermore, some of the diagrams we have to calculate already showed up in this reference, which allows us to perform valuable cross-checks.

Calculation of $\delta Z_e^{(1)}$

In the MS-renormalisation scheme, $\delta Z_e^{(1)}$ has to cancel all divergent terms stemming from one-particle irreducible diagrams which contribute to the e_R -two-point function at one-loop level:

$$\begin{aligned}
 & \text{Diagram 1: } e_R \text{ (in) } \circlearrowleft \text{1PI} \text{ } e_R \text{ (out)} = \text{Diagram 2: } e_R \text{ (in) } \circlearrowleft \begin{matrix} \phi \\ L_L \end{matrix} e_R \text{ (out)} + \text{Diagram 3: } e_R \text{ (in) } \circlearrowleft \begin{matrix} k^{++} \\ e_R \end{matrix} e_R \text{ (out)} \\
 & + \text{Diagram 4: } e_R \text{ (in) } \circlearrowleft \begin{matrix} B \\ e_R \end{matrix} e_R \text{ (out)} + \text{Diagram 5: } e_R \text{ (in) } \square \text{ } e_R \text{ (out)} \stackrel{!}{=} \text{UV-finite.}
 \end{aligned} \quad (3.2.12)$$

We now present the calculation of the diagrams on the right-hand side of this equation. Here, we use the computational techniques summarised in Ref. [25] and the Feynman rules in App. C without further reference.

For the one-loop diagram with ϕ and L_L in the loop we get:

$$\begin{aligned}
i(\Sigma_{e_R}^\phi)_{JI} &\equiv \text{Diagram with } \phi_j \text{ and } (L_{K,L})_k \text{ in the loop} \\
&= [-i\mu^{\frac{\epsilon}{2}} (Y_e)_{JK} \delta_{kj}] [-i\mu^{\frac{\epsilon}{2}} (Y_e^\dagger)_{KI} \delta_{kj}] \int \frac{d^d k}{(2\pi)^d} P_L \frac{i(\not{p} + \not{k})}{(p+k)^2} P_R \frac{i}{k^2 - m_\phi^2} \\
&= \frac{i\pi^2}{(2\pi)^4} (Y_e Y_e^\dagger)_{JI} \delta_{jj} P_L \cdot \frac{\mu^\epsilon}{i\pi^2} \int d^d k \frac{\not{p} + \not{k}}{(p+k)^2 (k^2 - m_\phi^2)} \\
&= 2i\alpha (Y_e Y_e^\dagger)_{JI} \not{p} P_R \frac{1}{\epsilon} + \text{UV-finite.}
\end{aligned} \tag{3.2.13}$$

Analogously, for the one-loop diagram with k^{++} and e_R in the loop we get:

$$\begin{aligned}
i(\Sigma_{e_R}^k)_{JI} &\equiv \text{Diagram with } k^{++} \text{ and } e_{K,R} \text{ in the loop} \\
&= [-2i\mu^{\frac{\epsilon}{2}} g_{JK}^\dagger] [-2i\mu^{\frac{\epsilon}{2}} g_{KI}] \int \frac{d^d k}{(2\pi)^d} P_L \frac{-i(-\not{p} - \not{k})}{(p+k)^2} P_R \frac{i}{k^2 - m_k^2} \\
&= \frac{4i\pi^2}{(2\pi)^4} (g^\dagger g)_{JI} P_L \cdot \frac{\mu^\epsilon}{i\pi^2} \int d^d k \frac{\not{p} + \not{k}}{(p+k)^2 (k^2 - m_k^2)} \\
&= 4i\alpha (g^\dagger g)_{JI} \not{p} P_R \frac{1}{\epsilon} + \text{UV-finite.}
\end{aligned} \tag{3.2.14}$$

The one-loop diagram with B and e_R in the loop yields:

$$\begin{aligned}
i(\Sigma_{e_R}^B)_{JI} &\equiv \text{Diagram} \\
&= [+i\mu^{\frac{\epsilon}{2}} g_1 \delta_{JK}] [+i\mu^{\frac{\epsilon}{2}} g_1 \delta_{KI}] \\
&\quad \cdot \int \frac{d^d k}{(2\pi)^d} \gamma^\mu P_R \frac{i(\not{p} + \not{k})}{(p+k)^2} \gamma^\nu P_R \frac{i[-\eta_{\mu\nu} + (1-\xi_1) \frac{k_\mu k_\nu}{k^2}]}{k^2} \\
&= \frac{i\pi^2}{(2\pi)^4} g_1^2 \delta_{JI} P_L \cdot \frac{\mu^\epsilon}{i\pi^2} \int d^d k \frac{\gamma^\mu (\not{p} + \not{k}) \gamma^\nu [-\eta_{\mu\nu} + (1-\xi_1) \frac{k_\mu k_\nu}{k^2}]}{(p+k)^2 k^2} \\
&= 2i\alpha \xi_1 g_1^2 \delta_{JI} \not{p} P_R \frac{1}{\epsilon} + \text{UV-finite}.
\end{aligned} \tag{3.2.15}$$

Note that we denote the Minkowski metric by $\eta_{\mu\nu} \equiv (+1, -1, -1, -1)$.

Upon plugging these expressions into Eq. (3.2.12) we get

$$i(\Sigma_{e_R}^\phi|_{\text{div}})_{JI} + i(\Sigma_{e_R}^k|_{\text{div}})_{JI} + i(\Sigma_{e_R}^B|_{\text{div}})_{JI} + i\not{p}(\delta Z_e)_{JI} P_R \stackrel{!}{=} 0, \tag{3.2.16}$$

where we denoted the divergent parts by the subscript “div”. Solving for $\delta Z_e^{(1)}$ yields the final result:

$$\boxed{\delta Z_e^{(1)} = -\alpha [2Y_e Y_e^\dagger + 4g^\dagger g + 2\xi_1 g_1^2] \frac{1}{\epsilon}} \tag{3.2.17}$$

This result contains the gauge parameter ξ_1 . As we will see below, ξ_1 will drop out of physically measurable quantities such as β -functions, as to be expected, reflecting their gauge invariance.

Calculation of $\delta Z_L^{(1)}$

The defining equation for the one-loop wavefunction renormalisation constant $\delta Z_L^{(1)}$ corresponding to the left-handed lepton doublet L_L reads:

$$\begin{aligned}
 & \text{1PI} = \text{loop}(e_R) + \text{loop}(h^+) \\
 & + \text{loop}(B, W^A) + \delta Z_L^{(1)} \stackrel{!}{=} \text{UV-finite.}
 \end{aligned}
 \tag{3.2.18}$$

In the third diagram a summation over $A \in \{1, 2, 3\}$ is understood. This equation yields:

$$\delta Z_L^{(1)} = -\alpha \left[Y_e^\dagger Y_e + 4f^\dagger f + \frac{1}{2}\xi_1 g_1^2 + \frac{3}{2}\xi_2 g_2^2 \right] \frac{1}{\varepsilon}
 \tag{3.2.19}$$

Calculation of $\delta Z_\phi^{(1)}$

For the one-loop wavefunction renormalisation constant $\delta Z_\phi^{(1)}$ corresponding to the Higgs-doublet ϕ we have to evaluate the following equation:

$$\begin{aligned}
 & \text{1PI} = \text{loop}(\phi, h^+, k^{++}) + \text{loop}(e_R) \\
 & + \text{loop}(u_R, d_R) + \text{loop}(B, W^A) + \delta Z_\phi^{(1)} \stackrel{!}{=} \text{UV-finite.}
 \end{aligned}
 \tag{3.2.20}$$

3.3 EFT- h

In the previous section we presented the neutrino mass matrix in the full Zee-Babu model, and we also did some preparatory work for the computations in the EFTs. We will now discuss EFT- h , which follows from the full theory by integrating out the doubly charged scalar particle k^{++} . Thus, only the singly charged scalar h^+ remains accessible in addition to the SM, cf. Sec. 2.3.3. The residual effects of k^{++} are now described by a set of effective operators, which we will present Sec. 3.3.1. As already anticipated, it turns out that three effective couplings, namely κ_{21} , κ_{11} , and κ_W , are relevant for the mass matrix in EFT- h , as we will present in Sec. 3.3.4. Furthermore, these couplings get switched on at different loop orders. We will discuss this in detail in Sec. 3.3.3. Finally, we will derive the RGEs in Sec. 3.3.5. Here, the main work will be the computation of the RGEs of the effective couplings. For this, we will need their counterterms as well as the wavefunction renormalisation constants which we have already computed in the full theory. Furthermore, we will see that some of the counterterms of the effective couplings are not only needed to compute the RGEs, but also to cancel infinities in the equations for the mass matrix and the matching. Therefore, we have to compute them first, cf. Sec. 3.3.2.

3.3.1 Effective Operators

EFT- h derives from the full theory by integrating out k^{++} . Therefore, we obtain the Lagrangian of EFT- h from the Lagrangian of the full theory as given in Eq. (2.3.12) by omitting the gauge-kinetic term of k^{++} and by setting all couplings to k^{++} to zero:

$$g = 0, \quad \mu_k^2 = 0, \quad \lambda_k = 0, \quad \lambda_{\phi k} = 0, \quad \lambda_{hk} = 0, \quad \mu_{hk} = 0. \quad (3.3.1)$$

Furthermore, we add all effective operators of mass dimension $\mathcal{D} = 5$, which follow from the SM particle content extended by h^+ and which are allowed by gauge symmetry. We label those effective operators \mathcal{O} (and the corresponding effective couplings κ) by two indices: the first one denotes the number of h^+ -particles involved in the coupling, and the second one enumerates the different operators and couplings of this type. Furthermore, we use the notations \mathcal{O}_W and κ_W for the Weinberg operator, which is the effective $\mathcal{D} = 5$ operator coupling only SM particles, cf. Sec. 2.3.1.

One finds the following effective operators with mass-dimension $\mathcal{D} = 5$:

$$\mathcal{O}_W = -\kappa_W \overline{(L_{I,L})^c}_i (L_{J,L})_j \phi_k \phi_l \epsilon_{ik} \epsilon_{jl} + \text{h.c.} \quad (3.3.2a)$$

$$\mathcal{O}_{11} = -\kappa_{11, IJ} \overline{(L_{I,L})}_i e_{J,R} \phi_k^\dagger \epsilon_{ik}^T h^+ + \text{h.c.} \quad (3.3.2b)$$

$$\mathcal{O}_{12} = -\kappa_{12} \phi_i^\dagger \phi_j^\dagger \epsilon_{ij} \phi_k^\dagger \phi_k h^+ + \text{h.c.} \quad (3.3.2c)$$

$$\mathcal{O}_{13} = -\kappa_{13} (D_\mu \phi^\dagger)_i (D^\mu \phi^\dagger)_j \epsilon_{ij} h^+ + \text{h.c.} \quad (3.3.2d)$$

$$\mathcal{O}_{14} = -\kappa_{14} \phi_i^\dagger (D^\mu \phi^\dagger)_j \epsilon_{ij} (D_\mu h^+) + \text{h.c.} \quad (3.3.2e)$$

$$\mathcal{O}_{21} = -\kappa_{21, IJ} \overline{(e_{I,R})^c}_i e_{J,R} h^+ h^+ + \text{h.c.} \quad (3.3.2f)$$

$$\mathcal{O}_{31} = -\kappa_{31} \phi_i^\dagger \phi_j^\dagger \epsilon_{ij} (h^+ h^-) h^+ + \text{h.c.} \quad (3.3.2g)$$

As κ_W and κ_{21} multiply operators which are symmetric in the flavour indices, only their symmetric parts can be physical. We define κ_W and κ_{21} to denote those symmetric parts, which coincides with the convention we used for the Majorana mass matrix, and for the Yukawa coupling g in the full theory. Note that κ_{11} does not have any particular symmetry properties.

We will find that only the three effective couplings κ_{21} , κ_{11} , and κ_W are relevant for the computation of the neutrino mass matrix. Therefore, we need not consider the matching or the running of any other effective coupling.

3.3.2 Calculation of the Counterterms

We now present the computation of the counterterms which we will need for the mass matrix, the matching equations, and the RGEs. Recall from Sec. 3.1 that, in order to compute the RGEs of the effective couplings consistently up to three-loop order, we need the the wavefunction renormalisation constants δZ_e , δZ_L , δZ_ϕ , and δZ_h , as well as the counterterm of the effective coupling κ_{21} at one-loop order. Furthermore, we need the counterterm of the effective coupling κ_{11} at one- and two-loop order, and the counterterm of the effective coupling κ_W at two- and three-loop order.

As already mentioned above, we will find that in the diagrams we have to calculate for the mass matrix as well as for the matching, infinities occur. Those will have to be cancelled by the counterterm of κ_{11} at one- and the counterterm of κ_W at two-loop order. In this chapter, we will calculate the counterterms independently from the equations for the mass matrix and the matching. This provides us with a useful possibility to cross-check the results, as $\delta\kappa_{11}^{(1)}$ and $\delta\kappa_W^{(2)}$ have to cancel the aforementioned infinities.

Wavefunction Renormalisation Constants

As described at the beginning of this chapter, the counterterms of the wavefunction renormalisation constants can be easily deduced from those we already calculated in the full theory in Sec. 3.2.3. To this end, we just set those full-theory couplings which are not existent anymore in EFT- h to zero, i.e., we apply Eq. (3.3.1). In principle, there could be additional diagrams containing effective couplings relevant here. Fortunately, it turns out that there are no diagrams of this type to consider at one-loop order. So, we arrive at the following expressions:

$$\delta Z_\phi^{(1)} = -\alpha \left[2T - \frac{1}{2} (3 - \xi_1) g_1^2 - \frac{3}{2} (3 - \xi_2) g_2^2 \right] \frac{1}{\varepsilon} \quad (3.3.3a)$$

$$\delta Z_h^{(1)} = -\alpha \left[8\text{Tr} (f^\dagger f) + 2(3 - \xi_1) g_1^2 \right] \frac{1}{\varepsilon} \quad (3.3.3b)$$

$$\delta Z_e^{(1)} = -\alpha \left[2Y_e Y_e^\dagger + 2\xi_1 g_1^2 \right] \frac{1}{\varepsilon} \quad (3.3.3c)$$

$$\delta Z_L^{(1)} = -\alpha \left[Y_e^\dagger Y_e + 4f^\dagger f + \frac{1}{2} \xi_1 g_1^2 + \frac{3}{2} \xi_2 g_2^2 \right] \frac{1}{\varepsilon} \quad (3.3.3d)$$

Calculation of $\delta\kappa_{21}^{(1)}$

The defining equation for the one-loop counterterm $\delta\kappa_{21}^{(1)}$ of the effective coupling κ_{21} reads:

(3.3.4)

The factors of two in front of the diagrams involving the B -gauge bosons come from the symmetry of the diagrams under exchange of the external h^+ -particles. As the external e_R -particles carry family indices (which we omit in the diagrams for clarity), the two diagrams in which B connects an external h^+ - with an external e_R -particle give different contributions.

By evaluating the diagrams in the above equation and collecting the UV-divergent parts, we get for the one-loop counterterm corresponding to κ_{21} :

$$\delta\kappa_{21}^{(1)} = \alpha (4\lambda_h + 24g_1^2 - 4\xi_1 g_1^2) \kappa_{21}^{(0)} \frac{1}{\varepsilon} \quad (3.3.5)$$

Note that $\delta\kappa_{21}^{(1)}$ starts beyond tree-level, since $\kappa_{21}^{(0)}$ gets switched on already at tree level, as was to be expected from the discussion in Sec. 3.1.

Calculation of $\delta\kappa_{11}^{(1)}$ and $\delta\kappa_{11}^{(2)}$

The defining equation for the one-loop counterterm $\delta\kappa_{11}^{(1)}$ of the effective coupling κ_{11} reads:

$$\begin{array}{c} \text{1PI} \end{array} = \begin{array}{c} \text{one-loop diagram} \\ \kappa_{21}^{(0)} \end{array} + \delta\kappa_{11}^{(1)} \stackrel{!}{=} \text{UV-finite}. \quad (3.3.6)$$

Note that we have already used this equation in Sec. 3.1 as an example of how counterterms of effective couplings, which get switched on at some loop order beyond tree-level, can receive contributions at the same loop order. Here, we use the tree-level effective coupling $\kappa_{21}^{(0)}$ in a one-loop diagram, which yields a one-loop contribution to the counterterm of the one-loop effective coupling $\kappa_{11}^{(1)}$. This is the only diagram which contributes at one-loop order, so that we find:

$$\boxed{\delta\kappa_{11}^{(1)} = 16\alpha f^\dagger Y_e^T \kappa_{21}^{(0)} \frac{1}{\varepsilon}} \quad (3.3.7)$$

Additionally, we have discussed in Sec. 3.1 that, in order to calculate the running of the neutrino mass matrix consistently up to three-loop order, we also have to compute all two-loop contributions $\delta\kappa_{11}^{(2)}$ to the counterterm of κ_{11} . The defining equation at this order

Furthermore, we did not explicitly write down the two-loop diagrams contributing at two-loop order. These include all those diagrams which can be formed out of the diagram containing $\kappa_{21}^{(0)}$ in Eq. (3.3.6) by adding an additional loop using B - or W -gauge bosons. In principle, the computation these two-loop diagrams is possible but time-consuming. We did not perform them in this work but stress again that one has to include these contributions in order to compute the running of the neutrino mass matrix in full consistency at third loop order. Nevertheless, we will see in Sec. 4 that one can get useful approximate results by only using the leading order contribution as given in Eq. (3.3.7).

We give the the two-loop contributions stemming from the one-loop diagrams depicted in the above equation here for future reference. These yield the following subset of terms belonging to $\delta\kappa_{11}^{(2)}$:

$$\delta\kappa_{11}^{(2)} \supset \alpha \left(8f^\dagger f - Y_e^\dagger Y_e + 2\lambda_{\phi h} - 2g_1^2 + \frac{5}{2}\xi_1 g_1^2 - \frac{3}{2}\xi_2 g_2^2 \right) \left(\kappa_{11}^{(1)} + \delta\kappa_{11}^{(1)} \right) \frac{1}{\varepsilon} \quad (3.3.9)$$

The diagrams containing the counterterm $\delta\kappa_{11}^{(1)}$ generate terms proportional to $1/\varepsilon^2$, which we can see by using Eq. (3.3.9). These terms will therefore not contribute to the β -function of κ_{11} , since, according to Eq. (2.2.15), only the $1/\varepsilon$ -terms are relevant here. In contrast, the missing two-loop diagrams will give contributions to the β -functions, since they in general do generate additional $1/\varepsilon$ -terms. Thus, we have in fact not computed all diagrams which we need in order to evaluate the running of the neutrino mass matrix in EFT- h consistently up to three-loop order. We will discuss in Sec. 4, why we nevertheless obtain sensible numerical results from our equations.

Calculation of $\delta\kappa_{\mathbb{W}}^{(2)}$ and $\delta\kappa_{\mathbb{W}}^{(3)}$

The defining equation for the two-loop counterterm $\delta\kappa_{\mathbb{W}}^{(2)}$ of the effective coupling $\kappa_{\mathbb{W}}$ reads:

$$\begin{aligned}
& \text{1PI} = \text{Diagram 1} + (\phi \leftrightarrow \phi) \\
& + \text{Diagram 2} + (\phi \leftrightarrow \phi) + (L_L \leftrightarrow L_L) + \left(\begin{matrix} \phi \leftrightarrow \phi \\ L_L \leftrightarrow L_L \end{matrix} \right) \quad (3.3.10) \\
& + \left(\begin{matrix} \text{diagrams with} \\ \kappa_{11}^{(1)} \leftrightarrow \delta\kappa_{11}^{(1)} \end{matrix} \right) + \delta\kappa_{\mathbb{W}}^{(2)} \stackrel{!}{=} \text{UV-finite.}
\end{aligned}$$

The two-loop diagram involving the tree-level effective coupling $\kappa_{21}^{(0)\dagger}$ factorises, such that one effectively has to evaluate the product of two one-loop integrals. In order to obtain the $1/\varepsilon$ -divergent term of this diagram, we therefore do not only need the $1/\varepsilon$ -divergent terms of the individual one-loop integrals but their constant terms, too, as those are multiplied by the $1/\varepsilon$ -term of the respective other one-loop integral. One finds that the resulting $1/\varepsilon$ -terms cancel out of the result and only the $1/\varepsilon^2$ -term coming from multiplying both $1/\varepsilon$ -terms survives. Recall that such terms are irrelevant for the computation of β -functions, as only the $1/\varepsilon$ -terms enter Eq. (2.2.15).

Furthermore, one has to be careful to include all diagrams which arise from the ones depicted by swapping external particles. We indicated this using obvious notation. Note that L_L carries family indices, and both ϕ and L_L carry $SU(2)_L$ -indices, too. Evaluating the above equation with these remarks in mind amounts to some pages of tedious algebra, which result in:

$$\boxed{\delta\kappa_{\mathbb{W}}^{(2)} = -2\alpha \left[fY_e^\dagger \kappa_{11}^{(1)\dagger} - \left(fY_e^\dagger \kappa_{11}^{(1)\dagger} \right)^T \right] \frac{1}{\varepsilon} - 32\alpha^2 fY_e^\dagger \kappa_{21}^{(0)\dagger} Y_e^* f \frac{1}{\varepsilon^2}} \quad (3.3.11)$$

In analogy to the situation we already discussed for $\delta\kappa_{11}^{(2)}$, in the case of κ_W we need the third-order contribution $\delta\kappa_W^{(3)}$ to compute the third-order running of the mass matrix:

$$\begin{aligned}
& \text{1PI} = \kappa_W^{(2)} + \text{diagrams with } e_R \text{ and } \phi \text{ loop} + (\phi \leftrightarrow \phi) + (L_L \leftrightarrow L_L) + \left(\begin{array}{l} \phi \leftrightarrow \phi \\ L_L \leftrightarrow L_L \end{array} \right) \\
& + \text{diagrams with } B, W^A \text{ boson legs} + \text{diagrams with } \phi \text{ loop and } B, W^A \text{ boson legs} \\
& + \text{diagrams with } \phi \text{ loop and } B, W^A \text{ boson legs} + (\phi \leftrightarrow \phi) + (L_L \leftrightarrow L_L) + \left(\begin{array}{l} \phi \leftrightarrow \phi \\ L_L \leftrightarrow L_L \end{array} \right) \\
& + \left(\text{diagrams with } \kappa_W^{(2)} \leftrightarrow \delta\kappa_W^{(2)} \right) + \left(\text{two- and three-loop diagrams} \right) + \delta\kappa_W^{(3)} \stackrel{!}{=} \text{UV-finite.}
\end{aligned} \tag{3.3.12}$$

These diagrams are of similar type as those in Eq. (3.3.8), with $\kappa_{11}^{(1)}$ replaced by $\kappa_W^{(2)}$, but we have to keep in mind that not only B , but also W^A can connect the external legs of κ_W . Again, there are diagrams with more than one loop which contribute to $\delta\kappa_W^{(3)}$. We obtain

these diagrams by attaching an additional gauge boson loop to the one-loop diagrams in Eq. (3.3.10). The subset of three-loop contributions stemming only from the depicted one-loop diagrams yields the following terms:

$$\delta\kappa_W^{(3)} \supset \alpha \left\{ -2 \left[\kappa_W^{(2)} Y_e^\dagger Y_e + \left(\kappa_W^{(2)} Y_e^\dagger Y_e \right)^T \right] + \left[4\lambda_\phi + \left(\frac{3}{2} - \xi_1 \right) g_1^2 + \left(\frac{3}{2} - 3\xi_2 \right) g_2^2 \right] \kappa_W^{(2)} \right\} \frac{1}{\varepsilon} + \left(\kappa_W^{(2)} \leftrightarrow \delta\kappa_W^{(2)} \right) \quad (3.3.13)$$

Here, the same remarks as those below Eq. (3.3.9) apply.

3.3.3 Matching

Let us now derive the matching equations, describing the relationship between the couplings of the full theory and the effective couplings κ_{21} , κ_{11} , and κ_W . We will find that the lowest-order contributions to these couplings are $\kappa_{21}^{(0)}$, $\kappa_{11}^{(1)}$, and $\kappa_W^{(2)}$, respectively, a fact we already made use of when computing the counterterms in the previous section.

In what follows, we denote by μ_k^* the threshold energy at which k^{++} is integrated out, cf. Sec. 2.3.3. As we have to match three effective couplings to the full theory, we have to write down three independent matching equations. Those have to be evaluated at μ_k^* , which we will not always make explicit in order to keep the notation sufficiently uncluttered. We will use the general recipe introduced in Sec. 3.1 in order to consistently keep track of the loop orders: we recall that a n -loop diagram contains a factor of α^n and also expand the effective couplings in orders of α . Then, the matching amounts to equating the coefficients of corresponding powers of α . At this point, we want to draw the reader's attention to a technique named *Covariant Derivative Expansion* [78, 79], which we used at several points of the calculations as a useful cross-check of the results.

We will perform the matching in the broken phase. This has several computational advantages: first, we will again have to evaluate one-loop integrals in this section. However, the calculations differ from those we performed when computing the counterterms by the fact that we now need not only the UV-divergent terms of the one-loop integrals anymore. Indeed, the UV-divergent terms will be cancelled by the counterterms, and the relevant terms will now be the UV-finite ones. This makes the calculations considerably more complicated. Therefore, we are interested in saving as much work as possible. Now, consider an n -point one-loop integral stemming from a loop to which m Higgs particles ϕ are attached in the unbroken phase. Considering the same loop in the broken phase, by replacing ϕ by its vev $\langle\phi\rangle$ and evaluating the summand coming with v , such an integral reduces to an $(n - m)$ -point integral that is considerably easier to evaluate. An additional advantage of working in the broken phase is that many of the diagrams we have to compute for the matching will appear again in the equation for the neutrino mass matrix. Clearly, there we *have to* work in the broken phase, as otherwise all neutrinos are massless and

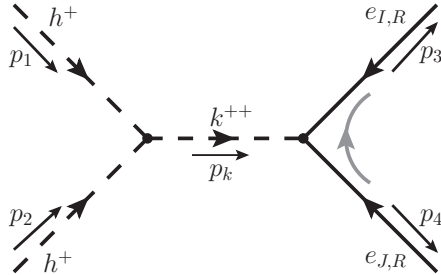
the calculations do not make sense. Thus, working in the broken phase already in the matching process makes it possible to simply reuse the results of this section later for the computation of the mass matrix.

First matching equation: $\kappa_{21}^{(0)}$

κ_{21} gets switched on at tree level as described by the first matching equation which we present now. Indeed, the lowest order contribution to the process

$$h^+ h^+ \rightarrow (e_{I,R})^c (e_{J,R})^c, \quad (3.3.14)$$

given in EFT- h by the point-like interaction described by κ_{21} , is mediated in the full theory at tree level via the following diagram:



The diagram shows two incoming dashed lines representing h^+ particles with momenta p_1 and p_2 . They meet at a vertex and a dashed line representing a scalar mediator k^{++} with momentum p_k extends to the right. At the second vertex, the mediator splits into two outgoing lines: a solid line representing $e_{I,R}$ with momentum p_3 and a dashed line representing $e_{J,R}$ with momentum p_4 . A curved arrow indicates the flow of the process.

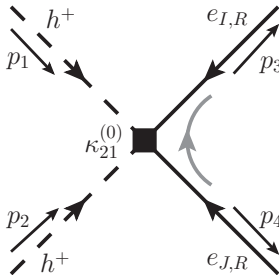
$$i\mathcal{M}_{ZB,IJ}^{(0)} \equiv \quad (3.3.15)$$

$$= [-2ig_{IJ}P_R] \frac{i}{p_k^2 - m_k^2} [-2i\mu_{hk}] = \frac{-4i\mu_{hk}g_{IJ}}{p_k^2 - m_k^2} P_R$$

$$= \frac{4i\mu_{hk}g_{IJ}}{m_k^2} P_R + \mathcal{O}\left(\frac{p_k^2}{m_k^2}\right),$$

where $p_k = p_1 + p_2 = p_3 + p_4$.

In EFT- h , at lowest order this process is pointlike and described by the effective coupling κ_{21} :



The diagram shows a pointlike interaction represented by a solid black square vertex. Two incoming dashed lines represent h^+ particles with momenta p_1 and p_2 . Two outgoing lines represent $e_{I,R}$ (solid line, momentum p_3) and $e_{J,R}$ (dashed line, momentum p_4). A curved arrow indicates the process.

$$i\mathcal{M}_{h,IJ}^{(0)} \equiv \kappa_{21}^{(0)} = -4i\kappa_{21,IJ}^{(0)} P_R. \quad (3.3.16)$$

We already added a superscript (0) to κ_{21} here, since we found above that in the full theory this process occurs at tree level.

The matching equation arising from comparing the zeroth-order coefficients of the α -expansion of the process $h^+ h^+ \rightarrow (e_{I,R})^c (e_{J,R})^c$ in the full theory and in EFT- h reads:

$$i\mathcal{M}_{h,IJ}^{(0)} \stackrel{!}{=} i\mathcal{M}_{ZB,IJ}^{(0)}. \quad (3.3.17)$$

This yields for external momenta small compared to m_k the following final result:

$$\boxed{\kappa_{21,IJ}^{(0)} = -\frac{\mu_{hk}g_{IJ}}{m_k^2}} \quad (3.3.18)$$

Second matching equation: $\kappa_{11}^{(1)}$

In the broken phase, by replacing ϕ by its vev v , κ_{11} gives a pointlike contribution to the process

$$h^+ \rightarrow (e_{I,R})^c \nu_{J,L}. \quad (3.3.19)$$

As described above, it is advantageous to use this process in the matching, as we only have to evaluate a three- instead of a four-point function, which simplifies the evaluation of the loop integral.

In the full theory, the lowest-order contribution to this process is at one-loop level via the following diagram (we set $d = 4$ as it is finite by power counting):

$$i\mathcal{M}_{\text{ZB},IJ}^{(1)} \equiv \text{Diagram} \quad (3.3.20)$$

$$\begin{aligned} &= \int \frac{d^4q}{(2\pi)^4} [-2ig_{IK}P_R] \frac{i(p_2 + m_{e,K})}{p_2^2 - m_{e,K}^2} [-2if_{KJ}^\dagger P_R] \frac{i}{p_1^2 - m_h^2} [-2i\mu_{hk}] \frac{i}{q^2 - m_k^2} \\ &= \frac{8i\alpha v}{\sqrt{2}} g_{IK}y_K \mathcal{I}_{2,K} f_{KJ}^\dagger \mu_{hk} P_R. \end{aligned}$$

Here we have defined the one-loop integral $\mathcal{I}_{2,K}$ via:

$$\begin{aligned} &i\alpha \mathcal{I}_{2,K} (m_h^2, m_k^2, m_{e,I}^2, m_{e,K}^2) \\ &\equiv \int \frac{d^4q}{(2\pi)^4} \frac{1}{[q^2 - m_k^2][(q + p_h)^2 - m_h^2][(q + p_e)^2 - m_{e,K}^2]}. \end{aligned} \quad (3.3.21)$$

Note that the dependence on $m_{e,I}^2$ enters implicitly through the external momentum p_e . To evaluate this integral, we introduce three Feynman parameters x , y , and z to obtain

$$\begin{aligned} i\alpha\mathcal{I}_{2,K} &= \int \frac{d^4q}{(2\pi)^4} \int_0^1 dx \int_0^1 dy \int_0^1 dz \delta(x+y+z-1) \frac{2!}{D_K^3} \\ &= \int \frac{d^4q}{(2\pi)^4} \int_0^1 dx \int_0^{1-x} dy \frac{2!}{D_K^3} \Big|_{z=1-x-y}, \end{aligned} \quad (3.3.22)$$

where in the denominator we have:

$$D_K|_{z=1-x-y} = x[(p_e + q)^2 - m_{e,K}^2] + y[(p_h + q)^2 - m_h^2] + (1-x-y)[q^2 - m_k^2] \equiv \ell^2 - \Delta_K. \quad (3.3.23)$$

Here, we completed the square,

$$q^2 + 2q(xp_e + yp_h) = (q + xp_e + yp_h)^2 - (xp_e + yp_h)^2, \quad (3.3.24)$$

in order to obtain a denominator of the form $[\ell^2 - \Delta_K]^3$ with Δ_K independent of the shifted momentum ℓ , which is given by:

$$\ell \equiv q + xp_e + yp_h. \quad (3.3.25)$$

Δ_K reads:

$$\Delta_K = x^2 p_e^2 + y^2 p_h^2 + 2xyp_e \cdot p_h - xp_e^2 - yp_h^2 + xm_{e,K}^2 + ym_h^2 + (1-x-y)m_k^2. \quad (3.3.26)$$

We can simplify this expression by using the relation $p_\nu = p_h - p_e$, leading to:

$$p_\nu^2 = p_h^2 + p_e^2 - 2p_h \cdot p_e. \quad (3.3.27)$$

Furthermore, we use the fact that the external particles are on-shell, i.e. $p_h^2 = m_h^2$, $p_e^2 = m_{e,I}^2$, and $p_\nu^2 = m_{\nu,J}^2 = 0$. Using these relations in Eq. (3.3.26) yields:

$$\Delta_K = m_{e,I}^2(x^2 + 2xy - x) + m_h^2(y^2 + 2xy) + xm_{e,K}^2 + (1-x-y)m_k^2. \quad (3.3.28)$$

Note that we have $\Delta_K > 0$ on the integration domain, so we do not run into problems with divergences. Putting everything together, we are left with:

$$i\alpha\mathcal{I}_{2,K} = 2! \int_0^1 dx \int_0^{1-x} dy \int \frac{d^4\ell}{(2\pi)^4} \frac{1}{[\ell^2 - \Delta_K]^3}. \quad (3.3.29)$$

Here, we switched the order of integrations and shifted the momentum from q to ℓ using Eq. (3.3.25). Notice that $d^4q = d^4\ell$. The momentum integral evaluates to

$$\int \frac{d^4\ell}{(2\pi)^4} \frac{1}{[\ell^2 - \Delta_K]^3} = -i\alpha \frac{1}{2\Delta_K}, \quad (3.3.30)$$

the third diagram contributing at one-loop order:

$$\begin{aligned}
&= \int \frac{d^d q}{(2\pi)^d} \left[-4i\mu^\varepsilon \kappa_{21,IK}^{(0)} P_R \right] \frac{i(\not{p}_1 + m_{e,K})}{p_1^2 - m_{e,K}^2} \left[-2i\mu^{\frac{\varepsilon}{2}} f_{KJ}^\dagger P_R \right] \frac{i}{q^2 - m_h^2} \\
&= \frac{8i\alpha\mu^{\frac{\varepsilon}{2}} v}{\sqrt{2}} \kappa_{21,IK}^{(0)} y_K \mathcal{I}_{3,K} f_{KJ}^\dagger P_R.
\end{aligned}$$

The one-loop integral $\mathcal{I}_{3,K}$ is defined as:

$$i\alpha \mathcal{I}_{3,K}(m_h^2, m_{e,K}^2) \equiv \mu^\varepsilon \int \frac{d^d q}{(2\pi)^d} \frac{1}{[q^2 - m_h^2] [(q - p_\nu)^2 - m_{e,K}^2]}. \quad (3.3.35)$$

We can evaluate it by performing the same steps as above (we only have to introduce two Feynman parameters here instead of three). This leads to:

$$i\alpha \mathcal{I}_{3,K} = \mu^\varepsilon \int_0^1 dx \int \frac{d^d \ell}{(2\pi)^d} \frac{1}{[\ell^2 - \Delta_K]^2}, \quad (3.3.36)$$

with $\ell \equiv q - xp_\nu$, and

$$\Delta_K = xm_{e,K}^2 + (1-x)m_h^2 > 0. \quad (3.3.37)$$

The momentum integral evaluates to

$$\begin{aligned}
\mu^\varepsilon \int \frac{d^d \ell}{(2\pi)^d} \frac{1}{[\ell^2 - \Delta_K]^2} &= \frac{i\mu^\varepsilon \Gamma(2 - \frac{d}{2})}{(4\pi)^{\frac{d}{2}}} \left(\frac{1}{\Delta_K} \right)^{2 - \frac{d}{2}} \\
&= i\alpha \left[\frac{2}{\varepsilon} + \log(4\pi) - \gamma_E - \log\left(\frac{\Delta_K}{\mu^2}\right) + \mathcal{O}(\varepsilon) \right],
\end{aligned} \quad (3.3.38)$$

where we used $d = 4 - \varepsilon$ and performed an expansion in ε . The UV-divergent part proportional to $1/\varepsilon$ will be cancelled by the counterterm $\delta\kappa_{11}^{(1)}$. It will prove convenient to give names to the first few expansion coefficients of \mathcal{I}_3 as we will need them later:

$$\mathcal{I}_{3,K} \equiv \mathcal{I}_{3,K}^{(-1)} \frac{1}{\varepsilon} + \mathcal{I}_{3,K}^{(0)} + \mathcal{I}_{3,K}^{(1)} \varepsilon + \mathcal{O}(\varepsilon^2). \quad (3.3.39)$$

Note that the superscripts do not denote coefficients of an expansion in loop orders here. Rather, they denote coefficients of a (Laurent-)expansion in the regularisation parameter ε . We just found:

$$\mathcal{I}_{3,K}^{(-1)} = \int_0^1 dx \, 2 = 2, \quad (3.3.40)$$

$$\mathcal{I}_{3,K}^{(0)}(\mu) = \log(4\pi) - \gamma_E - \int_0^1 dx \log\left(\frac{\Delta_K}{\mu^2}\right). \quad (3.3.41)$$

Let us have a closer look at $\mathcal{I}_{3,K}^{(0)}$. We can perform the integral over x analytically:

$$\int_0^1 dx \log\left(\frac{\Delta_K}{\mu^2}\right) = \frac{2m_{e,K}^2}{m_{e,K}^2 - m_h^2} \log\left(\frac{m_{e,K}}{\mu}\right) - \frac{2m_h^2}{m_{e,K}^2 - m_h^2} \log\left(\frac{m_h}{\mu}\right) - 1. \quad (3.3.42)$$

Therefore, we have:

$$\mathcal{I}_{3,K}^{(0)}(\mu) = \log(4\pi) - \gamma_E + 1 - \frac{2m_{e,K}^2}{m_{e,K}^2 - m_h^2} \log\left(\frac{m_{e,K}}{\mu}\right) + \frac{2m_h^2}{m_{e,K}^2 - m_h^2} \log\left(\frac{m_h}{\mu}\right). \quad (3.3.43)$$

We will see below that it is not necessary for our purposes to calculate $\mathcal{I}_{3,K}^{(1)}$, since it drops out of the final results in any case.

We are now ready to evaluate the matching equations arising from comparing the coefficients of the α -expansions of the process $h^+ \rightarrow (e_{I,R})^c \nu_{J,L}$ in the full theory as well as in EFT- h . As there is no diagram at tree level in the full theory contributing to this process, we immediately find:

$$\boxed{\kappa_{11}^{(0)} = 0} \quad (3.3.44)$$

At first loop order we have:

$$i\mathcal{M}_{\text{ZB},IJ}^{(1)} \stackrel{!}{=} i\mathcal{M}_{h,1,IJ}^{(1)} + i\mathcal{M}_{h,2,IJ}^{(1)} + i\mathcal{M}_{h,3,IJ}^{(1)}. \quad (3.3.45)$$

Using Eq. (3.3.7), we find that $\mathcal{M}_{h,2,IJ}^{(1)}$ indeed cancels the divergent terms of $\mathcal{M}_{h,3,IJ}^{(1)}$. This provides a useful cross-check for the correctness of our calculations. By equating the

convergent terms, we arrive at our final result:

$$\begin{aligned} \kappa_{11,IJ}^{(1)} &= -8\alpha \left(f_{IK}^\dagger \mathcal{I}_{2,K} y_K g_{KJ} \mu_{hk} - f_{IK}^\dagger \mathcal{I}_{3,K}^{(0)} y_K \kappa_{21,KJ}^{(0)} \right) \\ &= -8\alpha f_{IK}^\dagger \left(\mathcal{I}_{2,K} + \frac{\mathcal{I}_{3,K}^{(0)}}{m_k^2} \right) y_K g_{KJ} \mu_{hk} \end{aligned} \quad (3.3.46)$$

In the second line, we substituted our previous result Eq. (3.3.18). Note that, as already anticipated above, κ_{11} gets switched on at first loop order.

Third matching equation: $\kappa_W^{(2)}$

In the broken phase, the Weinberg operator gives a pointlike contribution to the neutrino mass matrix if we replace both ϕ -legs by the Higgs vev v . Therefore, we use the condition that the mass matrices in the full theory and in EFT- h have to coincide at the matching scale as the third matching equation. This is advantageous, as we have already computed the mass matrix in the full theory. Furthermore, we still have to compute the mass matrix in EFT- h in any case. Therefore, it makes sense to use this result for the matching, too.

In the full theory, the lowest-order contribution to the mass matrix is at two-loop level, cf. Eq. (3.2.3):

$$\begin{aligned} i\mathcal{M}_{\nu,IJ}^{\text{ZB}} &= \begin{array}{c} \begin{array}{c} \text{---} h^+ \text{---} \\ \text{---} k^{++} \text{---} \\ \text{---} h^+ \text{---} \end{array} \\ \begin{array}{c} \nu_{I,L} \leftarrow e_{K,L} \leftarrow e_{K,R} \leftarrow e_{M,R} \leftarrow e_{M,L} \leftarrow \nu_{J,L} \\ \langle \phi \rangle \quad \langle \phi \rangle \\ \longleftarrow \end{array} \end{array} \quad (3.2.3) \\ &= -8i\alpha^2 v^2 \mu_{hk} f_{IK}^\dagger y_K g_{KM} \mathcal{I}_{1,KM} y_M f_{MJ}^\dagger P_R. \end{aligned}$$

In EFT- h , at two-loop level, there are seven diagrams contributing to the neutrino mass matrix. We will consistently set the external momentum to zero and denote the loop-momentum by q . The first diagram is the point-like contribution via κ_W :

$$i\mathcal{M}_{h,1,IJ}^{(2)} \equiv \begin{array}{c} \begin{array}{c} \kappa_W^{(2)\dagger} \\ \text{---} \text{---} \text{---} \end{array} \\ \begin{array}{c} \nu_{I,L} \leftarrow \nu_{J,L} \\ \langle \phi \rangle \quad \langle \phi \rangle \\ \longleftarrow \end{array} \end{array} = -iv^2 \kappa_{W,IJ}^{(2)\dagger} P_R. \quad (3.3.47)$$

As described in App. C, we had to leave out a symmetry factor of 2 here when deducing the Feynman rules in the broken from those in the unbroken phase. As shown in Sec. 3.3.2,

Furthermore, there are two similar diagrams involving κ_{11} and $\delta\kappa_{11}$, respectively:

$$i\mathcal{M}_{h,5,IJ}^{(2)} \equiv \begin{array}{c} \begin{array}{c} \text{---} \nu_{I,L} \text{---} \left[\text{---} \kappa_{11}^{(1)} \text{---} \right] \text{---} e_{K,R} \text{---} \left[\text{---} \langle \phi \rangle \text{---} \right] \text{---} e_{K,L} \text{---} \nu_{J,L} \text{---} \\ \text{---} \langle \phi \rangle \text{---} \left[\text{---} h^+ \text{---} \right] \text{---} \langle \phi \rangle \text{---} \\ \text{---} \langle \phi \rangle \text{---} \end{array} \end{array} = -i\alpha v^2 \kappa_{11,IK}^{(1)} y_K \mathcal{I}_{3,K} f_{KJ}^\dagger P_R, \quad (3.3.51)$$

as well as:

$$i\mathcal{M}_{h,6,IJ}^{(2)} \equiv \begin{array}{c} \begin{array}{c} \text{---} \nu_{I,L} \text{---} \left[\text{---} \delta\kappa_{11}^{(1)} \text{---} \right] \text{---} e_{K,R} \text{---} \left[\text{---} \langle \phi \rangle \text{---} \right] \text{---} e_{K,L} \text{---} \nu_{J,L} \text{---} \\ \text{---} \langle \phi \rangle \text{---} \left[\text{---} h^+ \text{---} \right] \text{---} \langle \phi \rangle \text{---} \\ \text{---} \langle \phi \rangle \text{---} \end{array} \end{array} = -i\alpha v^2 \delta\kappa_{11,IK}^{(1)} y_K \mathcal{I}_{3,K} f_{KJ}^\dagger P_R. \quad (3.3.52)$$

Finally, there is a two-loop diagram containing $\kappa_{21}^{(0)}$, thus contributing at two-loop order:

$$i\mathcal{M}_{h,7,IJ}^{(2)} \equiv \begin{array}{c} \begin{array}{c} \text{---} \nu_{I,L} \text{---} \left[\text{---} \langle \phi \rangle \text{---} \right] \text{---} e_{K,L} \text{---} \left[\text{---} \langle \phi \rangle \text{---} \right] \text{---} e_{K,R} \text{---} \left[\text{---} \kappa_{21}^{(0)} \text{---} \right] \text{---} e_{M,R} \text{---} \left[\text{---} \langle \phi \rangle \text{---} \right] \text{---} e_{M,L} \text{---} \nu_{J,L} \text{---} \\ \text{---} \langle \phi \rangle \text{---} \left[\text{---} h^+ \text{---} \right] \text{---} \langle \phi \rangle \text{---} \left[\text{---} h^+ \text{---} \right] \text{---} \langle \phi \rangle \text{---} \\ \text{---} \langle \phi \rangle \text{---} \end{array} \end{array} \quad (3.3.53)$$

$$\begin{aligned} &= \int \frac{d^d q}{(2\pi)^d} \int \frac{d^d q'}{(2\pi)^d} \left[-2i\mu^{\frac{\epsilon}{2}} f_{IK}^\dagger \varepsilon_{12} P_R \right] \frac{i(-\not{q} + m_{e,K})}{q^2 - m_{e,K}^2} \left[-4i\mu^\epsilon \kappa_{21,KM}^{(0)} P_R \right] \\ &\quad \cdot \left[-2i\mu^{\frac{\epsilon}{2}} f_{MJ}^\dagger \varepsilon_{21} P_R \right] \frac{i}{q^2 - m_h^2} \frac{i}{q'^2 - m_h^2} \\ &= 8i\alpha^2 v^2 f_{IK}^\dagger \mathcal{I}_{3,K} y_K \kappa_{21,KM}^{(0)} \mathcal{I}_{3,M} y_M f_{MJ}^\dagger P_R. \end{aligned}$$

We are now ready to evaluate the matching equations arising from comparing the coefficients of the α -expansions of the neutrino mass matrix in the full theory as well as

in EFT- h . As there are no diagrams at tree level or at one-loop level in the full theory contributing to the mass matrix, we immediately find:

$$\boxed{\kappa_W^{(0)} = \kappa_W^{(1)} = 0} \quad (3.3.54)$$

Equating the α^2 -coefficients leads to the equation:

$$i\mathcal{M}_{\nu,IJ}^{\text{ZB}} \stackrel{!}{=} \sum_{i=1}^7 i\mathcal{M}_{h,i,IJ}^{(2)}. \quad (3.3.55)$$

Plugging in the results of all diagrams we have just calculated, this equation reads:

$$\begin{aligned} 8\alpha^2 f_{IK}^\dagger y_K g_{KM} \mathcal{I}_{1,KM} y_M f_{MJ}^\dagger \mu_{hk} &= \kappa_{W,IJ}^{(2)\dagger} + \delta\kappa_{W,IJ}^{(2)\dagger} \\ &\quad - \alpha f_{IK}^\dagger y_K \mathcal{I}_{3,K} \kappa_{11,KJ}^{(1)T} - \alpha f_{IK}^\dagger y_K \mathcal{I}_{3,K} \delta\kappa_{11,KJ}^{(1)T} \\ &\quad + \alpha \kappa_{11,IK}^{(1)} y_K \mathcal{I}_{3,K} f_{KJ}^\dagger + \alpha \delta\kappa_{11,IK}^{(1)} y_K \mathcal{I}_{3,K} f_{KJ}^\dagger \\ &\quad - 8\alpha^2 f_{IK}^\dagger \mathcal{I}_{3,K} y_K \kappa_{21,KM}^{(0)} \mathcal{I}_{3,M} y_M f_{MJ}^\dagger. \end{aligned} \quad (3.3.56)$$

Let us first check that the counterterms $\delta\kappa_{11}^{(1)}$ and $\delta\kappa_W^{(2)}$ that we have calculated in Sec. 3.3.2 indeed cancel the divergences. To this end, we equate only the divergent terms appearing in this equation:

$$\begin{aligned} 0 &= \delta\kappa_{W,IJ}^{(2)\dagger} - \alpha f_{IK}^\dagger y_K \mathcal{I}_{3,K} \Big|_{\text{div}} \kappa_{11,KJ}^{(1)T} - \alpha f_{IK}^\dagger y_K \mathcal{I}_{3,K} \Big|_{\text{conv}} \delta\kappa_{11,KJ}^{(1)T} \\ &\quad - \alpha f_{IK}^\dagger y_K \mathcal{I}_{3,K} \Big|_{\text{div}} \delta\kappa_{11,KJ}^{(1)T} + \alpha \kappa_{11,IK}^{(1)} \mathcal{I}_{3,K} \Big|_{\text{div}} f_{KJ}^\dagger \\ &\quad + \alpha \delta\kappa_{11,IK}^{(1)} \mathcal{I}_{3,K} \Big|_{\text{conv}} f_{KJ}^\dagger + \alpha \delta\kappa_{11,IK}^{(1)} \mathcal{I}_{3,K} \Big|_{\text{div}} f_{KJ}^\dagger \\ &\quad - 8\alpha^2 f_{IK}^\dagger \mathcal{I}_{3,K} \Big|_{\text{conv}} y_K \kappa_{21,KM}^{(0)} \mathcal{I}_{3,M} \Big|_{\text{div}} y_M f_{MJ}^\dagger \\ &\quad - 8\alpha^2 f_{IK}^\dagger \mathcal{I}_{3,K} \Big|_{\text{div}} y_K \kappa_{21,KM}^{(0)} \mathcal{I}_{3,M} \Big|_{\text{conv}} y_M f_{MJ}^\dagger \\ &\quad - 8\alpha^2 f_{IK}^\dagger \mathcal{I}_{3,K} \Big|_{\text{div}} y_K \kappa_{21,KM}^{(0)} \mathcal{I}_{3,M} \Big|_{\text{div}} y_M f_{MJ}^\dagger. \end{aligned} \quad (3.3.57)$$

Here, we denoted the UV-divergent part (i.e. the $1/\varepsilon$ -term) of the loop-integral \mathcal{I}_3 by a subscript ‘‘div’’ did and analogously for the UV-convergent part (i.e. the terms starting at ε^0), cf. Eq. (3.3.39). We now use the results from Eqs. (3.3.40) and (3.3.41) and substitute the expressions for the counterterms Eqs. (3.3.7) and (3.3.11). Let us first have a look at the $\mathcal{O}(\varepsilon^{-1})$ -terms we get in the limit $d = 4$:

$$\begin{aligned} 0 &= 2\alpha f_{IK}^\dagger y_K \kappa_{11,KJ}^{(1)T} - 2\alpha \kappa_{11,IK}^{(1)} y_K f_{KJ}^\dagger - 2\alpha f_{IK}^\dagger y_K \kappa_{11,KJ}^{(1)T} + 2\alpha \kappa_{11,IK}^{(1)} y_K f_{KJ}^\dagger \\ &\quad + 16\alpha^2 f_{IK}^\dagger y_K \mathcal{I}_{3,K}^{(0)} \kappa_{21,KM}^{(0)} y_M f_{MJ}^\dagger + 16\alpha^2 f_{IK}^\dagger y_K \kappa_{21,KM}^{(0)} y_M \mathcal{I}_{3,M}^{(0)} f_{MJ}^\dagger \\ &\quad - 16\alpha^2 f_{IK}^\dagger y_K \mathcal{I}_{3,K}^{(0)} \kappa_{21,KM}^{(0)} y_M f_{MJ}^\dagger - 16\alpha^2 f_{IK}^\dagger y_K \kappa_{21,KM}^{(0)} y_M \mathcal{I}_{3,M}^{(0)} f_{MJ}^\dagger. \end{aligned} \quad (3.3.58)$$

We see that the right-hand side indeed adds up to zero. Analogously, we get for the $\mathcal{O}(\varepsilon^{-2})$ -terms:

$$\begin{aligned} 0 &= -32\alpha^2 f_{IK}^\dagger y_K \kappa_{21,KM}^{(0)} y_M f_{MJ}^\dagger + 32\alpha^2 f_{IK}^\dagger y_K \kappa_{21,KM}^{(0)} y_M f_{MJ}^\dagger \\ &\quad + 32\alpha^2 f_{IK}^\dagger y_K \kappa_{21,KM}^{(0)} y_M f_{MJ}^\dagger - 32\alpha^2 f_{IK}^\dagger y_K \kappa_{21,KM}^{(0)} y_M f_{MJ}^\dagger. \end{aligned} \quad (3.3.59)$$

This equation is satisfied, too. The fact that the counterterms indeed cancel the divergences as expected, confirms our results for the counterterms as well as the integrity of the matching equation.

We now turn to the calculation of the Weinberg operator at the matching scale. Retaining only the convergent terms in Eq. (3.3.56) yields:

$$\begin{aligned}
8\alpha^2 f_{IK}^\dagger y_K g_{KM} \mathcal{I}_{1,KM} y_M f_{MJ}^\dagger \mu_{hk} &= \kappa_{W,IJ}^{(2)\dagger} - \alpha f_{IK}^\dagger y_K \mathcal{I}_{3,K}|_{\text{conv}} \kappa_{11,KJ}^{(1)T} \\
&- \alpha f_{IK}^\dagger y_K \mathcal{I}_{3,K}|_{\text{conv}} \delta \kappa_{11,KJ}^{(1)T} + \alpha \kappa_{11,IK}^{(1)} y_K \mathcal{I}_{3,K}|_{\text{conv}} f_{KJ}^\dagger \\
&+ \alpha \delta \kappa_{11,IK}^{(1)} y_K \mathcal{I}_{3,K}|_{\text{conv}} f_{KJ}^\dagger - 8\alpha^2 f_{IK}^\dagger \mathcal{I}_{3,K}|_{\text{conv}} y_K \kappa_{21,KM}^{(0)} \mathcal{I}_{3,M}|_{\text{conv}} y_M f_{MJ}^\dagger \\
&- 8\alpha^2 f_{IK}^\dagger \mathcal{I}_{3,K}|_{\text{div}} y_K \kappa_{21,KM}^{(0)} \mathcal{I}_{3,M}|_{\text{conv}} y_M f_{MJ}^\dagger \\
&- 8\alpha^2 f_{IK}^\dagger \mathcal{I}_{3,K}|_{\text{conv}} y_K \kappa_{21,KM}^{(0)} \mathcal{I}_{3,M}|_{\text{div}} y_M f_{MJ}^\dagger.
\end{aligned} \tag{3.3.60}$$

If we now plug in the result for $\delta \kappa_{11}^{(1)}$ as well as the convergent part of the loop integral $\mathcal{I}_{3,K}$, we find for $d = 4$:

$$\begin{aligned}
\kappa_{W,IJ}^{(2)\dagger} &= 8\alpha^2 f_{IK}^\dagger y_K g_{KM} \mathcal{I}_{1,KM} y_M f_{MJ}^\dagger \mu_{hk} + \alpha f_{IK}^\dagger y_K \mathcal{I}_{3,K}^{(0)} \kappa_{11,KJ}^{(1)T} \\
&- 16\alpha^2 f_{IK}^\dagger y_K \mathcal{I}_{3,K}^{(1)} \kappa_{21,KM}^{(0)} y_M f_{MJ}^\dagger - \alpha \kappa_{11,IK}^{(1)} y_K \mathcal{I}_{3,K}^{(0)} f_{KJ}^\dagger \\
&- 16\alpha^2 f_{IK}^\dagger y_K \kappa_{21,KM}^{(0)} y_M \mathcal{I}_{3,M}^{(1)} f_{MJ}^\dagger + 8\alpha^2 f_{IK}^\dagger \mathcal{I}_{3,K}^{(0)} y_K \kappa_{21,KM}^{(0)} \mathcal{I}_{3,M}^{(0)} y_M f_{MJ}^\dagger \\
&+ 16\alpha^2 f_{IK}^\dagger y_K \kappa_{21,KM}^{(0)} y_M \mathcal{I}_{3,M}^{(1)} f_{MJ}^\dagger + 16\alpha^2 f_{IK}^\dagger y_K \mathcal{I}_{3,K}^{(1)} \kappa_{21,KM}^{(0)} y_M f_{MJ}^\dagger \\
&= \alpha f_{IK}^\dagger y_K \mathcal{I}_{3,K}^{(0)} \kappa_{11,KJ}^{(1)T} - \alpha \kappa_{11,IK}^{(1)} y_K \mathcal{I}_{3,K}^{(0)} f_{KJ}^\dagger \\
&+ 8\alpha^2 f_{IK}^\dagger y_K g_{KM} \mathcal{I}_{1,KM} y_M f_{MJ}^\dagger \mu_{hk} + 8\alpha^2 f_{IK}^\dagger y_K \mathcal{I}_{3,K}^{(0)} \kappa_{21,KM}^{(0)} \mathcal{I}_{3,M}^{(0)} y_M f_{MJ}^\dagger.
\end{aligned} \tag{3.3.61}$$

Note that the terms containing $\mathcal{I}_{3,K}^{(1)}$ cancel. We anticipated this result above and therefore did not calculate the $\mathcal{O}(\varepsilon)$ -coefficient of the loop integral \mathcal{I}_3 . Our final result for the Weinberg operator reads:

$$\boxed{
\begin{aligned}
\kappa_{W,IJ}^{(2)} &= \alpha \left(f_{IK}^T \kappa_{11,KJ}^{(1)\dagger} - \kappa_{11,IK}^{(1)*} f_{KJ}^T \right) y_K \mathcal{I}_{3,K}^{(0)} \\
&+ 8\alpha^2 f_{IK} y_K \left(g_{KM}^* \mathcal{I}_{1,KM} \mu_{hk} + \mathcal{I}_{3,K}^{(0)} \kappa_{21,KM}^{(0)*} \mathcal{I}_{3,M}^{(0)} \right) y_M f_{MJ}
\end{aligned}
} \tag{3.3.62}$$

3.3.4 Mass Matrix

We saw in the previous section that in EFT- h there are seven diagrams inducing the neutrino mass matrix at two-loop order:

$$\begin{aligned}
 i\mathcal{M}_{\nu,IJ}^h \equiv & \text{Diagram 1} + \text{Diagram 2} \\
 & + \text{Diagram 3} + \text{Diagram 4} \\
 & + \text{Diagram 5} + \text{Diagram 6} \\
 & + \text{Diagram 7} .
 \end{aligned}
 \tag{3.3.63}$$

We already calculated all diagrams appearing in this equation in the previous section when performing the matching of the effective operators. The evaluation of Eq. (3.3.63) is therefore analogous to the calculations above. In particular, we saw that the divergences arising from the loop diagrams get cancelled by the counterterms. Substituting everything into Eq. (3.1.22), we arrive at the two-loop contribution to the neutrino mass matrix in EFT- h :

$$\begin{aligned}
 M_{\nu,IJ}^h = v^2 & \left[\kappa_{W,IJ}^{(2)\dagger} + \alpha \left(\kappa_{11,IK}^{(1)} f_{KJ}^\dagger - f_{IK}^\dagger \kappa_{11,KJ}^{(1)T} \right) y_K \mathcal{I}_{3,K}^{(0)} \right. \\
 & \left. - 8\alpha^2 f_{IK}^\dagger \mathcal{I}_{3,K}^{(0)} y_K \kappa_{21,KM}^{(0)} \mathcal{I}_{3,M}^{(0)} y_M f_{MJ}^\dagger \right]
 \end{aligned}
 \tag{3.3.64}$$

3.3.5 Renormalisation Group Equations

We now present the RGEs for EFT- h . We discussed at the beginning of this chapter that the RGEs of the full-theory couplings which are still present in EFT- h can be obtained from

the RGEs of the full theory presented in Sec. 3.2.2, by setting the couplings which are not existent anymore to zero, cf. Eq. (3.3.1). Indeed, one finds that no new terms containing effective couplings appear in the β -functions of full-theory couplings at one-loop order. We showed in Sec. 3.1 that we need these β -functions only at one-loop order in order to compute the running of the neutrino mass matrix at three-loop order. This is not true for the β -functions of the effective couplings: we found that we need $\beta_{\kappa_{21}}^{(1)}$, $\beta_{\kappa_{11}}^{(1)}$, $\beta_{\kappa_{21}}^{(2)}$, $\beta_{\kappa_W}^{(2)}$, and $\beta_{\kappa_W}^{(3)}$. We will compute these β -functions in what follows using the results of Sec. 3.3.2.

As in the full theory, we present the RGEs in blocks of coupled equations. The first block again consists of the β -functions of the gauge parameters. In the absence of k^{++} the β -function of g_1 changes slightly compared to the full theory. The other two β -functions stay unchanged, as k^{++} carries only a $U(1)$ -hypercharge but is a singlet under $SU(2)_L$ and $SU(3)_C$:

$$\alpha\beta_{g_1}^{(1)} = \frac{43}{10}g_1^3, \quad (3.3.65a)$$

$$\alpha\beta_{g_2}^{(1)} = -\frac{19}{6}g_2^3, \quad (3.3.65b)$$

$$\alpha\beta_{g_3}^{(1)} = -7g_3^3. \quad (3.3.65c)$$

As discussed above, the running of the Yukawa couplings can be obtained from the equations of the full theory by setting $g = 0$. Note that the terms containing the gauge parameters stay unchanged, because those terms arise solely from diagrams which contribute to the correction of the Yukawa vertices via loops containing gauge bosons and those diagrams are still present and unchanged in EFT- h . We obtain:

$$\alpha\beta_{Y_u}^{(1)} = Y_u \left[\frac{3}{2}Y_u^\dagger Y_u - \frac{3}{2}Y_d^\dagger Y_d + T - \frac{17}{20}g_1^2 - \frac{9}{4}g_2^2 - 8g_3^2 \right], \quad (3.3.66a)$$

$$\alpha\beta_{Y_d}^{(1)} = Y_d \left[-\frac{3}{2}Y_u^\dagger Y_u + \frac{3}{2}Y_d^\dagger Y_d + T - \frac{1}{4}g_1^2 - \frac{9}{4}g_2^2 - 8g_3^2 \right], \quad (3.3.66b)$$

$$\alpha\beta_{Y_e}^{(1)} = Y_e \left[\frac{3}{2}Y_e^\dagger Y_e + 2f^\dagger f + T - \frac{9}{4}g_1^2 - \frac{9}{4}g_2^2 \right], \quad (3.3.66c)$$

$$\alpha\beta_f^{(1)} = f \left[\frac{1}{2}Y_e^\dagger Y_e + 4f^\dagger f + 4\text{Tr}(f^\dagger f) - \frac{9}{10}g_1^2 - \frac{9}{2}g_2^2 \right] + \left[\frac{1}{2}(Y_e^\dagger Y_e)^T \right] f. \quad (3.3.66d)$$

Following the same reasoning, we obtain the β -functions for the remaining scalar couplings:

$$\alpha\beta_{\lambda_\phi}^{(1)} = 4\lambda_\phi T - 2T_4 + 24\lambda_\phi^2 + \lambda_{\phi h}^2 - \frac{9}{5}\lambda_\phi g_1^2 + \frac{27}{200}g_1^4 - 9\lambda_\phi g_2^2 + \frac{9}{8}g_2^4 + \frac{9}{20}g_1^2 g_2^2, \quad (3.3.67a)$$

$$\alpha\beta_{\lambda_h}^{(1)} = 16\lambda_h \text{Tr}(f^\dagger f) - 32\text{Tr}(f^\dagger f f^\dagger f) + 20\lambda_h^2 + 2\lambda_{\phi h}^2 - \frac{36}{5}\lambda_h g_1^2 + \frac{54}{25}g_1^4, \quad (3.3.67b)$$

$$\begin{aligned} \alpha\beta_{\lambda_{\phi h}}^{(1)} &= 2\lambda_{\phi h} T + 8\lambda_{\phi h} \text{Tr}(f^\dagger f) - 16\text{Tr}(f^\dagger f Y_e^\dagger Y_e) \\ &\quad + 12\lambda_\phi \lambda_{\phi h} + 8\lambda_h \lambda_{\phi h} + 4\lambda_{\phi h}^2 + \frac{27}{25}g_1^4 - \frac{9}{2}\lambda_{\phi h} g_1^2 - \frac{9}{2}\lambda_{\phi h} g_2^2. \end{aligned} \quad (3.3.67c)$$

The running of the remaining scalar mass parameters is determined by:

$$\alpha\beta_{\mu_\phi^2}^{(1)} = 2\mu_\phi^2 T + 12\lambda_\phi\mu_\phi^2 + 2\lambda_{\phi h}\mu_h^2 - \frac{9}{10}\mu_\phi^2 g_1^2 - \frac{9}{2}\mu_\phi^2 g_2^2, \quad (3.3.68a)$$

$$\alpha\beta_{\mu_h^2}^{(1)} = 8\mu_h^2 \text{Tr}(f^\dagger f) + 4\lambda_{\phi h}\mu_\phi^2 + 8\lambda_h\mu_h^2 - \frac{18}{5}\mu_h^2 g_1^2. \quad (3.3.68b)$$

Finally, we need the β -functions for the effective couplings. Let us start with $\beta_{\kappa_{21}}$. In order to apply the central Eq. (2.2.15), we need to express the bare coupling $\kappa_{21,B}$ in terms of the renormalised one which we denote by $\kappa_{21,R}$.⁴ Using the definition of $\kappa_{21,B}$ in Eq. (3.3.2f) together with the explanations in Sec. 2.2.1, we find:

$$\kappa_{21,B} = (Z_e^T)^{-\frac{1}{2}} \mu^\varepsilon (\kappa_{21,R} + \delta\kappa_{21}) (Z_e)^{-\frac{1}{2}} (Z_h)^{-1}. \quad (3.3.69)$$

Now we can use the results for the wavefunction renormalisation constants δZ_h and δZ_e as given in Eqs. (3.3.3b) and (3.3.3c) as well as the counterterm $\delta\kappa_{21}^{(1)}$ as given in Eq. (3.3.5) in Eq. (2.2.15) to obtain after some algebra the one-loop β -function of κ_{21} :

$$\alpha\beta_{\kappa_{21}}^{(1)} = 2 \left[\kappa_{21}^{(0)} Y_e Y_e^\dagger + \left(\kappa_{21}^{(0)} Y_e Y_e^\dagger \right)^T \right] + [16\text{Tr}(f^\dagger f) + 4\lambda_h + 18g_1^2] \kappa_{21}^{(0)} \quad (3.3.70)$$

Analogously, for κ_{11} , we find the relation

$$\kappa_{11,B} = (Z_L)^{-\frac{1}{2}} \mu^\varepsilon (\kappa_{11,R} + \delta\kappa_{11}) (Z_e)^{-\frac{1}{2}} (Z_h)^{-\frac{1}{2}} (Z_\phi)^{-\frac{1}{2}}, \quad (3.3.71)$$

which yields, using the one-loop counterterm $\delta\kappa_{11}^{(1)}$ from Eq. (3.3.7), the one-loop β -function

$$\alpha\beta_{\kappa_{11}}^{(1)} = 16f^\dagger Y_e^T \kappa_{21}^{(0)} \quad (3.3.72)$$

The subset of terms we have calculated of the two-loop counterterm $\delta\kappa_{11}^{(2)}$ as given in Eq. (3.3.9) yields the subset of terms of the two-loop β -function:

$$\alpha\beta_{\kappa_{11}}^{(2)} \supset \kappa_{11}^{(1)} [Y_e Y_e^\dagger] + \left[10f^\dagger f - \frac{1}{2} Y_e^\dagger Y_e + T + 4\text{Tr}(f^\dagger f) + 2\lambda_{\phi h} - \frac{23}{4} g_1^2 - \frac{9}{4} g_2^2 \right] \kappa_{11}^{(1)} \quad (3.3.73)$$

Finally, for the Weinberg operator we have:

$$\kappa_{W,B} = (Z_L^T)^{-\frac{1}{2}} \mu^\varepsilon (\kappa_{W,R} + \delta\kappa_W) (Z_L)^{-\frac{1}{2}} (Z_\phi)^{-1}. \quad (3.3.74)$$

Using $\delta\kappa_W^{(2)}$ from Eq. (3.3.11) yields the two-loop β -function:

$$\alpha\beta_{\kappa_W}^{(2)} = -2 \left[f Y_e^\dagger \kappa_{11}^{(1)\dagger} + \left(f Y_e^\dagger \kappa_{11}^{(1)\dagger} \right)^T \right] \quad (3.3.75)$$

⁴Recall that the Lagrangian given in Sec. 2.3.2 as well as in Sec. 3.3.1 is defined in terms of *bare* parameters. Note further that we consistently omitted the subscripts B there for brevity.

while the subset of terms of $\delta\kappa_{\text{W}}^{(3)}$ given in Eq. (3.3.11) yield the following terms of the three-loop β -function:

$$\alpha\beta_{\kappa_{\text{W}}}^{(3)} \supset \kappa_{\text{W}}^{(2)} \left(2f^\dagger f - \frac{3}{2} Y_e^\dagger Y_e \right) + \left[\kappa_{\text{W}}^{(2)} \left(2f^\dagger f - \frac{3}{2} Y_e^\dagger Y_e \right) \right]^T + [2T + 4\lambda_\phi - 3g_2^2] \kappa_{\text{W}}^{(2)} \quad (3.3.76)$$

These are the final results in EFT- h .

3.4 EFT- k

We now present the same calculations as we did in the previous section in EFT- h in EFT- k . This effective theory follows from the full theory by integrating out the singly charged scalar particle h^+ . Thus, only the doubly charged scalar k^{++} remains in addition to the SM, cf. Sec. 2.3.3. The residual effects of h^+ are now described by a set of effective couplings, which we will present Sec. 3.4.1. It turns out that the structure of EFT- k is much simpler, as only one effective coupling of mass dimension $\mathcal{D} = 5$, namely κ_{W} , is relevant for the mass matrix, which we will present in Sec. 3.4.3. The matching of κ_{W} is therefore comparably simple and will be discussed in in Sec. 3.4.2. Note that there appear no infinite diagrams contributing to the mass matrix or in the matching equations. Therefore, we need the counterterms only for the computation of the RGEs, which we present in Sec. 3.4.4.

3.4.1 Effective Operators

EFT- k derives from the full theory by integrating out h^+ . Therefore, we obtain the Lagrangian of EFT- k from the Lagrangian of the full theory as given in Eq. (2.3.12) by omitting the gauge-kinetic term of h^+ and by setting all couplings to h^+ to zero:

$$f = 0, \quad \mu_h^2 = 0, \quad \lambda_h = 0, \quad \lambda_{\phi h} = 0, \quad \lambda_{hk} = 0, \quad \mu_{hk} = 0. \quad (3.4.1)$$

Furthermore, we add all effective operators of mass dimension $\mathcal{D} = 5$, which follow from the SM particle content extended by k^{++} , and which are allowed by gauge symmetry. In contrast to EFT- h , one finds only one effective operator of this type, namely the Weinberg operator κ_{W} as given in Eq. (3.3.2a). In particular, there are no effective operators of mass dimension $\mathcal{D} = 5$ involving k^{++} , as there is no combination of particles which could compensate the two units of $U(1)_Y$ -hypercharge.

3.4.2 Matching

As in Sec. 3.3.3, the matching equation of the Weinberg operator arises from the condition that the neutrino mass matrices in the full theory and in EFT- k coincide. We know the

lowest order contribution in the full theory is at two-loop level, cf. Eq. (3.2.3):

$$\begin{aligned}
 i\mathcal{M}_{\nu,IJ}^{\text{ZB}} = & \quad \begin{array}{c} \text{Diagram: A two-loop diagram for } i\mathcal{M}_{\nu,IJ}^{\text{ZB}}. \text{ It features a central horizontal line with vertices } \nu_{I,L}, e_{K,L}, e_{K,R}, e_{M,R}, e_{M,L}, \nu_{J,L}. \text{ A dashed arc above the line connects } e_{K,L} \text{ and } e_{M,L} \text{ via } h^+ \text{ bosons. A vertical dashed line connects } e_{K,R} \text{ and } e_{M,R} \text{ via } k^{++} \text{ boson. Two vertical dashed lines connect } e_{K,L} \text{ and } e_{M,L} \text{ to } \langle \phi \rangle \text{ lines. A long horizontal arrow below the line points left.} \end{array} \quad (3.2.3) \\
 = & -8i\alpha^2 v^2 \mu_{hk} f_{IK}^\dagger y_K g_{KM} \mathcal{I}_{1,KM} y_M f_{MJ}^\dagger P_R.
 \end{aligned}$$

In EFT- k , we only have the contribution of the Weinberg operator Eq. (3.3.47) at this order, since, in contrast to EFT- h , there are no effective couplings which are switched on at tree level or at one-loop level:

$$\begin{aligned}
 i\mathcal{M}_{k,1,IJ}^{(2)} \equiv & \quad \begin{array}{c} \text{Diagram: A Weinberg operator diagram. A central square vertex is connected to } \nu_{I,L} \text{ and } \nu_{J,L} \text{ by solid lines. Two dashed lines connect the vertex to } \langle \phi \rangle \text{ lines. A long horizontal arrow below the vertex points left.} \end{array} \quad (3.3.47) \\
 = & -iv^2 \kappa_{\text{W},IJ}^{(2)\dagger} P_R.
 \end{aligned}$$

We are now ready to evaluate the matching equations arising from comparing the coefficients of the α -expansions of the neutrino mass matrix in the full theory as well as in EFT- k . As there are no diagrams at tree level or at one-loop level in the full theory contributing to the mass matrix, we immediately find:

$$\boxed{\kappa_{\text{W}}^{(0)} = \kappa_{\text{W}}^{(1)} = 0} \quad (3.4.2)$$

Equating the α^2 -coefficients leads to the equation:

$$i\mathcal{M}_{\nu,IJ}^{\text{ZB}} \stackrel{!}{=} i\mathcal{M}_{k,1,IJ}^{(2)}. \quad (3.4.3)$$

Plugging in the results of the above diagrams, this equation yields:

$$\boxed{\kappa_{\text{W},IJ}^{(2)} = \frac{1}{v^2} (M_{\nu,IJ}^{\text{ZB}})^\dagger = 8i\alpha^2 \mu_{hk} f_{IK} y_K g_{KM}^* \mathcal{I}_{1,KM} y_M f_{MJ}} \quad (3.4.4)$$

3.4.3 Mass Matrix

In EFT- k the neutrino mass matrix at two-loop order is given only by the Weinberg operator:

$$\begin{aligned}
 i\mathcal{M}_{\nu,IJ}^k \equiv & \quad \begin{array}{c} \text{Diagram: A Weinberg operator diagram. A central square vertex is connected to } \nu_L \text{ and } \nu_L \text{ by solid lines. Two dashed lines connect the vertex to } \langle \phi \rangle \text{ lines. A long horizontal arrow below the vertex points left.} \end{array} \quad (3.4.5) \\
 = & -iv^2 \kappa_{\text{W},IJ}^{(2)\dagger} P_R.
 \end{aligned}$$

Using this in Eq. (3.1.22), we find:

$$\boxed{M_{\nu,IJ}^k = v^2 \kappa_{\text{W},IJ}^{(2)\dagger}} \quad (3.4.6)$$

3.4.4 Renormalisation Group Equations

As was done in Sec. 3.3.5, we can deduce the RGEs of all full-theory couplings by applying Eq. (3.4.1) to the RGEs of the full theory as given in Sec. 3.2.2. In addition, we need the β -function of the effective coupling κ_W at three-loop order, cf. Sec. 3.1. To compute it, we need the wavefunction renormalisation constants $\delta Z_\phi^{(1)}$, $\delta Z_L^{(1)}$, as well as the counterterm $\delta\kappa_W^{(3)}$. We present their calculations first and use the results afterwards to compute the β -functions.

Wavefunction Renormalisation Constants and Counterterm

The wavefunction renormalisation constants can be deduced from the ones calculated in the full theory in Sec. 3.2.3 by applying Eq. (3.4.1). This yields:

$$\delta Z_\phi^{(1)} = -\alpha \left[2T - \frac{1}{2}(3 - \xi_1)g_1^2 - \frac{3}{2}(3 - \xi_2)g_2^2 \right] \frac{1}{\varepsilon} \quad (3.4.7a)$$

$$\delta Z_L^{(1)} = -\alpha \left[Y_e^\dagger Y_e + \frac{1}{2}\xi_1 g_1^2 + \frac{3}{2}\xi_2 g_2^2 \right] \frac{1}{\varepsilon} \quad (3.4.7b)$$

Similarly, the computation of the counterterm $\delta\kappa_W$ of the Weinberg operator is greatly simplified, as we already computed all relevant diagrams in EFT- h in Sec. 3.3.2. Indeed, let us first have a look at the analogue of Eq. (3.3.10) in EFT- k . The loop diagrams depicted there contain κ_{21} as well as κ_{11} and are therefore not existent in EFT- k . Furthermore, note that there are no additional diagrams containing k^{++} contributing at this order. Therefore, we find:

$$\delta\kappa_W^{(2)} = 0 \quad (3.4.8)$$

This was to be expected, as we already discussed in Sec. 3.1 that counterterms of effective couplings may only have contributions at the same loop order at which the effective coupling itself is switched on if we have other, lower-order, effective couplings at our disposal. These can then be used in loop diagrams to give contributions at the relevant order. This is what happened in EFT- h for both κ_{11} and κ_W . In contrast, in EFT- k , we have only one single effective coupling κ_W , which is switched on at two-loop order, thus leading to $\delta\kappa_W$ starting *beyond* two-loop order.

All diagrams depicted in Eq. (3.3.12) are also present in EFT- k , with the exception of the two- and three-loop diagrams. Indeed, in EFT- k , we do not have to consider these two- and three-loop diagrams, as they contain the effective couplings κ_{21} and κ_{11} which are not present in EFT- k . Furthermore, there are again no additional diagrams containing k^{++} to consider here. Therefore, all three-loop contributions to the counterterm of κ_W in EFT- k come from the one-loop diagrams depicted in Eq. (3.3.12). Using these observations in

Eq. (3.3.13) together with Eq. (3.4.8) yields the result:

$$\delta\kappa_{\mathbb{W}}^{(3)} = \alpha \left\{ -2 \left[\kappa_{\mathbb{W}}^{(2)} Y_e^\dagger Y_e + \left(\kappa_{\mathbb{W}}^{(2)} Y_e^\dagger Y_e \right)^T \right] + \left[4\lambda_\phi + \left(\frac{3}{2} - \xi_1 \right) g_1^2 + \left(\frac{3}{2} - 3\xi_2 \right) g_2^2 \right] \kappa_{\mathbb{W}}^{(2)} \right\} \frac{1}{\varepsilon} \quad (3.4.9)$$

RGEs

We are now ready to compute the RGEs of EFT- k .

As was the case in EFT- h , the β -function of the gauge coupling g_1 changes slightly, while the β -functions of g_2 and g_3 stay unchanged in comparison to the full theory:

$$\alpha\beta_{g_1}^{(1)} = \frac{49}{10}g_1^3, \quad (3.4.10a)$$

$$\alpha\beta_{g_2}^{(1)} = -\frac{19}{6}g_2^3, \quad (3.4.10b)$$

$$\alpha\beta_{g_3}^{(1)} = -7g_3^3. \quad (3.4.10c)$$

For the running of the remaining Yukawa couplings we get:

$$\alpha\beta_{Y_u}^{(1)} = Y_u \left[\frac{3}{2}Y_u^\dagger Y_u - \frac{3}{2}Y_d^\dagger Y_d + T - \frac{17}{20}g_1^2 - \frac{9}{4}g_2^2 - 8g_3^2 \right], \quad (3.4.11a)$$

$$\alpha\beta_{Y_d}^{(1)} = Y_d \left[-\frac{3}{2}Y_u^\dagger Y_u + \frac{3}{2}Y_d^\dagger Y_d + T - \frac{1}{4}g_1^2 - \frac{9}{4}g_2^2 - 8g_3^2 \right], \quad (3.4.11b)$$

$$\alpha\beta_{Y_e}^{(1)} = Y_e \left[\frac{3}{2}Y_e^\dagger Y_e + T - \frac{9}{4}g_1^2 - \frac{9}{4}g_2^2 \right] + [2gg^\dagger] Y_e, \quad (3.4.11c)$$

$$\alpha\beta_g^{(1)} = g \left[(Y_e Y_e^\dagger)^T + 4g^\dagger g + 2\text{Tr}(g^\dagger g) - \frac{18}{5}g_1^2 \right] + [Y_e Y_e^\dagger] g. \quad (3.4.11d)$$

The β -functions of the remaining scalar couplings read:

$$\alpha\beta_{\lambda_\phi}^{(1)} = 4\lambda_\phi T - 2T_4 + 24\lambda_\phi^2 + \lambda_{\phi k}^2 - \frac{9}{5}\lambda_\phi g_1^2 + \frac{27}{200}g_1^4 - 9\lambda_\phi g_2^2 + \frac{9}{8}g_2^4 + \frac{9}{20}g_1^2 g_2^2, \quad (3.4.12a)$$

$$\alpha\beta_{\lambda_k}^{(1)} = 8\lambda_k \text{Tr}(g^\dagger g) - 16\text{Tr}(g^\dagger g g^\dagger g) + 20\lambda_k^2 + 2\lambda_{\phi k}^2 - \frac{144}{5}\lambda_k g_1^2 + \frac{864}{25}g_1^4, \quad (3.4.12b)$$

$$\alpha\beta_{\lambda_{\phi k}}^{(1)} = 2\lambda_{\phi k} T + 4\lambda_{\phi k} \text{Tr}(g^\dagger g) - 16\text{Tr}(g g^\dagger Y_e Y_e^\dagger) + 12\lambda_\phi \lambda_{\phi k} + 8\lambda_k \lambda_{\phi k} + 4\lambda_{\phi k}^2 + \frac{108}{25}g_1^4 - \frac{153}{10}\lambda_{\phi k} g_1^2 - \frac{9}{2}\lambda_{\phi k} g_2^2. \quad (3.4.12c)$$

The running of the remaining scalar mass parameters is given by:

$$\alpha\beta_{\mu_\phi^2}^{(1)} = 2\mu_\phi^2 T + 12\lambda_\phi \mu_\phi^2 + 2\lambda_{\phi k} \mu_k^2 - \frac{9}{10}\mu_\phi^2 g_1^2 - \frac{9}{2}\mu_\phi^2 g_2^2, \quad (3.4.13a)$$

$$\alpha\beta_{\mu_k^2}^{(1)} = 4\mu_k^2 \text{Tr}(g^\dagger g) + 4\lambda_{\phi k} \mu_\phi^2 + 8\lambda_k \mu_k^2 - \frac{72}{5}\mu_k^2 g_1^2. \quad (3.4.13b)$$

Note that we do not need the running of μ_ϕ^2 for the calculation of the running of the neutrino mass matrix. Nevertheless, as explained above, we calculate the running of all model parameters in order to check if they run out of physically sensible ranges.

Finally, for the β -function of the Weinberg operator we find, using Eq. (3.3.74) together with Eqs. (3.4.7), (3.4.8), and (3.4.9) in Eq. (2.2.15):

$$\beta_{\kappa_W}^{(2)} = 0 \quad (3.4.14a)$$

$$\alpha\beta_{\kappa_W}^{(3)} = -\frac{3}{2} \left[\kappa_W^{(2)} Y_e^\dagger Y_e + \left(\kappa_W^{(2)} Y_e^\dagger Y_e \right)^T \right] + [2T + 4\lambda_\phi - 3g_2^2] \kappa_W^{(2)} \quad (3.4.14b)$$

At first glance, this result is interesting as it does not contain the Yukawa coupling g . In contrast, in EFT- h , the function $\beta_{\kappa_W}^{(3)}$ does contain the Yukawa coupling f , which entered solely through δZ_L . As k^{++} does not couple to L_L , it was to be expected that g would not appear in $\beta_{\kappa_W}^{(3)}$ in EFT- k . Nevertheless, note that the running of κ_W is influenced indirectly by the running of g , as this influences the running of Y_e , T , and λ_ϕ .

3.5 EFT-0

In the last part of this chapter, we will present the neutrino mass matrix and the RGEs in EFT-0, which we obtain by integrating out both BSM particles h^+ and k^{++} . We therefore end up with the SM particle content described by the Lagrangian given in Eq. (2.1.3). The residual effects of the charged scalars are described by the Weinberg operator κ_W as given in Eq. (3.3.2a). In this respect, EFT-0 does not differ from EFT- k . It follows that the computations in both EFT- k and EFT-0 are pretty much the same. Therefore, we will only present the final results without unnecessary detailed remarks.

3.5.1 Matching

Recall from Sec. 2.3.3 that we have to distinguish two cases for the matching in EFT-0, depending on whether we have derived it from EFT- h or EFT- k . Although in both cases the resulting EFT-0 is described by the same Lagrangian, the matching conditions are formally different, leading to different initial parameter configurations. We distinguish these two cases by the names EFT-0 h (if we came from EFT- h) and EFT-0 k (if we came from EFT- k). In both cases, the form of the matching equation coincides with Eq. (3.4.4). In particular, the Weinberg operator is switched on at two-loop level, which was to be expected, cf. Eq. (3.4.2).

EFT-0 h

In EFT-0 h , the matching condition is that the neutrino mass matrix in EFT- h coincides with the neutrino mass matrix in EFT-0 h , which is given solely by the Weinberg operator

at two-loop level. This leads to:

$$\boxed{\kappa_{\mathbb{W},IJ}^{(2)} = \frac{1}{v^2} (M_{\nu,IJ}^h)^\dagger} \quad (3.5.1)$$

Here, $M_{\nu,IJ}^h$ is given in Eq. (3.3.64).

EFT-0k

Analogously, in EFT-0k we have:

$$\boxed{\kappa_{\mathbb{W},IJ}^{(2)} = \frac{1}{v^2} (M_{\nu,IJ}^k)^\dagger} \quad (3.5.2)$$

Now, $M_{\nu,IJ}^k$ is given in Eq. (3.4.6).

3.5.2 Mass Matrix

In the previous section, we already used the fact that, in EFT-0, the neutrino mass matrix $M_{\nu,IJ}^0$ at two-loop order is given solely by the Weinberg operator. This yields:

$$\boxed{M_{\nu,IJ}^0 = v^2 \kappa_{\mathbb{W},IJ}^{(2)\dagger}} \quad (3.5.3)$$

3.5.3 Renormalisation Group Equations

The RGEs of full-theory couplings which are still present in EFT-0 can be obtained from the RGEs of the full theory by applying both Eqs. (3.3.1) and (3.4.1), leading to the well-known RGEs of the SM couplings. Furthermore, as already noted, there is no formal difference between the calculation of the counterterm of the Weinberg operator in EFT-0 compared to EFT-k, so we can re-use the result from Eq. (3.4.9) to compute the β -function of the Weinberg operator. These considerations lead to the following RGEs in EFT-0.

The running of the gauge couplings is given by the β -functions of the SM:

$$\alpha\beta_{g_1}^{(1)} = \frac{41}{10}g_1^3, \quad (3.5.4a)$$

$$\alpha\beta_{g_2}^{(1)} = -\frac{19}{6}g_2^3, \quad (3.5.4b)$$

$$\alpha\beta_{g_3}^{(1)} = -7g_3^3. \quad (3.5.4c)$$

For the remaining Yukawa-couplings we have:

$$\alpha\beta_{Y_u}^{(1)} = Y_u \left[\frac{3}{2}Y_u^\dagger Y_u - \frac{3}{2}Y_d^\dagger Y_d + T - \frac{17}{20}g_1^2 - \frac{9}{4}g_2^2 - 8g_3^2 \right], \quad (3.5.5a)$$

$$\alpha\beta_{Y_d}^{(1)} = Y_d \left[-\frac{3}{2}Y_u^\dagger Y_u + \frac{3}{2}Y_d^\dagger Y_d + T - \frac{1}{4}g_1^2 - \frac{9}{4}g_2^2 - 8g_3^2 \right], \quad (3.5.5b)$$

$$\alpha\beta_{Y_e}^{(1)} = Y_e \left[\frac{3}{2}Y_e^\dagger Y_e + T - \frac{9}{4}g_1^2 - \frac{9}{4}g_2^2 \right]. \quad (3.5.5c)$$

The β -function of the Higgs self-coupling is given by:

$$\alpha\beta_{\lambda_\phi}^{(1)} = 4\lambda_\phi T - 2T_4 + 24\lambda_\phi^2 - \frac{9}{5}\lambda_\phi g_1^2 + \frac{27}{200}g_1^4 - 9\lambda_\phi g_2^2 + \frac{9}{8}g_2^4 + \frac{9}{20}g_1^2 g_2^2. \quad (3.5.6)$$

We obtain for the running of the Higgs mass parameter:

$$\alpha\beta_{\mu_\phi^2}^{(1)} = 2\mu_\phi^2 T + 12\lambda_\phi \mu_\phi^2 - \frac{9}{10}\mu_\phi^2 g_1^2 - \frac{9}{2}\mu_\phi^2 g_2^2. \quad (3.5.7)$$

Finally, the β -function of κ_W reads:

$$\beta_{\kappa_W}^{(2)} = 0 \quad (3.5.8a)$$

$$\alpha\beta_{\kappa_W}^{(3)} = -\frac{3}{2} \left[\kappa_W^{(2)} Y_e^\dagger Y_e + \left(\kappa_W^{(2)} Y_e^\dagger Y_e \right)^T \right] + [2T + 4\lambda_\phi - 3g_2^2] \kappa_W^{(2)} \quad (3.5.8b)$$

This result coincides with the one given in Refs. [35, 88].

Numerical Results

In this chapter we present the results obtained by processing the equations from the previous chapter numerically. In particular, we discuss the numerical solution of the RGEs of the Zee-Babu model in some detail. This yields the running of the neutrino mass matrix and thus the running of the neutrino masses and leptonic mixing angles. We start with describing how these parameters can be extracted from the neutrino mass matrix and subsequently turn to the numerical solution of the RGEs. Finally, we present the results for some sample initial parameter configurations in a top-down approach.

4.1 Evaluation of the Neutrino Mass Matrix

As discussed in Sec. 2.1.2, neutrino masses as well as leptonic mixing angles and phases are encoded in the neutrino mass matrix M_ν . In the Zee-Babu model neutrinos acquire a mass term of Majorana type, which is why M_ν is (complex) symmetric. Such a matrix can be diagonalised using a single unitary matrix U (in contrast to the bi-unitary diagonalisation of general complex matrices),

$$U^T M_\nu U = D_\nu = \text{diag}(m_1, m_2, m_3), \quad (4.1.1)$$

yielding three real and positive diagonal entries m_i representing the neutrino masses. This is known as *Takagi factorisation* [27]. We used the algorithm described in Ref. [92] to perform this factorisation numerically.

Recall from Sec. 3.2.1 that, in the Zee-Babu model, one neutrino is exactly massless at leading order. Thus, assuming normal ordering, we have

$$D_\nu = \text{diag}(0, m_2, m_3), \quad (4.1.2)$$

with $m_2 \ll m_3$ according to experimental data [16]. In our numerical treatment, we will always assume normal ordering. However, the analysis can easily be adapted to the case of inverted ordering.

We work in a basis where the charged lepton Yukawa matrix Y_e is diagonal. We know from above that in this case the matrix U is in fact the PMNS-matrix U^{PMNS} , which contains information on the leptonic mixing angles θ_{12} , θ_{13} , and θ_{23} , as well as on the Dirac and Majorana phases. In our numerical treatment, we focused on the running of the mixing angles, which can be extracted from the PMNS-matrix via the following equations [28]:

$$\theta_{13} = \arcsin(|U_{13}|), \quad (4.1.3a)$$

$$\theta_{12} = \begin{cases} \arctan\left(\frac{|U_{12}|}{|U_{11}|}\right) & \text{if } U_{11} \neq 0, \\ \frac{\pi}{2} & \text{otherwise,} \end{cases} \quad (4.1.3b)$$

$$\theta_{23} = \begin{cases} \arctan\left(\frac{|U_{23}|}{|U_{33}|}\right) & \text{if } U_{33} \neq 0, \\ \frac{\pi}{2} & \text{otherwise.} \end{cases} \quad (4.1.3c)$$

These equations follow from the standard parameterisation of the PMNS-matrix as given in Eq. (2.1.40).

4.2 Solution of the RGEs

We start the discussion of the numerical solution of the RGEs by describing some approximations, which make the numerical computations less costly, without reducing the accuracy of the results significantly. Then, we discuss the problem of finding sensible initial values for the running parameters in a top-down approach. As we will see, this is a rather delicate issue, since not all parameters are fixed at the same energy scale.

4.2.1 Simplification and Solution of the RGEs

Due to the large number of coupled equations, the numerical solution of the full set of RGEs may be numerically expensive. Particularly, the block of β -functions for the Yukawa couplings represents a large set of coupled RGEs. Fortunately, one can safely neglect the running of all the SM Yukawa couplings except for the top-quark coupling y_t . This is justified because y_t is much larger than all the other SM Yukawa couplings [14, 17, 93]. Thus we can fix those Yukawa couplings at their measured values and keep them constant during the running. As we basically do not know anything about the strength of the BSM Yukawa couplings f and g , we cannot neglect their running a priori. Furthermore, based on the measured values, we neglect terms containing Y_e^2 and Y_d^2 compared to g_i^2 on the right-hand side of the RGEs. The resulting simplified RGEs are summarised in App. D.

The solution of the simplified RGEs turns out to be quite harmless from a numerical point of view. Indeed, the usage of standard numerical routines for non-stiff ODEs yields fast and stable results. However, we would like to point out one exception: for parameter configurations with large differences between the dimensionful parameters μ_ϕ^2 , μ_h^2 , μ_k^2 , and μ_{hk} , the running of these parameters is generically very strong. This issue is well-known in the SM setting as the *hierarchy problem*, and discussed in great detail in Ref. [94]. Although

we did not inspect such cases in detail in this thesis, one presumably has to resort to stiff ODE-solvers in such settings due to the big difference in the dynamics of the running of different parameters.

4.2.2 Initial Values for the RGEs

We discussed in Sec. 2.3.3 the top-down approach of RG running: we want to investigate whether we can find a parameter configuration of the Zee-Babu model at the high energy scale μ_{GUT} , which on the one hand corresponds to a bimaximal leptonic mixing pattern at μ_{GUT} , and on the other hand reproduces the available data of neutrino measurements at the low scale μ_{EW} .¹ The parameter configurations at the high and low energy scales are connected via the RGEs. In this section we want to discuss in detail the procedure of finding suitable initial values for the RGEs of the full theory at μ_{GUT} . Note that the initial values for the RGEs in the EFTs are fixed by the matching equations.

The Connection of the BSM parameters to the Leptonic Mixing Pattern

Let us first discuss how we have to choose the BSM parameters of the Zee-Babu model in order to end up with a given leptonic mixing pattern specified by the three mixing angles θ_{12} , θ_{13} , and θ_{23} . We will eventually use the resulting equations to fix a bimaximal mixing pattern at μ_{GUT} .

The mixing pattern is encoded in the neutrino mass matrix which is given in the Zee-Babu model by Eq. (3.2.3):

$$M_{\nu, IJ}^{\text{ZB}} = 8\alpha^2 v^2 \mu_{hk} f_{IK}^\dagger y_K g_{KM} \mathcal{I}_{1, KM} y_M f_{MJ}^\dagger. \quad (3.2.3)$$

It is clear that the BSM parameters contained in this equation, namely f , g , μ_{hk} , as well as the scalar masses m_h and m_k (through \mathcal{I}_1), are not fixed completely by a given mass matrix M_{ν}^{ZB} . This can be seen by counting the number of parameters on both sides of the above equation: as described in Secs. 2.1.2 and 3.2.1, M_{ν}^{ZB} is parameterised by 2 mass eigenvalues, 3 angles, and 2 phases, yielding a total of 7 real parameters. In contrast, f , g , μ_{hk} , m_h , and m_k constitute 12 moduli and 5 phases, i.e., 17 real parameters. Therefore, we expect to find that a given mixing pattern does not fix 10 of those 17 BSM parameters.

¹We also noted in Sec. 2.3.3 that the parameters have to stay confined to physically meaningful bounds on the way down from the high to the low scale. For example, the scalar potential has to be bounded from below at every energy value. Furthermore, all equations derived in this thesis only make sense for small values of the couplings as otherwise perturbativity would be violated. In Ref. [17] these constraints are quantified for the Zee-Babu model. However, in our numerical treatment, we focused on a basic investigation of the running of neutrino masses and leptonic mixing angles and did not consider these issues in detail. We only remark that particularly vacuum stability seems to be a delicate issue in the Zee-Babu model, as we found that the quartic scalar self-couplings λ_ϕ , λ_h and λ_k have the tendency to attain negative values during the running. Furthermore, we would like to point out that our results are taylormade for an extended analysis including checks for such range violations, since we deduced the RGEs of *all* model parameters in Chap. 3. Thus, using our equations, one can check at every single energy value if the current parameter configuration is physically reasonable. If not, one can immediately discard the corresponding initial values.

To make the basic structure of the mass matrix more evident, let us rewrite Eq. (3.2.3) in the following form [16, 17]:²

$$M_\nu^{\text{ZB}} = \zeta f^\dagger \omega f^\dagger. \quad (4.2.1)$$

Here we have defined:

$$\zeta \equiv 8\alpha^2 v^2 \mu_{hk}, \quad (4.2.2a)$$

$$\omega_{IJ} \equiv y_I g_{IJ} \mathcal{I}_{1,IJ} y_J. \quad (4.2.2b)$$

Note that, in the definition of ω , no summation over family indices is involved. Thus, we can solve for g given ω and \mathcal{I}_1 .

As f^\dagger is antisymmetric, $\det f^\dagger = 0$, and we have an eigenvector v_0 of f^\dagger with zero eigenvalue:

$$v_0 = (1, -\xi, \xi')^T. \quad (4.2.3)$$

Here, ξ and ξ' are given by the ratios:

$$\xi \equiv \frac{f_{e\tau}^\dagger}{f_{\mu\tau}^\dagger}, \quad \xi' \equiv \frac{f_{e\mu}^\dagger}{f_{\mu\tau}^\dagger}. \quad (4.2.4)$$

Note that our choice of $f_{\mu\tau}$ as normalisation is arbitrary. Clearly, we could have used any other element of f here.

We multiply Eq. (4.2.1) from the right with v_0 to obtain:

$$M_\nu^{\text{ZB}} v_0 = 0. \quad (4.2.5)$$

This is the central equation of this section: given any valid mass matrix of the Zee-Babu model, i.e., given any complex symmetric matrix M_ν^{ZB} with $\det M_\nu^{\text{ZB}} = 0$, we can solve for f in terms of the mixing angles θ_{12} , θ_{13} , θ_{23} , and the Dirac phase δ . To this end, consider the Takagi factorisation of the mass matrix,

$$M_\nu^{\text{ZB}} = U^* D_\nu U^\dagger, \quad (4.2.6)$$

with U the PMNS-matrix as described in Sec. 4.1. The following depends on the mass hierarchy we impose at the high scale, i.e., on the entries of the diagonal matrix D_ν . In this thesis, we consider normal ordering as given in Eq. (4.1.2). Our procedure can be easily

²Note that we cannot employ the *Casas-Ibarra parameterisation* [38, 88, 95] here. Indeed, the structure of the neutrino mass matrix in the Zee-Babu model is more complicated than in the models where the Casas-Ibarra parameterisation is useful, like in seesaw-type scenarios or the scotogenic model. Indeed, the structure of the neutrino mass matrix in such models is $M \sim h^T \Lambda h$, with Λ a given matrix and h one *single* Yukawa matrix we want to solve for. In particular, h does not have any symmetry properties. In contrast, in the Zee-Babu model, *two* unknown Yukawa matrices f and g are involved. Additionally, f is defined to be antisymmetric and g is defined to be symmetric. The Casas-Ibarra parameterisation does not allow to solve for the unknown Yukawa matrices in this case.

adapted to the case of inverted ordering. Substituting Eqs. (4.2.6), (4.1.2), and (2.1.40) into Eq. (4.2.5), we obtain:

$$\xi = \frac{\cos \theta_{23}}{\cos \theta_{13}} \tan \theta_{12} + \tan \theta_{13} \sin \theta_{23} e^{i\delta}, \quad (4.2.7a)$$

$$\xi' = \frac{\sin \theta_{23}}{\cos \theta_{13}} \tan \theta_{12} - \tan \theta_{13} \sin \theta_{23} e^{i\delta}. \quad (4.2.7b)$$

Therefore, after fixing any real³ $f_{\mu\tau}$, the Yukawa matrix f is completely determined by the mixing angles and by the Dirac phase.

Finally, we can fix any three (complex) elements of ω as well as the real parameter ζ (or, equivalently, μ_{hk}) and use Eq. (4.2.1) to solve for the remaining three elements of ω . For example, if we fix ω_{ee} , $\omega_{e\mu}$, and $\omega_{e\tau}$ we find:

$$\omega_{\mu\mu} = -\frac{1}{\zeta} M_{\nu,\tau\tau}^{\text{ZB}} - 2\omega_{e\mu}\xi - \omega_{ee}\xi^2, \quad (4.2.8a)$$

$$\omega_{\mu\tau} = +\frac{1}{\zeta} M_{\nu,\mu\tau}^{\text{ZB}} - \omega_{e\tau}\xi + \omega_{e\mu}\xi' + \omega_{ee}\xi\xi', \quad (4.2.8b)$$

$$\omega_{\tau\tau} = -\frac{1}{\zeta} M_{\nu,\mu\mu}^{\text{ZB}} - 2\omega_{e\tau}\xi' - \omega_{ee}\xi'^2. \quad (4.2.8c)$$

Having computed ω , the Yukawa matrix g is fixed after choosing scalar masses m_h and m_k (and thus fixing \mathcal{I}_1) by Eq. (4.2.2b).

Note that, as expected, we found that 10 BSM parameters are not fixed by specifying the leptonic mixing pattern: we are free to choose one real entry of f , 3 complex entries of ω (and therefore of g) as well as the 3 real parameters μ_{hk} , m_h , and m_k .

Initialising the RGEs in a Top-Down Approach

We discussed in the previous section that imposing a bimaximal mixing pattern at μ_{GUT} only fixes a subset of the elements of the Yukawa matrices f and g , while leaving the other BSM parameters unconstrained. These unconstrained parameters span the space which has to be scanned for configurations which lead to the measured neutrino masses and leptonic mixing angles at the low scale as given in Sec. 2.1.2. However, these are not the only running parameters which are fixed by experiment at the low scale. Indeed, the SM parameters listed in Tab. 4.1 also enter the neutrino mass matrix in our setting.

In summary, we are facing the situation that some of the running parameters are fixed at the high scale, others at the low scale, and the mixing angles at both scales. This requirement makes the numerical treatment of the RGEs somewhat more involved compared to a pure initial value problem, where all quantities are given at the *same* energy scale. However, we came up with a heuristic procedure for finding initial values at μ_{GUT} that works rather well: for the SM parameters listed in Tab. 4.1, we start with the measured values at the low scale and run them *up* to the high scale using the RGEs

³We know from Sec. 2.3.2 that f contains only two physical phases, allowing us to choose $f_{\mu\tau}$ real.

Parameter	Value	Unit
$\sqrt{3/5}g_1$	0.357	-
g_2	0.652	-
g_3	1.22	-
y_t	0.995	-
λ_ϕ	0.129	-
μ_ϕ^2	$-7.81 \cdot 10^{+3}$	GeV ²

Table 4.1: Measured values [26] of those SM parameters of which we inspect the running because they enter the neutrino mass matrix. We only specify the values we used in the numerical calculations and suppress information about the precision of the measurements.

of the *full theory*.⁴ Afterwards, we use the resulting high-scale values as initial values in the top-down run. Clearly, this is not correct, as we should use the RGEs of the EFTs at low energies. However, this is not possible due to our ignorance of the mass thresholds of the scalars h^+ and k^{++} in a bottom-up run. Nevertheless, we found that using the “wrong” RGEs introduces no substantial error in most cases. This can be easily verified by checking that one hits the measured values (with deviations that lie within the experimental uncertainties) at the low scale in the subsequent top-down run again.

Now that we found suitable high-scale initial values for all relevant SM couplings, we are well-prepared to scan the parameter space of the free BSM couplings at the high scale for values, which lead to the measured neutrino masses and leptonic mixing angles at the low scale.

4.3 Discussion of the Results

We now present the results of the numerical evaluation of the running of the neutrino masses and leptonic mixing angles. A full scan of the space of free BSM parameters was beyond the scope of this thesis as this space has very high dimension. Nevertheless, we found initial parameter configurations at μ_{GUT} from which the running leads to values at μ_{EW} quite close to the measured ones. These results indicate that the running in the Zee-Babu model might indeed explain the deviation of neutrino data from a bimaximal mixing pattern. Furthermore, our results may serve as useful seed configurations for a more extensive parameter scan, which may be able to answer this question conclusively.

As explained in the previous section, there are plenty of free BSM parameters at the high scale. These are the dimensionless quartic scalar couplings λ_h , λ_k , $\lambda_{\phi h}$, $\lambda_{\phi k}$, and

⁴For the gauge parameters g_1 , g_2 , and g_3 , as well as for the top-quark coupling y_t , this procedure is trivial as these couplings do not depend on BSM parameters, which are fixed at the high scale. However, the RGEs of the quartic Higgs coupling λ_ϕ and the Higgs mass parameter μ_ϕ^2 do depend on the solutions of (or are coupled to) RGEs of BSM parameters. Thus, in practice, we performed several interlaced top-down and bottom-up runs. However, this is only a minor practical issue and thus we provide a simplified explanation in order to convey the general idea more clearly.

Parameter	Value	Unit
μ_{hk}	11	GeV
m_h	180	GeV
m_k	255	GeV
Δm_{21}^2	$5.5 \cdot 10^{-5}$	eV ²
Δm_{32}^2	$3.9 \cdot 10^{-3}$	eV ²

Table 4.2: Initial parameter configuration at the high scale leading to the EFT-route “full theory \rightarrow EFT- h \rightarrow EFT- $0h$ ” and the running displayed in Fig. 4.1.

λ_{hk} , as well as the Yukawa couplings $f_{\mu\tau}$, g_{ee} , $g_{e\mu}$, and $g_{e\tau}$. In addition, there are the dimensionful quantities μ_{hk} , m_h , m_k , and the two neutrino mass eigenvalues m_2 and m_3 .

We performed a scan of this high-dimensional parameter space, which we chose to constrain by fixing the aforementioned quartic scalar and Yukawa couplings all to the same value of 0.1 at μ_{GUT} . This choice is motivated by the constraints on perturbativity and vacuum stability given in Ref. [17]. However, the running is very sensitive to variations in these initial values, which is why they need to be included in a full parameter scan.

To summarise, we varied only the initial values of the dimensionful scalar parameters μ_h^2 , μ_k^2 , μ_{hk} , as well as the neutrino mass splittings Δm_{21}^2 and Δm_{32}^2 . Given the latter, also the neutrino masses m_2 and m_3 are fixed, since one neutrino is massless in the Zee-Babu model, $m_1 = 0$, given that we consider the case of normal hierarchy. As was to be expected from our discussion in the context of the hierarchy problem, the running of the neutrino parameters is very sensitive to variations of these dimensionful quantities.

EFT-route: “full theory \rightarrow EFT- h \rightarrow EFT- $0h$ ” Fig. 4.1 shows the running of the neutrino masses and leptonic mixing angles for the initial parameter configuration given in Tab. 4.2. This configurations leads to the EFT-route

$$\text{full theory} \rightarrow \text{EFT-}h \rightarrow \text{EFT-}0h,$$

i.e., k^{++} hits its mass threshold before h^+ does. Therefore, k^{++} has to be integrated out first. This was to be expected, since we adjusted for m_k to be significantly larger than m_h at μ_{GUT} . This must not be taken as a general rule, though, since there might be alternative initial values leading to a running in which the scalar mass parameters cross between the high and the low scale.

As is evident from Fig. 4.1a, we hit the measured 3σ -ranges of the mixing angles θ_{23} and θ_{13} . This indicates that in the Zee-Babu model the running might indeed explain the deviation of the measured mixing angles from a bimaximal mixing pattern. The fact that the mixing angle θ_{12} shows barely any running and therefore does not hit its measured value does not have to contradict this assumption, as we only scanned a small part of the free BSM parameter space. There might well be different initial values featuring a stronger running of θ_{12} . However, if one finds this not to be the case, one should look for a structural argument, which explains why in the Zee-Babu model strong running of θ_{12} is prohibited.

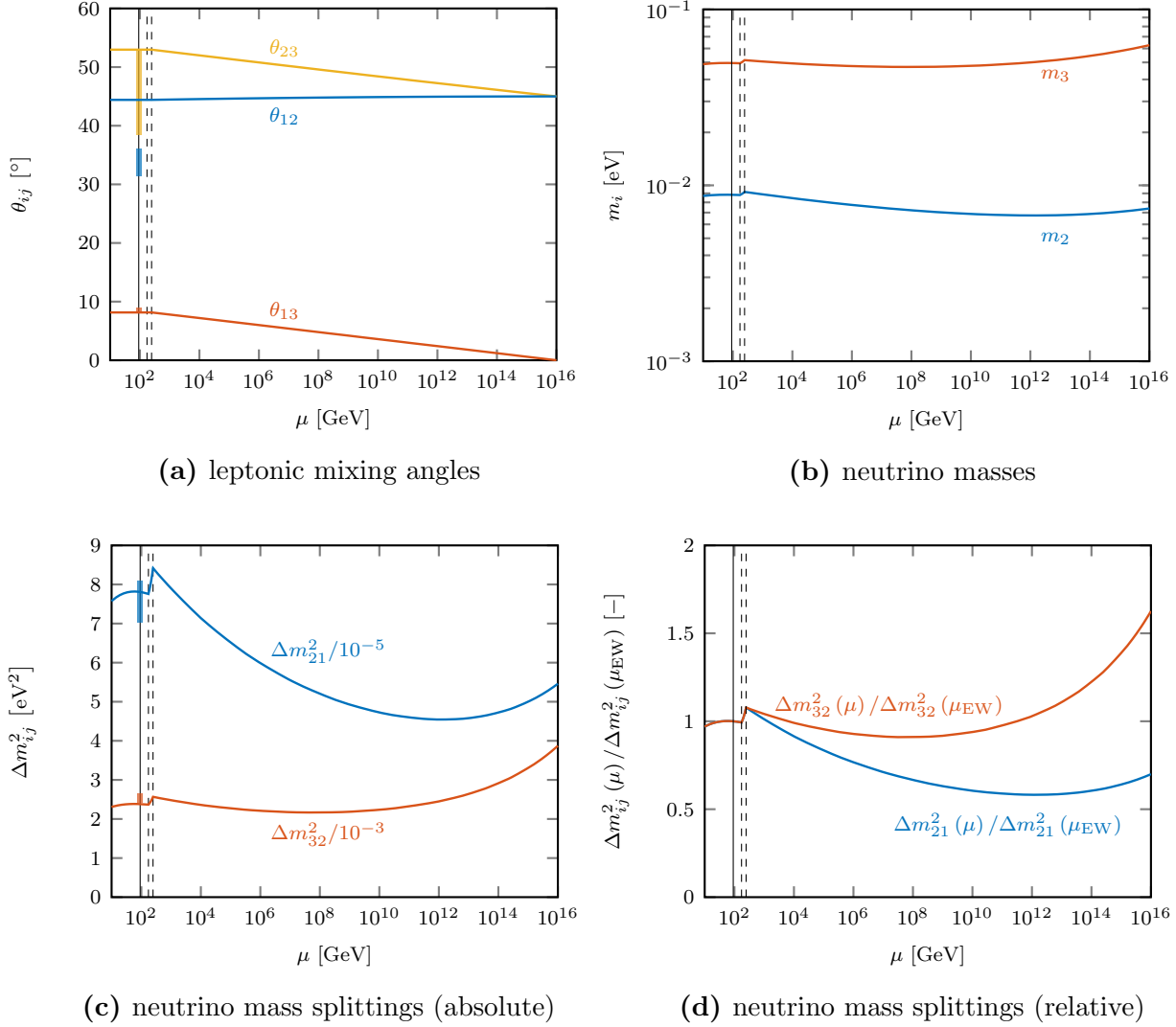


Figure 4.1: Results of the numerical evaluation of the RGEs of neutrino masses and leptonic mixing angles for an initial parameter configuration leading to the EFT-route “full theory \rightarrow EFT- $h \rightarrow$ EFT- $0h$ ”. The solid vertical line indicates the electroweak scale μ_{EW} , while the dashed vertical lines indicate the mass thresholds of k^{++} (right line) and h^+ (left line). Thus, we are in the full theory for energies above the rightmost dashed vertical line, in EFT- h between the vertical lines, and in EFT- $0h$ below the left vertical line. In the case of mixing angles and mass-splittings we indicate the 3σ -ranges from experiments by coloured rectangles.

Depending on the initial configuration, the neutrino masses can exhibit very strong running. From Fig. 4.1d we find that, for our current example configuration, the mass splittings change by factors of roughly 2 (for Δm_{21}^2) and 3/2 (for Δm_{32}^2) due to the running, which is a rather moderate change compared to other cases. As can be seen from Fig. 4.1c, we hit the measured 3σ -ranges of both mass splittings.

There is another important issue that we would like to point out. Recall that in Secs. 3.1 and 3.3 we learned that, due to the complex operator structure of EFT- h , the running of the neutrino mass matrix therein receives contributions already at second loop order. In contrast, in the full theory as well as in all other EFTs, the running starts at third loop order. If we wanted to be fully consistent, we would have to compute the running up to *the same* loop order in the full theory as well as in *all* EFTs. We chose to go up to third loop order (otherwise there was only running in EFT- h), which implies that for EFT- h we have to consider not only leading but also next-to leading order effects. Although possible in principle, their computation turned out to be infeasible within the scope of this work. Thus, we computed only the leading, i.e., second order effects in EFT- h . Fig. 4.1 is based on these results.

Although necessary for full consistency, the incorporation of third order effects in EFT- h would most certainly not lead to any substantial changes of the low-energy values of the running parameters in our example. The justification for this statement is the fact that the mass thresholds of h^+ and k^{++} lie very close together. Thus, we use the equations of EFT- h only in a very small energy range (namely the range between the dashed vertical lines in the plots). In cases where this energy range was bigger, one would clearly have to include third order effects in EFT- h to make viable predictions as they then might lead to changes in the low-scale values which are of the same order as those stemming from the third order effects in the full theory and in EFT- $0h$. However, in our case the third order effects only will lead to negligible changes. We remark that the mass thresholds turn out to lie close together for a wide range of input scalar masses m_h and m_k , such that our approach can safely be used for basic studies of the Zee-Babu model. Furthermore, these are probably the cases most relevant for colliders.

Following the discussion above, one would expect the running in EFT- h to be stronger compared to the full theory and to the other EFTs, since it sets in at a lower loop order. From our plots in Fig. 4.1, one might get the impression that this is indeed the case as the slope of the running neutrino masses is bigger (and even changes sign) in EFT- h . This is particularly apparent in the plots for the mass splittings. However, we did not quantify this behaviour in this thesis. Nevertheless, this is a very interesting point, as it would underpin the usefulness of the loop order expansion as described in Sec. 3.1. More importantly, from a conceptual point of view, one might learn much more about the running in EFTs by having a closer look at this issue. In this context, deriving analytical formulae for the running of the neutrino masses and leptonic mixing angles as was done for example in Refs. [14, 85] might be a promising starting point.

Parameter	Value	Unit
μ_{hk}	10	GeV
m_h	320	GeV
m_k	175	GeV
Δm_{21}^2	$6.0 \cdot 10^{-5}$	eV ²
Δm_{32}^2	$4.5 \cdot 10^{-3}$	eV ²

Table 4.3: Initial parameter configuration leading to the EFT-route “full theory \rightarrow EFT- $k \rightarrow$ EFT-0 k ” and the running displayed in Fig. 4.2.

EFT-route: “full theory \rightarrow EFT- $k \rightarrow$ EFT-0 k ” Fig. 4.2 represents an example in which the running leads to the EFT-route

$$\text{full theory} \rightarrow \text{EFT-}k \rightarrow \text{EFT-0}k. \quad (4.3.1)$$

The corresponding initial parameter configuration is given in Tab. 4.3. Note that here m_h was chosen to be larger than m_k in order to force h^+ to be integrated out before k^{++} .

In this setting we did manage to find an initial parameter configuration in which we hit the 3σ -range of θ_{23} and Δm_{21}^2 . As mentioned earlier, this motivates a more thorough parameter scan involving also the scalar and Yukawa couplings. This might then give enough freedom to hit all measured values at the low scale. Note that the running of the neutrino masses in this example is rather large compared to the case we discussed before, cf. Fig. 4.2d.

We would like to point out that the results shown in Fig. 4.2 incorporate the running at third loop order in full consistency. Recall that, in EFT- k , the leading-order effects of the running are of third loop order, which is why they can be computed with maintainable effort. At first sight, we get the impression that the running in EFT- k is indeed not altered that much as it was the case above in EFT- h .

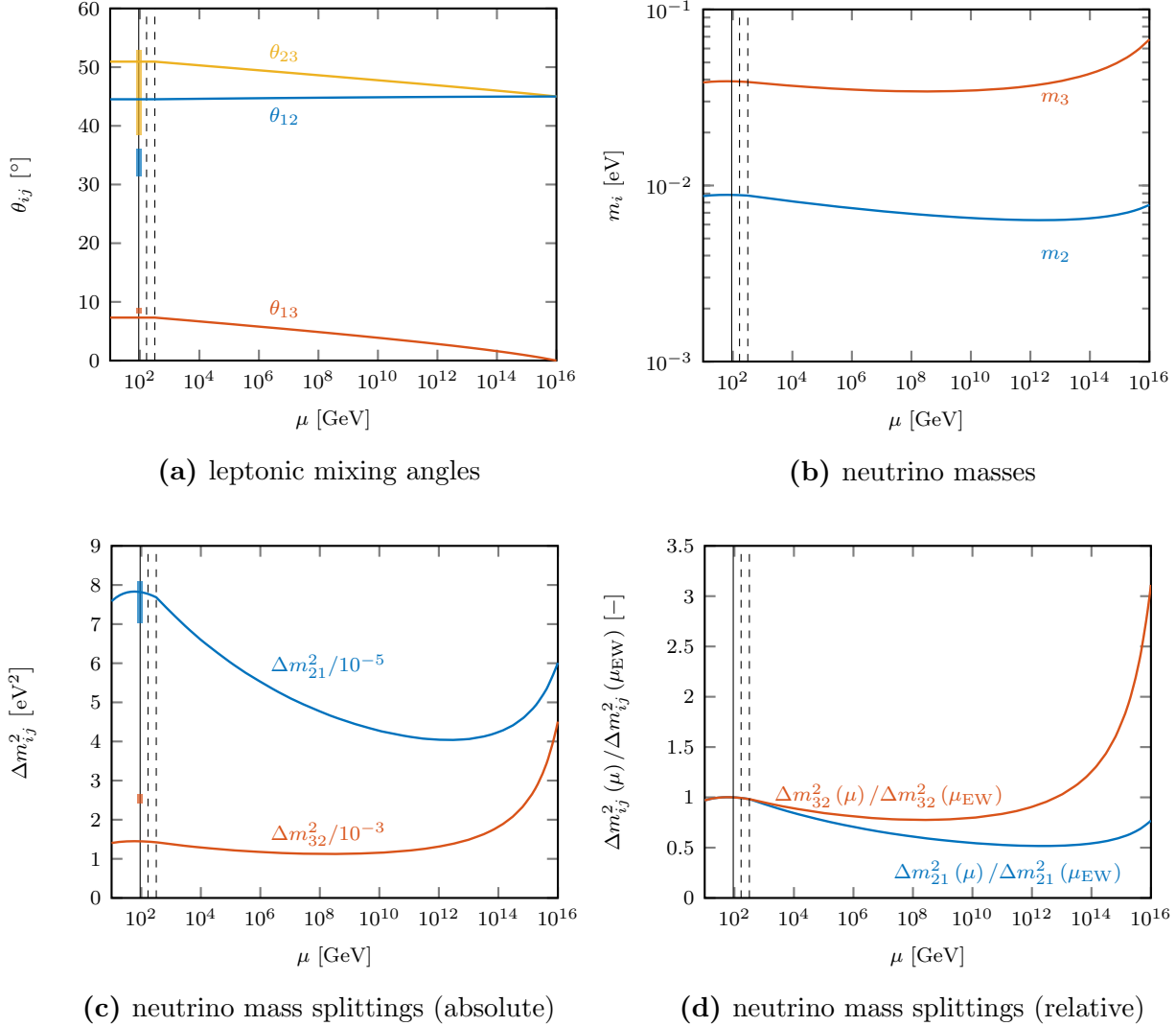


Figure 4.2: Results of the numerical evaluation of the RGEs of neutrino masses and leptonic mixing angles for an initial parameter configuration leading to the EFT-route “full theory \rightarrow EFT- $k \rightarrow$ EFT- $0k$ ”. The solid vertical line indicates the electroweak scale μ_{EW} , while the dashed vertical lines indicate the mass thresholds of k^{++} (left line) and h^+ (right line). Thus, we are in the full theory for energies above the rightmost dashed vertical line, in EFT- k between the vertical lines, and in EFT- $0k$ below the left vertical line. In the case of mixing angles and mass-splittings we indicate the 3σ -ranges from experiments by coloured rectangles.

Conclusions and Outlook

We studied the Zee-Babu model, an economical extension of the SM by only two charged scalar particles, leading to radiative neutrino masses at two-loop order. Our main result is the full set of RGEs of the full theory and of the EFTs, which we obtain by subsequently integrating out the additional scalars according to their mass hierarchy. It turned out to be quite intricate to keep track of which effects are to be taken into account in the computation, in order to eventually obtain a given accuracy of the running. This motivated us to refine a method of organising the calculations of the neutrino mass matrix, the β -functions of full-theory parameters and of effective couplings, as well as the matching process, in loop orders. This enables us to decide which effects have to be considered in order to obtain the running at some fixed target accuracy, i.e., up to some targeted loop order. We presented this method in a general manner, making it easily applicable to a wide range of models and moreover yielding valuable insights from a conceptual point of view. In particular, we learned that the running in EFTs may be stronger than in the full theory in the sense that it starts at lower loop orders.

The RGEs contain the full information about the running of neutrino masses and leptonic mixing angles in the Zee-Babu model. We performed a first numerical evaluation of the running in a top-down approach, meaning to start at some very high energy scale with a theoretically well-motivated mixing pattern. We then studied, whether the running can account for deviations from neutrino data taken at energies below the electroweak scale. Our results indicate that this might indeed be the case, thereby motivating a more thorough analysis of the running in future work. Moreover, we found that the mixing angle θ_{12} shows barely any running for the initial high-energy parameter configurations we looked at, raising the question whether this is a generic property of the Zee-Babu model. Furthermore, it would be interesting to compare in more detail the running in the full theory and in the various EFTs, as both our results from the loop expansion and the numerical evaluation indicate substantial differences. For both questions, it seems promising to try to approximate the RGEs in such a way that they become soluble analytically, possibly giving further insights into the general structure of the running.

Acknowledgements

An dieser Stelle möchte ich all denjenigen danken, welche mich beim Verfassen dieser Arbeit unterstützt und das vergangene Jahr am Max-Planck-Institut für Physik für mich zu einer großartigen Zeit gemacht haben. Insbesondere gebührt mein Dank Georg Raffelt, der es mir ermöglicht hat, diese Masterarbeit in der Astroteilchenphysik-Arbeitsgruppe am MPI anzufertigen.

Mein Betreuer Alex Merle hat ganz wesentlich zum Gelingen der Arbeit beigetragen. Seine Tür stand jederzeit offen, um (nicht nur) fachliche Fragen zu diskutieren, und ich bin immer mit nützlichen Antworten und Anregungen (und manchmal auch amüsanten Ablenkungen) wieder zurück an die Arbeit gegangen. Er hat eine angenehm freundschaftliche Atmosphäre geschaffen, in der eigenverantwortliches Arbeiten ermöglicht und gefördert wurde. Trotzdem haben unzählige hilfreiche Tips zur richtigen Zeit mir den Übergang vom Studium in das Forschungsumfeld sehr erleichtert. Insbesondere haben Alex' Ratschläge mich an vielen Stellen davor bewahrt, zu viel Zeit mit Details und Kleinigkeiten zu vertrödeln und den Blick fürs Wesentliche nicht zu verlieren.

Auch die Hilfe von Tanja Geib war unheimlich wertvoll. Ich möchte ihr danken für die vielen hilfreichen Antworten auf die vielen hilflosen Fragen eines Teilchenphysik-Neulings, zu (gefühl) jeder Tages- und Nachtzeit. Außerdem werden mir die musikreichen Tage auf Schloss Ringberg in überragend guter Erinnerung bleiben, wobei natürlich auch Frank Steffen und Alex Millar genannt werden müssen.

Überdies danke ich Alex und Tanja (und Alex) für das Korrekturlesen meiner Arbeit in den letzten Wochen und Tagen. Eure Ratschläge haben mich nochmal ein gutes Stück voran gebracht!

Auch dank Manuel, Max, Ignacio, Edoardo, Hendrik, Ludo, Annette, Daniela, Flo, Kilian und Abhiram wird mir das Jahr am MPI in sehr guter Erinnerung bleiben.

Zum Schluss möchte ich meiner Familie, allen voran meinen Eltern Petra und Herbert, für ihre Liebe und Unterstützung danken. Gut, wenn es etwas gibt, auf das man sich *immer* verlassen kann!

Appendix A

Symbols and Notation

We use the following symbols in this thesis:

Symbol	Description
$\mu, \nu, \dots \in \{0, 1, 2, 3\}$	Lorentz indices
$i, j, k, \dots \in \{1, 2\}$	$SU(2)_L$ -indices ((anti-)fundamental representation)
$A \in \{1, 2, 3\}$	$SU(2)_L$ -index (adjoint representation)
$B \in \{1, \dots, 8\}$	$SU(3)_C$ -index (adjoint representation)
$I, J, K, \dots \in \{1, 2, 3\}$	Family indices
$\eta_{\mu\nu} \equiv \text{diag}(+1, -1, -1, -1)$	Minkowski metric
γ^μ, γ_5	Dirac γ -matrices
$\epsilon_{ij}, \epsilon_{12} \equiv +1$	Completely antisymmetric tensor
σ^A	Pauli matrices
λ^B	Gell-Mann matrices
d	Number of spacetime dimensions
\mathcal{D}	Mass dimension of operators
$\varepsilon \equiv 4 - d$	Regularisation parameter in dimreg
$Q_L \equiv (u_L, d_L)$	Left-handed quark doublet
u_R	Right-handed up-type quarks
d_R	Right-handed down-type quarks
$L_L \equiv (\nu_L, e_L)$	Left-handed lepton doublet
e_R	Right-handed leptons
$\phi \equiv 1/\sqrt{2}(\phi^+, \phi^0)$	Higgs doublet
ϕ_H	Physical Higgs particle
$v = 246 \text{ GeV}$	Higgs vev

Table A.1: Symbols used in this thesis.

Symbol	Description
B_μ	$U(1)_Y$ -gauge boson
W_μ^A	$SU(2)_L$ -gauge bosons
G_μ^B	$SU(3)_C$ -gauge bosons
h^+	Singly charged scalar (Zee-Babu model)
k^{++}	Doubly charged scalar (Zee-Babu model)
Y_u	Up-quark Yukawa matrix
Y_d	Down-quark Yukawa matrix
Y_e	Charged lepton Yukawa matrix
T	Quadratic Yukawa trace terms
T_4	Quartic Yukawa trace terms
f	Yukawa matrix for h^+
g	Yukawa matrix for k^{++}
y_t	Top-quark Yukawa coupling
y_I	Diagonal entries of Y_e in mass eigenbasis
$m_{e,I}$	Masses of the charged leptons
M_ν	Neutrino mass matrix
m_I	Neutrino masses
U^{PMNS}	Leptonic mixing matrix
$\theta_{12}, \theta_{13}, \theta_{23}$	Leptonic mixing angles
δ	Dirac phase
ϕ_1, ϕ_2	Majorana phases
$\mu_\phi^2, \mu_h^2, \mu_k^2$	Scalar mass parameters
μ_{hk}	Trilinear scalar coupling
$\lambda_\phi, \lambda_h, \lambda_k, \lambda_{\phi h}, \lambda_{\phi k}, \lambda_{hk}$	Quartic scalar couplings
m_H	Mass of physical Higgs particle
m_h	Mass of h^+
m_k	Mass of k^{++}
ξ_1, ξ_2, ξ_3	Gauge parameters
μ	Energy scale
$\mu_{\text{EW}} \approx 100 \text{ GeV}$	Scale of electroweak symmetry breaking (“low scale”)
$\mu_{\text{GUT}} \approx 10^{16} \text{ GeV}$	Scale of grand unification (“high scale”)
μ_h^*, μ_k^*	Mass thresholds of h^+, k^{++}
$\alpha \equiv 1/(16\pi^2)$	Loop factor
$\mathcal{I}_1, \mathcal{I}_2, \mathcal{I}_3$	Loop integrals

Table A.1: Symbols used in this thesis – continued.

Furthermore, we use the following notational conventions.

- We exclusively use Dirac spinor notation. Notice the conventions introduced in App. B.
- We suppress colour indices and always make $SU(2)_L$ -indices explicit.
- We make family indices explicit whenever it clarifies notation. In unambiguous cases, we use matrix notation for contracting family indices.
- For charged scalars we use the following abbreviations:

$$h^- \equiv (h^+)^\dagger, \quad k^{--} \equiv (k^{++})^\dagger.$$

- For objects carrying $SU(2)_L$ -indices we write:

$$\psi_i^\dagger \equiv (\psi^\dagger)_i, \quad \psi_i^c \equiv (\psi^c)_i, \quad \psi_i^T \equiv (\psi^T)_i.$$

We use analogous relations for objects carrying family indices.

Appendix **B**

Spinor Algebra

We list without proof the most important rules and notational conventions for calculations with Dirac spinors.

Given a Dirac spinor ψ we define

$$\bar{\psi} \equiv \psi^\dagger \gamma^0, \quad \psi^c \equiv C \bar{\psi}^T, \quad (\text{B.0.1})$$

where the charge conjugation matrix C obeys the relations:

$$C^\dagger = C^{-1}, \quad C^T = -C, \quad C^{-1} \gamma^\mu C = -(\gamma^\mu)^T, \quad C^{-1} \gamma_5 C = \gamma_5^T. \quad (\text{B.0.2})$$

Furthermore, we define the left- and right-handed chirality projectors via:

$$P_L \equiv \frac{1 - \gamma_5}{2}, \quad P_R \equiv \frac{1 + \gamma_5}{2}. \quad (\text{B.0.3})$$

They obey the following relations:

$$P_L^2 = P_L, \quad P_R^2 = P_R, \quad P_L P_R = P_R P_L = 0, \quad P_L + P_R = 1. \quad (\text{B.0.4})$$

We denote the projections of ψ onto its left- and right-handed components by:

$$\psi_L \equiv P_L \psi, \quad \psi_R \equiv P_R \psi. \quad (\text{B.0.5})$$

Note that

$$\bar{\psi}_L = \bar{\psi} P_R, \quad \bar{\psi}_R = \bar{\psi} P_L, \quad (\text{B.0.6})$$

and

$$(\psi_L)^c = P_R \psi^c, \quad (\psi_R)^c = P_L \psi^c. \quad (\text{B.0.7})$$

Furthermore, we need the important relations

$$(\bar{\psi}_1 \psi_2)^\dagger = \bar{\psi}_2 \psi_1, \quad (\bar{\psi}_1 \gamma^\mu \psi_2)^\dagger = \bar{\psi}_2 \gamma^\mu \psi_1, \quad (\bar{\psi}_1 \gamma_5 \psi_2)^\dagger = -\bar{\psi}_2 \gamma_5 \psi_1, \quad (\text{B.0.8})$$

as well as [96]:

$$\bar{\psi}_1 \psi_2 = \bar{\psi}_2^c \psi_1^c, \quad \bar{\psi}_1 \gamma^\mu \psi_2 = -\bar{\psi}_2^c \gamma^\mu \psi_1^c, \quad \bar{\psi}_1 \gamma_5 \psi_2 = \bar{\psi}_2^c \gamma_5 \psi_1^c. \quad (\text{B.0.9})$$

Feynman Rules of the Zee-Babu Model

We present the Feynman rules for the lepton and scalar sectors of the Zee-Babu model and its derived effective theories in $d = 4 - \varepsilon$ dimensions, which makes them directly applicable in dimensional regularisation. The standard techniques for deriving Feynman rules from a given Lagrangian presented in most of the introductory textbooks on QFT are only applicable if the interactions of the model conserve fermion number [25, 34, 58]. Diagrammatically, this is reflected by the fact that there are no clashing arrows on fermion lines, yielding a unique direction for applying the Feynman rules in a diagram. In models containing Majorana fermions or, more generally, in models with fermion number-violating interactions such as the Zee-Babu model, the situation is more involved. Fortunately, there exist several techniques which make the derivation and application of Feynman rules nearly as convenient as in the case where fermion number is conserved. In this thesis we use the technique proposed in Ref. [96], which relies on the introduction of an (arbitrary) *fermion flow* direction through a diagram which takes the place of the fermion number flow in fermion number-conserving models. We indicate this direction by a grey arrow next to fermion lines.

C.1 Unbroken Phase

First, we present the Feynman rules in the unbroken phase, i.e., in the case of vanishing Higgs vev, $v = 0$. From these, the Feynman rules in the broken phase can be deduced easily as described in the following section.

The Feynman rule for the counterterm δc of a coupling c follows by the replacement $c \rightarrow \delta c$ in the Feynman rule for c , since we renormalise all couplings additively. Therefore, we do not present the Feynman rules for the counterterms of couplings separately. However, as the situation is a bit more involved for the wavefunction renormalisation counterterms, we give their Feynman rules explicitly.

C.1.1 Propagators and Wavefunction Renormalisation Counterterms

We omit $SU(2)_L$ -indices in the following diagrams and Feynman rules, as both the propagators and the wavefunction renormalisation constants are diagonal in the $SU(2)_L$ -indices. Furthermore, note that the $i\varepsilon$ -terms in the denominators of the propagators play no role in the calculations in the main part of this thesis, which is why we omit them there consistently.

Fermions

$$\mathcal{L}_{\text{ZB}} \supset \overline{f_{I,L}} (i\not{\partial} f_{J,L}) (\delta_{IJ} + \delta Z_{f,IJ}) = -\overline{(f_{J,L})^c} \left[i\not{\partial} (f_{I,L})^c \right] (\delta_{IJ} + \delta Z_{f,JI}^T)$$

$$\begin{array}{c} \xrightarrow{p} \\ \overline{f_{J,L}} \longrightarrow \longrightarrow f_{I,L} \end{array} = \frac{i\not{p}}{p^2 + i\varepsilon} \delta_{IJ}$$

$$\begin{array}{c} \xrightarrow{p} \\ \overline{f_{J,L}} \longrightarrow \boxed{\otimes} \longrightarrow f_{I,L} \end{array} = i\not{p} \delta Z_{f,IJ} P_L$$

$$\begin{array}{c} \xrightarrow{p} \\ \overline{f_{J,L}} \longleftarrow \longleftarrow f_{I,L} \end{array} = \frac{-i\not{p}}{p^2 + i\varepsilon} \delta_{JI}$$

$$\begin{array}{c} \xrightarrow{p} \\ \overline{f_{J,L}} \longleftarrow \boxed{\otimes} \longleftarrow f_{I,L} \end{array} = -i\not{p} \delta Z_{f,JI}^T P_R$$

The corresponding Feynman rules for right-handed fermions f_R follow by the replacement $P_L \leftrightarrow P_R$ in the above expressions.

Scalars

$$\mathcal{L}_{\text{ZB}} \supset (\partial_\mu \varphi) (\partial^\mu \varphi)^\dagger (1 + \delta Z_\varphi) - (m_\varphi^2 + \delta m_\varphi^2) \varphi^\dagger \varphi$$

$$\begin{array}{c} \xrightarrow{p} \\ \overline{\varphi} \longrightarrow \longrightarrow \varphi \end{array} = \frac{i}{p^2 - m_\varphi^2 + i\varepsilon}$$

$$\begin{array}{c} \xrightarrow{p} \\ \overline{\varphi} \longrightarrow \boxed{\otimes} \longrightarrow \varphi \end{array} = i(p^2 \delta Z_\varphi - \delta m_\varphi^2)$$

Gauge Bosons

$$\begin{array}{c} \xrightarrow{p} \\ A_\mu \text{ (wavy)} \longrightarrow \longrightarrow A_\nu \text{ (wavy)} \end{array} = i \frac{-\eta_{\mu\nu} + (1 - \xi_A) \frac{p_\mu p_\nu}{p^2}}{p^2 + i\varepsilon}$$

Here, we denote by ξ_A the gauge parameter corresponding to the gauge field A_μ .

C.1.2 Leptonic Gauge Couplings

e_R -gauge-vertices

$$\mathcal{L}_{\text{ZB}} \supset +\mu^{\frac{\epsilon}{2}} g_1 \overline{e_{I,R}} \gamma^\mu e_{I,R} B_\mu = -\mu^{\frac{\epsilon}{2}} g_1 \overline{(e_{I,R})^c} \gamma^\mu (e_{I,R})^c B_\mu$$

$$= +i\mu^{\frac{\epsilon}{2}} g_1 \gamma^\mu \delta_{IJ} P_R$$

$$= -i\mu^{\frac{\epsilon}{2}} g_1 \gamma^\mu \delta_{IJ} P_L$$

L_L -gauge-vertices

$$\begin{aligned} \mathcal{L}_{\text{ZB}} \supset & +\frac{1}{2}\mu^{\frac{\epsilon}{2}} g_1 \overline{(L_{I,L})_i} \gamma^\mu (L_{I,L})_i B_\mu - \frac{1}{2}\mu^{\frac{\epsilon}{2}} g_2 \overline{(L_{I,L})_i} \gamma^\mu (L_{I,L})_j \sigma_{ij}^A W_\mu^A \\ & = -\frac{1}{2}\mu^{\frac{\epsilon}{2}} g_1 \overline{(L_{I,L})^c_i} \gamma^\mu (L_{I,L})^c_i B_\mu + \frac{1}{2}\mu^{\frac{\epsilon}{2}} g_2 \overline{(L_{I,L})^c_i} \gamma^\mu (L_{I,L})^c_j (\sigma^A)^T_{ij} W_\mu^A \end{aligned}$$

$$= +\frac{i}{2}\mu^{\frac{\epsilon}{2}} g_1 \gamma^\mu \delta_{IJ} \delta_{ij} P_L$$

$$= -\frac{i}{2}\mu^{\frac{\epsilon}{2}} g_1 \gamma^\mu \delta_{IJ} \delta_{ij} P_R$$

$$= -\frac{i}{2}\mu^{\frac{\epsilon}{2}} g_2 \gamma^\mu \delta_{IJ} \sigma_{ij}^A P_L$$

$$= +\frac{i}{2}\mu^{\frac{\epsilon}{2}} g_2 \gamma^\mu \delta_{IJ} (\sigma^A)^T_{ij} P_R$$

ϕ -gauge-vertices

$$\begin{aligned} \mathcal{L}_{\text{ZB}} \supset & -\frac{i}{2}\mu^{\frac{\varepsilon}{2}}g_1 \left[\phi_i^\dagger (\partial^\mu \phi_i) - (\partial_\mu \phi_i^\dagger) \phi_i \right] B_\mu - \frac{i}{2}\mu^{\frac{\varepsilon}{2}}g_2 \left[\phi_i^\dagger (\partial^\mu \phi_j) - (\partial_\mu \phi_i^\dagger) \phi_j \right] \sigma_{ij}^A W_\mu^A \\ & + \frac{1}{4}\mu^\varepsilon g_1^2 B_\mu B^\mu \phi_i^\dagger \phi_i + \frac{1}{4}\mu^\varepsilon g_2^2 W_\mu^A W^{A,\mu} \phi_i^\dagger \phi_i + \frac{1}{2}\mu^\varepsilon g_1 g_2 B_\mu W^{A,\mu} \phi_i^\dagger \phi_j \sigma_{ij}^A \end{aligned}$$

$$\begin{array}{c} \phi_i \\ \nearrow p_2 \\ \phi_j \\ \nearrow p_1 \end{array} \text{---} B_\mu = -\frac{i}{2}\mu^{\frac{\varepsilon}{2}}g_1 (p_{1\mu} + p_{2\mu}) \delta_{ij}$$

$$\begin{array}{c} \phi_i \\ \nearrow p_2 \\ \phi_j \\ \nearrow p_1 \end{array} \text{---} W_\mu^A = -\frac{i}{2}\mu^{\frac{\varepsilon}{2}}g_2 (p_{1\mu} + p_{2\mu}) \sigma_{ij}^A$$

$$\begin{array}{c} \phi_i \\ \nearrow \\ \phi_j \\ \nearrow \end{array} \text{---} B_\mu, B_\nu = +\frac{i}{2}\mu^\varepsilon g_1^2 \eta_{\mu\nu} \delta_{ij}$$

$$\begin{array}{c} \phi_i \\ \nearrow \\ \phi_j \\ \nearrow \end{array} \text{---} W_\mu^A, W_\nu^B = +\frac{i}{2}\mu^\varepsilon g_1^2 \eta_{\mu\nu} \delta_{ij} \delta_{AB}$$

$$\begin{array}{c} \phi_i \\ \nearrow \\ \phi_j \\ \nearrow \end{array} \text{---} W_\mu^A, B_\nu = +\frac{i}{2}\mu^\varepsilon g_1 g_2 \eta_{\mu\nu} \sigma_{ij}^A$$

C.1.3 Scalar Couplings

$$\begin{aligned} \mathcal{L}_{\text{ZB}} \supset & -\lambda_\phi (\phi_i^\dagger \phi_i)^2 - \lambda_h (h^+ h^-)^2 - \lambda_k (k^{++} k^{--})^2 - \lambda_{\phi h} (\phi_i^\dagger \phi_i) (h^+ h^-) \\ & - \lambda_{\phi k} (\phi_i^\dagger \phi_i) (k^{++} k^{--}) - \lambda_{hk} (h^+ h^-) (k^{++} k^{--}) - \mu_{hk} (h^+ h^+ k^{--} + h^- h^- k^{++}) \end{aligned}$$

$$\begin{array}{c} \phi_i \searrow \\ \phi_j \nearrow \\ \phi_k \nearrow \\ \phi_l \searrow \end{array} \begin{array}{c} \times \\ \times \\ \times \\ \times \end{array} = -2i\mu^\varepsilon \lambda_\phi (\delta_{ik}\delta_{jl} + \delta_{il}\delta_{jk})$$

$$\begin{array}{c} h^+ \searrow \\ h^+ \nearrow \\ h^+ \nearrow \\ h^+ \searrow \end{array} \begin{array}{c} \times \\ \times \\ \times \\ \times \end{array} = -4i\mu^\varepsilon \lambda_h$$

$$\begin{array}{c} k^{++} \searrow \\ k^{++} \nearrow \\ k^{++} \nearrow \\ k^{++} \searrow \end{array} \begin{array}{c} \times \\ \times \\ \times \\ \times \end{array} = -4i\mu^\varepsilon \lambda_k$$

$$\begin{array}{c} \phi_i \searrow \\ h^+ \nearrow \\ h^+ \nearrow \\ h^+ \searrow \end{array} \begin{array}{c} \times \\ \times \\ \times \\ \times \end{array} = -i\mu^\varepsilon \lambda_{\phi h} \delta_{ij}$$

$$\begin{array}{c} \phi_i \searrow \\ k^{++} \nearrow \\ k^{++} \nearrow \\ k^{++} \searrow \end{array} \begin{array}{c} \times \\ \times \\ \times \\ \times \end{array} = -i\mu^\varepsilon \lambda_{\phi k} \delta_{ij}$$

$$\begin{array}{c} h^+ \searrow \\ k^{++} \nearrow \\ k^{++} \nearrow \\ k^{++} \searrow \end{array} \begin{array}{c} \times \\ \times \\ \times \\ \times \end{array} = -i\mu^\varepsilon \lambda_{hk}$$

$$\begin{array}{c} h^+ \searrow \\ h^+ \nearrow \end{array} \begin{array}{c} \bullet \\ \bullet \end{array} \begin{array}{c} \longrightarrow \\ \longrightarrow \end{array} k^{++} = -2i\mu^{\frac{\varepsilon}{2}} \mu_{hk}$$

$$\begin{array}{c} h^+ \searrow \\ h^+ \nearrow \end{array} \begin{array}{c} \bullet \\ \bullet \end{array} \begin{array}{c} \longleftarrow \\ \longleftarrow \end{array} k^{++} = -2i\mu^{\frac{\varepsilon}{2}} \mu_{hk}$$

C.1.4 Leptonic Yukawa Couplings

$e_R L_L \phi$ -vertex

$$\begin{aligned} \mathcal{L}_{\text{ZB}} \supset & -\mu^{\frac{\xi}{2}} Y_{e,IJ} \overline{e_{I,R}} (L_{J,L})_i \phi_i^\dagger - \mu^{\frac{\xi}{2}} Y_{e,IJ}^\dagger (\overline{L_{I,L}})_i e_{J,R} \phi_i \\ & = -\mu^{\frac{\xi}{2}} Y_{e,IJ}^T (\overline{L_{I,L}})_i^c (e_{J,R})^c \phi_i^\dagger - \mu^{\frac{\xi}{2}} Y_{e,IJ}^* (\overline{e_{I,R}})^c (L_{J,L})_i^c \phi_i \end{aligned}$$

$$\begin{aligned} \text{Top-left: } & \begin{array}{c} e_{I,R} \\ \nearrow \\ \bullet \\ \nwarrow \\ (L_{J,L})_j \end{array} \rightarrow \phi_i = -i\mu^{\frac{\xi}{2}} Y_{e,IJ} \delta_{ij} P_L \\ \text{Top-right: } & \begin{array}{c} (L_{I,L})_i \\ \nearrow \\ \bullet \\ \nwarrow \\ e_{J,R} \end{array} \rightarrow \phi_j = -i\mu^{\frac{\xi}{2}} Y_{e,IJ}^\dagger \delta_{ij} P_R \\ \text{Bottom-left: } & \begin{array}{c} (L_{I,L})_i \\ \nearrow \\ \bullet \\ \nwarrow \\ e_{J,R} \end{array} \rightarrow \phi_j = -i\mu^{\frac{\xi}{2}} Y_{e,IJ}^T \delta_{ij} P_L \\ \text{Bottom-right: } & \begin{array}{c} e_{I,R} \\ \nearrow \\ \bullet \\ \nwarrow \\ (L_{J,L})_j \end{array} \rightarrow \phi_i = -i\mu^{\frac{\xi}{2}} Y_{e,IJ}^* \delta_{ij} P_R \end{aligned}$$

$e_R e_R k^{++}$ -vertex

$$\mathcal{L}_{\text{ZB}} \supset -\mu^{\frac{\xi}{2}} g_{IJ} \overline{(e_{I,R})^c} e_{J,R} k^{++} - \mu^{\frac{\xi}{2}} g_{IJ}^\dagger \overline{e_{I,R}} (e_{J,R})^c k^{--}, \text{ where } g_{IJ} = g_{JI}$$

$$\begin{aligned} \text{Left: } & \begin{array}{c} e_{I,R} \\ \nearrow \\ \bullet \\ \nwarrow \\ e_{J,R} \end{array} \rightarrow k^{++} = -2i\mu^{\frac{\xi}{2}} g_{IJ} P_R \\ \text{Right: } & \begin{array}{c} e_{I,R} \\ \nearrow \\ \bullet \\ \nwarrow \\ e_{J,R} \end{array} \rightarrow k^{++} = -2i\mu^{\frac{\xi}{2}} g_{IJ}^\dagger P_L \end{aligned}$$

$L_L L_L h^+$ -vertex

$$\mathcal{L}_{\text{ZB}} \supset -\mu^{\frac{\xi}{2}} f_{IJ} \overline{(L_{I,L})^c} (L_{J,L})_j \epsilon_{ij} h^+ - \mu^{\frac{\xi}{2}} f_{IJ}^\dagger (\overline{L_{I,L}})_i (L_{J,L})_j^c \epsilon_{ij}^T h^-, \text{ where } f_{IJ} = -f_{JI}$$

$$\begin{aligned} \text{Left: } & \begin{array}{c} (L_{I,L})_i \\ \nearrow \\ \bullet \\ \nwarrow \\ (L_{J,L})_j \end{array} \rightarrow h^+ = -2i\mu^{\frac{\xi}{2}} f_{IJ} \epsilon_{ij} P_L \\ \text{Right: } & \begin{array}{c} (L_{I,L})_i \\ \nearrow \\ \bullet \\ \nwarrow \\ (L_{J,L})_j \end{array} \rightarrow h^+ = -2i\mu^{\frac{\xi}{2}} f_{IJ}^\dagger \epsilon_{ij}^T P_R \end{aligned}$$

C.1.5 Effective Couplings

$e_R e_R h^+ h^+$ -vertex: κ_{21}

$$\mathcal{L}_{\text{ZB}} \supset -\mu^\varepsilon \kappa_{21, IJ} \overline{(e_{I,R})^c} e_{J,R} h^+ h^+ - \mu^\varepsilon \kappa_{21, IJ}^\dagger \overline{e_{I,R}} (e_{J,R})^c h^- h^-, \text{ where } \kappa_{21, IJ} = \kappa_{21, JI}$$

$$= -4i\mu^\varepsilon \kappa_{21, IJ} P_R$$

$$= -4i\mu^\varepsilon \kappa_{21, IJ}^\dagger P_L$$

$e_R L_L \phi h^+$ -vertex: κ_{11}

$$\begin{aligned} \mathcal{L}_{\text{ZB}} &\supset -\mu^\varepsilon \kappa_{11, IJ} (\overline{L_{I,L}})_i e_{J,R} \phi_k^\dagger \epsilon_{ik}^T h^+ - \mu^\varepsilon \kappa_{11, IJ}^\dagger \overline{e_{I,R}} (L_{J,L})_j \phi_k \epsilon_{jk}^T h^- \\ &= -\mu^\varepsilon \kappa_{11, IJ}^T \overline{(e_{I,R})^c} (L_{J,L})_j \phi_k^\dagger \epsilon_{jk}^T h^+ - \mu^\varepsilon \kappa_{11, IJ}^* \overline{(L_{I,L})^c}_i (e_{J,R})^c \phi_k \epsilon_{ik}^T h^- \end{aligned}$$

$$= -i\mu^\varepsilon \kappa_{11, IJ} \epsilon_{ik}^T P_R$$

$$= -i\mu^\varepsilon \kappa_{11, IJ}^\dagger \epsilon_{jk}^T P_L$$

$$= -i\mu^\varepsilon \kappa_{11, IJ}^T \epsilon_{jk}^T P_R$$

$$= -i\mu^\varepsilon \kappa_{11, IJ}^* \epsilon_{ik}^T P_L$$

$L_L L_L \phi \phi$ -vertex: κ_W

$$\mathcal{L}_{\text{ZB}} \supset -\mu^\varepsilon \kappa_{W,IJ} \overline{(L_{I,L})^c}_i (L_{J,L})_j \phi_k \phi_l \epsilon_{ik} \epsilon_{jl} - \mu^\varepsilon \kappa_{W,IJ}^\dagger \overline{(L_{I,L})}_i (L_{J,L})^c_j \phi_k^\dagger \phi_l^\dagger \epsilon_{ik} \epsilon_{jl},$$

where $\kappa_{W,IJ} = \kappa_{W,JI}$

$$= -2i\mu^\varepsilon \kappa_{W,IJ} (\epsilon_{ik} \epsilon_{jl} + \epsilon_{il} \epsilon_{jk}) P_L$$

$$= -2i\mu^\varepsilon \kappa_{W,IJ}^\dagger (\epsilon_{ik} \epsilon_{jl} + \epsilon_{il} \epsilon_{jk}) P_R$$

C.2 Broken Phase

The fields which are related by the $SU(2)_L$ -gauge symmetry in the unbroken phase are individual degrees of freedom in the broken phase. The Feynman rules in the broken phase follow easily from those in the unbroken phase by plugging in the $SU(2)_L$ -indices of the doublet-components which take part in the process at hand. Our conventions are summarised in Tab. 2.1.

However, in doing so, one has to be careful when dealing with vertices involving the Higgs doublet ϕ . Note that we defined the physical Higgs field ϕ_H with a prefactor of $1/\sqrt{2}$, cf. Eq. (2.1.8). Therefore, for every leg associated with a physical Higgs field ϕ_H , one has to add a factor of $1/\sqrt{2}$ to the vertex rule. Analogously, for every leg associated with the Higgs vev v , one has to add a factor of $v/\sqrt{2}$ and remove a factor of $\mu^{\frac{\varepsilon}{2}}$. In this case, one additionally may have to leave out symmetry factors which come from equivalent contractions in the unbroken phase. When in doubt, one can simply write down the Lagrangian in $d = 4 - \varepsilon$ dimensions in the broken phase and in unitarity gauge and read off the Feynman rules.

RGEs of the Zee-Babu Model and its EFTs

We summarise the simplified RGEs, which we used for the numerical evaluation of the results. Since the equations are not fully coupled, they do not have to be solved simultaneously. Rather, they can be solved in subsequent blocks, which we indicate by enumeration.

D.1 RGEs of the Full Theory

1. The analytical solutions of the RGEs of the gauge couplings:

$$g_i(t) = \frac{g_i(0)}{\sqrt{1 - \frac{b_i}{8\pi^2} g_i^2(0)t}}, \quad (\text{D.1.1})$$

where $b_i = (\frac{51}{10}, -\frac{19}{6}, -7)$.

2. The RGE for the top-quark Yukawa coupling y_t :

$$\alpha\beta_{y_t}^{(1)} = y_t \left[\frac{9}{2} y_t^2 - \frac{17}{20} g_1^2 - \frac{9}{4} g_2^2 - 8g_3^2 \right]. \quad (\text{D.1.2})$$

3. The RGEs for the antisymmetric Yukawa matrix f , which couples the left-handed leptonic doublets:

$$\alpha\beta_f^{(1)} = f \left[4f^\dagger f + 4\text{Tr}(f^\dagger f) - \frac{9}{10} g_1^2 - \frac{9}{2} g_2^2 \right]. \quad (\text{D.1.3})$$

4. The RGEs for the symmetric Yukawa matrix g , which couples the right-handed leptonic singlets:

$$\alpha\beta_g^{(1)} = g \left[4g^\dagger g + 2\text{Tr}(g^\dagger g) - \frac{18}{5} g_1^2 \right]. \quad (\text{D.1.4})$$

5. The RGEs for the quartic scalar couplings:

$$\begin{aligned} \alpha\beta_{\lambda_\phi}^{(1)} &= 12\lambda_\phi y_t^2 - 6y_t^4 + 24\lambda_\phi^2 + \lambda_{\phi h}^2 + \lambda_{\phi k}^2 \\ &\quad - \frac{9}{5}\lambda_\phi g_1^2 + \frac{27}{200}g_1^4 - 9\lambda_\phi g_2^2 + \frac{9}{8}g_2^4 + \frac{9}{20}g_1^2 g_2^2, \end{aligned} \quad (\text{D.1.5a})$$

$$\begin{aligned} \alpha\beta_{\lambda_h}^{(1)} &= 16\lambda_h \text{Tr}(f^\dagger f) - 32\text{Tr}(f^\dagger f f^\dagger f) + 20\lambda_h^2 + 2\lambda_{\phi h}^2 + \lambda_{hk}^2 \\ &\quad - \frac{36}{5}\lambda_h g_1^2 + \frac{54}{25}g_1^4, \end{aligned} \quad (\text{D.1.5b})$$

$$\begin{aligned} \alpha\beta_{\lambda_k}^{(1)} &= 8\lambda_k \text{Tr}(g^\dagger g) - 16\text{Tr}(g^\dagger g g^\dagger g) + 20\lambda_k^2 + 2\lambda_{\phi k}^2 + \lambda_{hk}^2 \\ &\quad - \frac{144}{5}\lambda_k g_1^2 + \frac{864}{25}g_1^4, \end{aligned} \quad (\text{D.1.5c})$$

$$\begin{aligned} \alpha\beta_{\lambda_{\phi h}}^{(1)} &= 6\lambda_{\phi h} y_t^2 + 8\lambda_{\phi h} \text{Tr}(f^\dagger f) - 16\text{Tr}(f^\dagger f Y_e^\dagger Y_e) \\ &\quad + 12\lambda_\phi \lambda_{\phi h} + 8\lambda_h \lambda_{\phi h} + 4\lambda_{\phi h}^2 + 2\lambda_{\phi k} \lambda_{hk} \\ &\quad + \frac{27}{25}g_1^4 - \frac{9}{2}\lambda_{\phi h} g_1^2 - \frac{9}{2}\lambda_{\phi h} g_2^2, \end{aligned} \quad (\text{D.1.5d})$$

$$\begin{aligned} \alpha\beta_{\lambda_{\phi k}}^{(1)} &= 6\lambda_{\phi k} y_t^2 + 4\lambda_{\phi k} \text{Tr}(g^\dagger g) - 16\text{Tr}(g g^\dagger Y_e Y_e^\dagger) \\ &\quad + 12\lambda_\phi \lambda_{\phi k} + 8\lambda_k \lambda_{\phi k} + 4\lambda_{\phi k}^2 + 2\lambda_{\phi h} \lambda_{hk} \\ &\quad + \frac{108}{25}g_1^4 - \frac{153}{10}\lambda_{\phi k} g_1^2 - \frac{9}{2}\lambda_{\phi k} g_2^2, \end{aligned} \quad (\text{D.1.5e})$$

$$\begin{aligned} \alpha\beta_{\lambda_{hk}}^{(1)} &= 8\lambda_{hk} \text{Tr}(f^\dagger f) + 4\lambda_{hk} \text{Tr}(g^\dagger g) \\ &\quad + 8\lambda_h \lambda_{hk} + 8\lambda_k \lambda_{hk} + 4\lambda_{\phi h} \lambda_{\phi k} + 4\lambda_{hk}^2 \\ &\quad - 18\lambda_{hk} g_1^2 + \frac{432}{25}g_1^4. \end{aligned} \quad (\text{D.1.5f})$$

6. The RGE for the trilinear scalar coupling μ_{hk} :

$$\alpha\beta_{\mu_{hk}}^{(1)} = \mu_{hk} \left[8\text{Tr}(f^\dagger f) + 2\text{Tr}(g^\dagger g) + 4\lambda_h + 4\lambda_{hk} - \frac{54}{5}g_1^2 \right]. \quad (\text{D.1.6})$$

7. The RGE for the scalar mass parameters:

$$\alpha\beta_{\mu_\phi^2}^{(1)} = 6\mu_\phi^2 y_t^2 + 12\lambda_\phi \mu_\phi^2 + 2\lambda_{\phi h} \mu_h^2 + 2\lambda_{\phi k} \mu_k^2 - \frac{9}{10}\mu_\phi^2 g_1^2 - \frac{9}{2}\mu_\phi^2 g_2^2, \quad (\text{D.1.7a})$$

$$\alpha\beta_{\mu_h^2}^{(1)} = 8\mu_h^2 \text{Tr}(f^\dagger f) + 4\lambda_{\phi h} \mu_\phi^2 + 8\lambda_h \mu_h^2 + 2\lambda_{hk} \mu_k^2 + 8\mu_{hk}^2 - \frac{18}{5}\mu_h^2 g_1^2, \quad (\text{D.1.7b})$$

$$\alpha\beta_{\mu_k^2}^{(1)} = 4\mu_k^2 \text{Tr}(g^\dagger g) + 4\lambda_{\phi k} \mu_\phi^2 + 2\lambda_{hk} \mu_h^2 + 8\lambda_k \mu_k^2 + 4\mu_{hk}^2 - \frac{72}{5}\mu_k^2 g_1^2. \quad (\text{D.1.7c})$$

D.2 RGEs of EFT- h

1. The analytical solutions of the RGEs of the gauge couplings:

$$g_i(t) = \frac{g_i(0)}{\sqrt{1 - \frac{b_i}{8\pi^2} g_i^2(0)t}}, \quad (\text{D.2.1})$$

where $b_i = (\frac{43}{10}, -\frac{19}{6}, -7)$.

2. The RGE for the top-quark Yukawa coupling y_t :

$$\alpha\beta_{y_t}^{(1)} = y_t \left[\frac{9}{2} y_t^2 - \frac{17}{20} g_1^2 - \frac{9}{4} g_2^2 - 8g_3^2 \right]. \quad (\text{D.2.2})$$

3. The RGEs for the antisymmetric Yukawa matrix f , which couples the left-handed leptonic doublets:

$$\alpha\beta_f^{(1)} = f \left[4f^\dagger f + 4\text{Tr}(f^\dagger f) - \frac{9}{10} g_1^2 - \frac{9}{2} g_2^2 \right]. \quad (\text{D.2.3})$$

4. The RGEs for the quartic scalar couplings:

$$\begin{aligned} \alpha\beta_{\lambda_\phi}^{(1)} &= 12\lambda_\phi y_t^2 - 6y_t^4 + 24\lambda_\phi^2 + \lambda_{\phi h}^2 - \frac{9}{5}\lambda_\phi g_1^2 + \frac{27}{200}g_1^4 - 9\lambda_\phi g_2^2 \\ &\quad + \frac{9}{8}g_2^4 + \frac{9}{20}g_1^2 g_2^2, \end{aligned} \quad (\text{D.2.4a})$$

$$\begin{aligned} \alpha\beta_{\lambda_h}^{(1)} &= 16\lambda_h \text{Tr}(f^\dagger f) - 32\text{Tr}(f^\dagger f f^\dagger f) + 20\lambda_h^2 + 2\lambda_{\phi h}^2 \\ &\quad - \frac{36}{5}\lambda_h g_1^2 + \frac{54}{25}g_1^4, \end{aligned} \quad (\text{D.2.4b})$$

$$\begin{aligned} \alpha\beta_{\lambda_{\phi h}}^{(1)} &= 6\lambda_{\phi h} y_t^2 + 8\lambda_{\phi h} \text{Tr}(f^\dagger f) - 16\text{Tr}(f^\dagger f Y_e^\dagger Y_e) \\ &\quad + 12\lambda_\phi \lambda_{\phi h} + 8\lambda_h \lambda_{\phi h} + 4\lambda_{\phi h}^2 + \frac{27}{25}g_1^4 - \frac{9}{2}\lambda_{\phi h} g_1^2 - \frac{9}{2}\lambda_{\phi h} g_2^2. \end{aligned} \quad (\text{D.2.4c})$$

5. The RGE for the scalar mass parameters:

$$\alpha\beta_{\mu_\phi^2}^{(1)} = 6\mu_\phi^2 y_t^2 + 12\lambda_\phi \mu_\phi^2 + 2\lambda_{\phi h} \mu_h^2 - \frac{9}{10}\mu_\phi^2 g_1^2 - \frac{9}{2}\mu_\phi^2 g_2^2, \quad (\text{D.2.5a})$$

$$\alpha\beta_{\mu_h^2}^{(1)} = 8\mu_h^2 \text{Tr}(f^\dagger f) + 4\lambda_{\phi h} \mu_\phi^2 + 8\lambda_h \mu_h^2 - \frac{18}{5}\mu_h^2 g_1^2. \quad (\text{D.2.5b})$$

6. The RGEs for the effective coupling κ_{21} :

$$\alpha\beta_{\kappa_{21}}^{(1)} = [16\text{Tr}(f^\dagger f) + 4\lambda_h + 18g_1^2] \kappa_{21}^{(0)}. \quad (\text{D.2.6})$$

7. The RGEs for the effective coupling κ_{11} :

$$\alpha\beta_{\kappa_{11}}^{(1)} = 16f^\dagger Y_e^T \kappa_{21}^{(0)}, \quad (\text{D.2.7a})$$

$$\alpha\beta_{\kappa_{11}}^{(2)} = 0. \quad (\text{D.2.7b})$$

$$(\text{D.2.7c})$$

8. The RGEs for the effective coupling κ_W :

$$\alpha\beta_{\kappa_W}^{(2)} = -2 \left[f Y_e^\dagger \kappa_{11}^{(1)\dagger} + \left(f Y_e^\dagger \kappa_{11}^{(1)\dagger} \right)^T \right], \quad (\text{D.2.8a})$$

$$\alpha\beta_{\kappa_W}^{(3)} = 0. \quad (\text{D.2.8b})$$

D.3 RGEs of EFT- k

1. The analytical solutions of the RGEs of the gauge couplings:

$$g_i(t) = \frac{g_i(0)}{\sqrt{1 - \frac{b_i}{8\pi^2} g_i^2(0)t}}, \quad (\text{D.3.1})$$

where $b_i = \left(\frac{49}{10}, -\frac{19}{6}, -7\right)$.

2. The RGE for the top-quark Yukawa coupling y_t :

$$\alpha\beta_{y_t}^{(1)} = y_t \left[\frac{9}{2} y_t^2 - \frac{17}{20} g_1^2 - \frac{9}{4} g_2^2 - 8g_3^2 \right]. \quad (\text{D.3.2})$$

3. The RGEs for the symmetric Yukawa matrix g , which couples the right-handed leptonic singlets:

$$\alpha\beta_g^{(1)} = g \left[4g^\dagger g + 2\text{Tr}(g^\dagger g) - \frac{18}{5} g_1^2 \right]. \quad (\text{D.3.3})$$

4. The RGEs for the quartic scalar couplings:

$$\begin{aligned} \alpha\beta_{\lambda_\phi}^{(1)} &= 12\lambda_\phi y_t^2 - 6y_t^4 + 24\lambda_\phi^2 + \lambda_{\phi k}^2 \\ &\quad - \frac{9}{5}\lambda_\phi g_1^2 + \frac{27}{200}g_1^4 - 9\lambda_\phi g_2^2 + \frac{9}{8}g_2^4 + \frac{9}{20}g_1^2 g_2^2, \end{aligned} \quad (\text{D.3.4a})$$

$$\begin{aligned} \alpha\beta_{\lambda_k}^{(1)} &= 8\lambda_k \text{Tr}(g^\dagger g) - 16\text{Tr}(g^\dagger g g^\dagger g) + 20\lambda_k^2 + 2\lambda_{\phi k}^2 \\ &\quad - \frac{144}{5}\lambda_k g_1^2 + \frac{864}{25}g_1^4, \end{aligned} \quad (\text{D.3.4b})$$

$$\begin{aligned} \alpha\beta_{\lambda_{\phi k}}^{(1)} &= 6\lambda_{\phi k} y_t^2 + 4\lambda_{\phi k} \text{Tr}(g^\dagger g) - 16\text{Tr}(g g^\dagger Y_e Y_e^\dagger) \\ &\quad + 12\lambda_\phi \lambda_{\phi k} + 8\lambda_k \lambda_{\phi k} + 4\lambda_{\phi k}^2 \\ &\quad + \frac{108}{25}g_1^4 - \frac{153}{10}\lambda_{\phi k} g_1^2 - \frac{9}{2}\lambda_{\phi k} g_2^2. \end{aligned} \quad (\text{D.3.4c})$$

5. The RGE for the scalar mass parameters:

$$\alpha\beta_{\mu_\phi^2}^{(1)} = 6\mu_\phi^2 y_t^2 + 12\lambda_\phi \mu_\phi^2 + 2\lambda_{\phi k} \mu_k^2 - \frac{9}{10}\mu_\phi^2 g_1^2 - \frac{9}{2}\mu_\phi^2 g_2^2, \quad (\text{D.3.5a})$$

$$\alpha\beta_{\mu_k^2}^{(1)} = 4\mu_k^2 \text{Tr}(g^\dagger g) + 4\lambda_{\phi k} \mu_\phi^2 + 8\lambda_k \mu_k^2 - \frac{72}{5}\mu_k^2 g_1^2. \quad (\text{D.3.5b})$$

6. The RGEs for the effective coupling κ_W :

$$\beta_{\kappa_W}^{(2)} = 0, \quad (\text{D.3.6a})$$

$$\alpha\beta_{\kappa_W}^{(3)} = [6y_t^2 + 4\lambda_\phi - 3g_2^2] \kappa_W^{(2)}. \quad (\text{D.3.6b})$$

D.4 RGEs of EFT-0

1. The analytical solutions of the RGEs of the gauge couplings:

$$g_i(t) = \frac{g_i(0)}{\sqrt{1 - \frac{b_i}{8\pi^2} g_i^2(0)t}}, \quad (\text{D.4.1})$$

where $b_i = (\frac{41}{10}, -\frac{19}{6}, -7)$.

2. The RGE for the top-quark Yukawa coupling y_t :

$$\alpha\beta_{y_t}^{(1)} = y_t \left[\frac{9}{2}y_t^2 - \frac{17}{20}g_1^2 - \frac{9}{4}g_2^2 - 8g_3^2 \right]. \quad (\text{D.4.2})$$

3. The RGEs for the quartic Higgs coupling λ_ϕ :

$$\alpha\beta_{\lambda_\phi}^{(1)} = 12\lambda_\phi y_t^2 - 6y_t^4 + 24\lambda_\phi^2 - \frac{9}{5}\lambda_\phi g_1^2 + \frac{27}{200}g_1^4 - 9\lambda_\phi g_2^2 + \frac{9}{8}g_2^4 + \frac{9}{20}g_1^2 g_2^2. \quad (\text{D.4.3})$$

4. The RGE for the Higgs mass parameter μ_ϕ^2 :

$$\alpha\beta_{\mu_\phi^2}^{(1)} = 6\mu_\phi^2 y_t^2 + 12\lambda_\phi \mu_\phi^2 - \frac{9}{10}\mu_\phi^2 g_1^2 - \frac{9}{2}\mu_\phi^2 g_2^2. \quad (\text{D.4.4})$$

5. The RGEs for the effective coupling κ_W :

$$\beta_{\kappa_W}^{(2)} = 0, \quad (\text{D.4.5a})$$

$$\alpha\beta_{\kappa_W}^{(3)} = [6y_t^2 + 4\lambda_\phi - 3g_2^2] \kappa_W^{(2)}. \quad (\text{D.4.5b})$$

Bibliography

- [1] R. Oerter. *The Theory of Almost Everything: The Standard Model, the Unsung Triumph of Modern Physics*. Pi Press, New York, 2006.
- [2] P. A. R. Ade et al. Planck 2015 Results. XIII. Cosmological Parameters. *Astron. Astrophys.*, 594:A13, 2016.
- [3] Y. Fukuda et al. Evidence for Oscillation of Atmospheric Neutrinos. *Phys. Rev. Lett.*, 81:1562–1567, 1998.
- [4] Q. R. Ahmad et al. Direct Evidence for Neutrino Flavor Transformation from Neutral Current Interactions in the Sudbury Neutrino Observatory. *Phys. Rev. Lett.*, 89:011301, 2002.
- [5] T. Araki et al. Measurement of Neutrino Oscillation with KamLAND: Evidence of Spectral Distortion. *Phys. Rev. Lett.*, 94:081801, 2005.
- [6] M. H. Ahn et al. Measurement of Neutrino Oscillation by the K2K Experiment. *Phys. Rev.*, D74:072003, 2006.
- [7] R. N. Mohapatra and P. B. Pal. *Massive Neutrinos in Physics and Astrophysics*. Third Edition. *World Sci. Lect. Notes Phys.*, 72, 2004.
- [8] M. Agostini et al. Results on Neutrinoless Double- β Decay of ^{76}Ge from Phase I of the GERDA Experiment. *Phys. Rev. Lett.*, 111(12):122503, 2013.
- [9] P. Minkowski. $\mu \rightarrow e\gamma$ at a Rate of One Out of 10^9 Muon Decays? *Phys. Lett.*, B67:421–428, 1977.
- [10] T. Yanagida. Horizontal Symmetry and Masses Of Neutrinos. *Conf. Proc.*, C7902131:95–99, 1979.
- [11] R. N. Mohapatra and G. Senjanovic. Neutrino Mass and Spontaneous Parity Violation. *Phys. Rev. Lett.*, 44:912, 1980.

- [12] Ernest Ma. Verifiable Radiative Seesaw Mechanism of Neutrino Mass and Dark Matter. *Phys. Rev.*, D73:077301, 2006.
- [13] R. Bouchand and A. Merle. Running of Radiative Neutrino Masses: The Scotogenic Model. *JHEP*, 07:084, 2012.
- [14] A. Merle and M. Platscher. Running of Radiative Neutrino Masses: The Scotogenic Model Revisited. *JHEP*, 11:148, 2015.
- [15] K. S. Babu. Model of “Calculable” Majorana Neutrino Masses. *Phys. Lett.*, B203:132–136, 1988.
- [16] K. S. Babu and C. Macesanu. Two-Loop Neutrino Mass Generation and Its Experimental Consequences. *Phys. Rev.*, D67:073010, 2003.
- [17] J. Herrero-Garcia, M. Nebot, N. Rius, and A. Santamaria. The Zee-Babu Model Revisited in the Light of New Data. *Nucl. Phys.*, B885:542–570, 2014.
- [18] S. F. Novaes. Standard Model: An Introduction. In *Particles and fields. Proceedings, 10th Jorge Andre Swieca Summer School, Sao Paulo, Brazil, February 6-12, 1999*, pages 5–102, 1999.
- [19] C. Burgess and G. Moore. *The Standard Model - A Primer*. Cambridge University Press, Cambridge, 2007.
- [20] M. D. Schwartz. *Quantum Field Theory and the Standard Model*. Cambridge University Press, Cambridge, 2014.
- [21] S. Pokorski. *Gauge Field Theories*. Cambridge University Press, Cambridge, 2000.
- [22] F. Englert and R. Brout. Broken Symmetry and the Mass of Gauge Vector Mesons. *Phys. Rev. Lett.*, 13:321–323, 1964.
- [23] P. W. Higgs. Broken Symmetries and the Masses of Gauge Bosons. *Phys. Rev. Lett.*, 13:508–509, 1964.
- [24] G. S. Guralnik, C. R. Hagen, and T. W. B. Kibble. Global Conservation Laws and Massless Particles. *Phys. Rev. Lett.*, 13:585–587, 1964.
- [25] M. E. Peskin and D. V. Schroeder. *An Introduction to Quantum Field Theory*. Westview Press, New York, 1995.
- [26] C. Patrignani et al. Review of Particle Physics. *Chin. Phys.*, C40(10):100001, 2016.
- [27] R. A. Horn and C. R. Johnson. *Matrix Analysis*. Cambridge University Press, Cambridge, 2. ed. edition, 2012.

- [28] S. Antusch, J. Kersten, M. Lindner, M. Ratz, and M. Schmidt. Mixing Parameter Tools 1.1, Documentation, 2015.
- [29] M. Gell-Mann and M. Levy. The Axial Vector Current in Beta Decay. *Nuovo Cim.*, 16:705, 1960.
- [30] N. Cabibbo. Unitary Symmetry and Leptonic Decays. *Phys. Rev. Lett.*, 10:531–533, 1963.
- [31] M. Kobayashi and T. Maskawa. CP Violation in the Renormalizable Theory of Weak Interaction. *Prog. Theor. Phys.*, 49:652–657, 1973.
- [32] L. Chau and W. Keung. Comments on the Parametrization of the Kobayashi-Maskawa Matrix. *Phys. Rev. Lett.*, 53:1802, 1984.
- [33] M. C. Gonzalez-Garcia and Y. Nir. Neutrino Masses and Mixing: Evidence and Implications. *Rev. Mod. Phys.*, 75:345–402, 2003.
- [34] M. Maggiore. *A Modern Introduction to Quantum Field Theory*. OUP Oxford, New York, London, 2004.
- [35] J. Kersten. Renormalisation Group Evolution of Neutrino Masses. *Masterarbeit an der Technischen Universität München*, 2001.
- [36] B. Pontecorvo. Inverse Beta Processes and Nonconservation of Lepton Charge. *Sov. Phys. JETP*, 7:172–173, 1958.
- [37] Z. Maki, M. Nakagawa, and S. Sakata. Remarks on the Unified Model of Elementary Particles. *Prog. Theor. Phys.*, 28:870–880, 1962.
- [38] A. Merle. keV Neutrino Model Building. *Int. J. Mod. Phys.*, D22:1330020, 2013.
- [39] J. W. F. Valle. Neutrino Physics Overview. *J. Phys. Conf. Ser.*, 53:473–505, 2006.
- [40] C. Giunti and C. W. Kim. *Fundamentals of Neutrino Physics and Astrophysics*. 2007.
- [41] M. Fukugita and T. Yanagida. *Physics of Neutrinos and Applications to Astrophysics*. 2003.
- [42] B. T. Cleveland, T. Daily, R. Davis, Jr., James R. D., K. Lande, C. K. Lee, P. S. Wildenhain, and J. Ullman. Measurement of the Solar Electron Neutrino Flux with the Homestake Chlorine Detector. *Astrophys. J.*, 496:505–526, 1998.
- [43] J. N. Abdurashitov et al. Measurement of the Solar Neutrino Capture Rate with Gallium Metal. *Phys. Rev.*, C60:055801, 1999.
- [44] B. Aharmim et al. An Independent Measurement of the Total Active B-8 Solar Neutrino Flux Using an Array of He-3 Proportional Counters at the Sudbury Neutrino Observatory. *Phys. Rev. Lett.*, 101:111301, 2008.

- [45] K. Abe et al. Solar Neutrino Measurements in Super-Kamiokande-IV. *Phys. Rev.*, D94(5):052010, 2016.
- [46] F. Kaether, W. Hampel, G. Heusser, J. Kiko, and T. Kirsten. Reanalysis of the GALLEX Solar Neutrino Flux and Source Experiments. *Phys. Lett.*, B685:47–54, 2010.
- [47] C. Arpesella et al. Direct Measurement of the Be-7 Solar Neutrino Flux with 192 Days of Borexino Data. *Phys. Rev. Lett.*, 101:091302, 2008.
- [48] R. Wendell et al. Atmospheric Neutrino Oscillation Analysis with Sub-Leading Effects in Super-Kamiokande I, II, and III. *Phys. Rev.*, D81:092004, 2010.
- [49] K. Abe et al. Indication of Electron Neutrino Appearance from an Accelerator-Produced Off-axis Muon Neutrino Beam. *Phys. Rev. Lett.*, 107:041801, 2011.
- [50] P. Adamson et al. An Improved Measurement of Muon Antineutrino Disappearance in MINOS. *Phys. Rev. Lett.*, 108:191801, 2012.
- [51] I. Esteban, M. C. Gonzalez-Garcia, M. Maltoni, I. Martinez-Soler, and T. Schwetz. Updated Fit to Three Neutrino Mixing: Exploring the Accelerator-Reactor Complementarity. *JHEP*, 01:087, 2017.
- [52] NuFit Collaboration. NuFit, 2016. <http://www.nu-fit.org/>, accessed 03-Mar-2017.
- [53] Ch. Kraus et al. Final Results from Phase II of the Mainz Neutrino Mass Search in Tritium Beta Decay. *Eur. Phys. J.*, C40:447–468, 2005.
- [54] V. N. Aseev et al. An Upper Limit on Electron Antineutrino Mass from Troitsk Experiment. *Phys. Rev.*, D84:112003, 2011.
- [55] J. Wolf. The KATRIN Neutrino Mass Experiment. *Nucl. Instrum. Meth.*, A623:442–444, 2010.
- [56] Xavier Sarazin. Review of Double Beta Experiments. 2012.
- [57] P. A. R. Ade et al. Planck 2013 Results. XVI. Cosmological Parameters. *Astron. Astrophys.*, 571:A16, 2014.
- [58] M. Srednicki. *Quantum Field Theory*. Cambridge University Press, Cambridge, 2007.
- [59] J. C. Collins. *Renormalization*, volume 26 of *Cambridge Monographs on Mathematical Physics*. Cambridge University Press, Cambridge, 1986.
- [60] S. Antusch, M. Drees, J. Kersten, M. Lindner, and M. Ratz. Neutrino Mass Operator Renormalization Revisited. *Phys. Lett.*, B519:238–242, 2001.

- [61] N. N. Bogoliubov and O. S. Parasiuk. On the Multiplication of the Causal Function in the Quantum Theory of Fields. *Acta Math.*, 97:227–266, 1957.
- [62] K. Hepp. Proof of the Bogolyubov-Parasiuk Theorem on Renormalization. *Commun. Math. Phys.*, 2:301–326, 1966.
- [63] W. Zimmermann. Convergence of Bogolyubov’s Method of Renormalization in Momentum Space. *Commun. Math. Phys.*, 15:208–234, 1969. [Lect. Notes Phys.558,217(2000)].
- [64] G. ’t Hooft. Renormalization of Massless Yang-Mills Fields. *Nucl. Phys.*, B33:173–199, 1971.
- [65] G. ’t Hooft. Renormalizable Lagrangians for Massive Yang-Mills Fields. *Nucl. Phys.*, B35:167–188, 1971.
- [66] G. ’t Hooft and M. J. G. Veltman. Regularization and Renormalization of Gauge Fields. *Nucl. Phys.*, B44:189–213, 1972.
- [67] G. ’t Hooft. Dimensional Regularization and the Renormalization Group. *Nucl. Phys.*, B61:455–468, 1973.
- [68] G. Passarino and M. J. G. Veltman. One Loop Corrections for e^+e^- Annihilation into $\mu^+\mu^-$ in the Weinberg Model. *Nucl. Phys.*, B160:151–207, 1979.
- [69] R. K. Ellis, Z. Kunszt, K. Melnikov, and G. Zanderighi. One-loop Calculations in Quantum Field Theory: From Feynman Diagrams to Unitarity Cuts. *Phys. Rept.*, 518:141–250, 2012.
- [70] K. Symanzik. Small Distance Behavior in Field Theory and Power Counting. *Commun. Math. Phys.*, 18:227–246, 1970.
- [71] K. Symanzik. Small Distance Behavior Analysis and Wilson Expansion. *Commun. Math. Phys.*, 23:49–86, 1971.
- [72] Curtis G. Callan, Jr. Broken Scale Invariance in Scalar Field Theory. *Phys. Rev.*, D2:1541–1547, 1970.
- [73] Curtis G. Callan, Jr. Broken Scale Invariance and Asymptotic Behavior. *Phys. Rev.*, D5:3202–3210, 1972.
- [74] H. Georgi. Effective Field Theory. *Ann. Rev. Nucl. Part. Sci.*, 43:209–252, 1993.
- [75] A. Pich. Effective Field Theory: Course. In *Probing the Standard Model of Particle Interactions. Proceedings, Summer School in Theoretical Physics, NATO Advanced Study Institute, 68th session, Les Houches, France, July 28-September 5, 1997. Pt. 1, 2*, pages 949–1049, 1998.

- [76] Steven Weinberg. Effective Field Theory, Past and Future. *PoS*, CD09:001, 2009.
- [77] T. Appelquist and J. Carazzone. Infrared Singularities and Massive Fields. *Phys. Rev.*, D11:2856, 1975.
- [78] B. Henning, X. Lu, and H. Murayama. How to Use the Standard Model Effective Field Theory. *JHEP*, 01:023, 2016.
- [79] B. Henning, X. Lu, and H. Murayama. One-loop Matching and Running with Covariant Derivative Expansion. 2016.
- [80] S. Weinberg. Baryon and Lepton Nonconserving Processes. *Phys. Rev. Lett.*, 43:1566–1570, 1979.
- [81] S. Weinberg. Varieties of Baryon and Lepton Nonconservation. *Phys. Rev.*, D22:1694, 1980.
- [82] M. Nebot, J. F. Oliver, D. Palao, and A. Santamaria. Prospects for the Zee-Babu Model at the CERN LHC and Low Energy Experiments. *Phys. Rev.*, D77:093013, 2008.
- [83] J. Herrero-Garcia, M. Nebot, N. Rius, and A. Santamaria. Testing the Zee-Babu Model via Neutrino Data, Lepton Flavour Violation and Direct Searches at the LHC. *Nucl. Part. Phys. Proc.*, 273-275:1678–1684, 2016.
- [84] V. D. Barger, S. Pakvasa, T. J. Weiler, and K. Whisnant. Bimaximal Mixing of Three Neutrinos. *Phys. Lett.*, B437:107–116, 1998.
- [85] S. Antusch, J. Kersten, M. Lindner, M. Ratz, and M. A. Schmidt. Running Neutrino Mass Parameters in See-Saw Scenarios. *JHEP*, 03:024, 2005.
- [86] F. Staub. Exploring New Models in all Detail with SARAH. *Adv. High Energy Phys.*, 2015:840780, 2015.
- [87] A. Vicente. Computer Tools in Particle Physics. 2015.
- [88] M. Platscher. Renormalisation of Radiative Neutrino Masses. *Masterarbeit am Max-Planck-Institut für Physik (Werner-Heisenberg-Institut)*, 2015.
- [89] K. L. McDonald and B. H. J. McKellar. Evaluating the Two Loop Diagram Responsible for Neutrino Mass in Babu’s Model. 2003.
- [90] J. van der Bij and M. J. G. Veltman. Two Loop Large Higgs Mass Correction to the ρ -Parameter. *Nucl. Phys.*, B231:205–234, 1984.
- [91] T. Geib, A. Merle, and M. Volpp. *Work in progress*.
- [92] T. Hahn. Routines for the Diagonalization of Complex Matrices. 2006.

- [93] S. Antusch, J. Kersten, M. Lindner, and M. Ratz. Running Neutrino Masses, Mixings and CP Phases: Analytical Results and Phenomenological Consequences. *Nucl. Phys.*, B674:401–433, 2003.
- [94] M. Malinsky. Fun with the Abelian Higgs Model. *Eur. Phys. J.*, C73:2415, 2013.
- [95] J. A. Casas and A. Ibarra. Massive Neutrinos and $\mu \rightarrow e, \gamma$. *Nucl. Phys. Proc. Suppl.*, 95:268–271, 2001.
- [96] A. Denner, H. Eck, O. Hahn, and J. Kublbeck. Feynman Rules for Fermion-Number-Violating Interactions. *Nucl. Phys.*, B387:467–481, 1992.

Erklärung

Ich versichere, die Arbeit selbstständig angefertigt und dazu nur die im Literaturverzeichnis angegebenen Quellen benutzt zu haben.

München, den 16. April 2017